Institut für Geoökologie
Lehrstuhl für Hydrologie und Klimatologie

# Reservoir Sedimentation in Dryland Catchments: Modelling and Management

**Dissertation**
**zur Erlangung des akademischen Grades**
**"doctor rerum naturalium"**
**(Dr. rer. nat.)**
**in der Wissenschaftsdisziplin Hydrologie**

**eingereicht an der**
**Mathematisch-Naturwissenschaftlichen Fakultät**
**der Universität Potsdam**

**von**
**George Leite Mamede**

**Potsdam, den 14. Januar 2008**

Elektronisch veröffentlicht auf dem
Publikationsserver der Universität Potsdam:
http://opus.kobv.de/ubp/volltexte/2008/1704/
urn:nbn:de:kobv:517-opus-17047
[http://nbn-resolving.de/urn:nbn:de:kobv:517-opus-17047]

Department of Geoecology
Chair for Hydrology and Climatology

# Reservoir Sedimentation in Dryland Catchments: Modelling and Management

**Dissertation for the Degree of**
**Doctor of Natural Sciences**

**Submitted to the Faculty of Mathematics and Sciences**
**at the University of Potsdam**

**by**

**George Leite Mamede**

**Potsdam, January 14. 2008**

# PREFACE

This research has been funded by the Brazilian Ministry of Education (CAPES) and developed within the framework of the SESAM Project (Sediment Export from Large Semi-Arid Catchments: Measurements and Modelling). The SESAM Project is an international cooperation programme involving the University of Potsdam (Germany), the GFZ Potsdam (Germany), the University of Lleida (Spain), the Forestry and Technology Center of Catalonia (Spain) and the Federal University of Ceará (Brazil). Overall, the goal of the SESAM Project was to develop an integrated model concept, which enables the simulation of erosion processes at the hillslope and sub-basin scale, the sediment transport processes in rivers and sediment deposition and management in reservoirs.

At first, I would like to express my utmost gratitude to my supervisor, Prof. Dr. Axel Bronstert, for his support and advice during the development of this thesis. I am particularly indebted to Prof. Dr. José Carlos de Araújo, for many helpful discussions which improved this research.

I would also like to acknowledge the colleagues from the SESAM team, particularly Prof. Dr. Ramon Batalla, Dr. Andreas Güntner and Dr. Eva Müller, for supporting this work with their experience, with critical questions and suggestions to improve it.

My special thanks go to colleagues Till Francke and Pedro Medeiros for helping on the progress of this research and for providing a pleasant work atmosphere.

I would also like to thank the colleagues who helped in carrying out the monitoring campaigns, particularly Benjamin Creutzfeldt, Paulo Belo, Carlos Germano, Roberto Silva and Alexandre Costa.

I would like to acknowledge the contributions of colleagues at several Institutions in Germany, Spain and Brazil in providing all the data I needed during the development of this research and equipment to carry out field measurements. In particular, I would like to mention the GFZ Potsdam, the University of Lleida, the Forestry and Technology Center of Catalonia, the Hydrological Confederation of the Ebro Basin (CHEBRO), the Water Management Company (COGERH) and the Water Resources and Meteorology Foundation (FUNCEME). The Brazilian Environmental Institute (IBAMA) made an important contribution in supporting monitoring campaigns in the study area in Brazil.

I would also like to thank all my colleagues at the Institute of Geoecology of the University of Potsdam, particularly Theresa Blume, Dominik Reusser, Andreas Bauer, Markus Morgner, Thomas Gräff, Daniel Bazant, Stefanie Erxleben, Sabine Schrader Saskia Förster, Knut Günther, Maik Heistermann, Heide Kraudelt and David Kneis.

Finally, I am deeply grateful to my wife, Gisele Mamede, for supporting me in all situations.

# CONTENTS

# FIGURES

## List of Figures

# List of Tables

# ABBREVIATIONS

## List of Abbreviations

| | |
|---|---|
| ASCE | American Society of Civil Engineers |
| CCHE1D | One-Dimensional Channel Network Model |
| CHEBRO | Hydrological Confederation of the Ebro Basin |
| COGERH | Water Management Company in the Federal State of Ceará |
| CONCEPTS | Conservation Channel Evolution and Pollutant Transport System |
| EFDC1D | One-Dimensional Hydrodynamic/Sediment Transport Model for Stream Networks |
| FUNCEME | Water Resources and Meteorology Foundation in the Federal State of Ceará |
| GFZ | GeoForschungsZentrum Potsdam |
| GSTARS | General Stream Tube Model for Alluvial River Simulation |
| HEC | Hydrologic Engineering Center |
| HISPAGUA | Spanish System of Information about Water |
| IBAMA | Brazilian Environmental Institute |
| IRTCES | International Research of Training Center on Erosion and Sedimentation |
| MUSLE | Modified Universal Soil Loss Equation |
| ORSTOM | French Scientific Research Institute for Development in Cooperation |
| QRF | Quantile Regression Forests model |
| SESAM | Sediment Export from Large Semi-Arid Catchments: Measurements and Modelling |
| SOTER | Soil and Terrain digital Database |
| SSC | Suspended Sediment Concentration |
| SSIIM | Model of Sediment Simulation in Intakes with Multiblock |
| UFC | Federal University of Ceará |
| USLE | Universal Soil Loss Equation |
| WASA | Model of Water Availability in Semi-Arid Environments |
| WASA-SED | WASA model with erosion and sediment transport modules |

# Summary

Semi-arid environments are mainly characterized by scarce water resources and are usually subject to risks of water stress. In these regions, water supply for drinking and irrigation purposes depends strongly on storage in surface reservoirs and sediment deposition in these reservoirs affects adversely the water storage.

In order to reproduce the complex behaviour of sediment deposition in reservoirs located in semi-arid environments and the effects of using sediment management techniques, a reservoir sedimentation model is developed and coupled within the WASA-SED model, which simulates rainfall-runoff processes and sediment transport within the hillslope and river network.

The reservoir sedimentation model consists of two modelling approaches, which may be applied according to reservoir size and data availability. For reservoirs with information about their geometric features (reservoir topography, stage-area and stage-volume curves) and physical properties of sediment deposits, such as deposition thickness, grain size distribution of sediment deposits and sediment densities, a detailed modelling approach to reservoir sedimentation may be applied. For reservoirs without those characteristics, a simplified modelling approach is used.

The detailed modelling approach of reservoir sedimentation enables the assessment of sediment deposition pattern in reservoirs and the evaluation of sediment release efficiency of sediment management techniques. It simulates sediment transport along the longitudinal profile of a reservoir. The reservoir is divided into cross-sections to elaborate the sediment budget. The sediment transport component is calculated using a non-uniform sediment transport approach based on the concept of sediment carrying capacity. Four different sediment-transport equations can be selected for the simulations.

The simplified modelling approach of reservoir sedimentation is suitable to simulate water and sediment transfer in dense reservoirs network. Nevertheless, it does not allow simulating either sediment management techniques, or spatial distribution of sedimentation. In this approach, the reservoirs are classified into *small* and *strategic* reservoirs according to their location and size. Strategic reservoirs are medium and large reservoirs located on main rivers at the sub-basin's outlet or reservoirs of particular interest. The small reservoirs are located on tributary streams and represented in the model in an aggregate manner by grouping them into size classes according to their storage capacity. A cascade routing scheme is used to describe the upstream-downstream position of the reservoir classes. The water and sediment balances of small reservoirs are computed for one hypothetical representative reservoir of mean characteristics. Sediment trapping efficiency and effluent grain size distribution are estimated using the overflow rate concept.

Three model applications are carried out within this research, as follows:

- The detailed modelling approach of reservoir sedimentation is applied to the 92.2 $Mm^3$ Barasona Reservoir, located in the foothills of the Central Pyrenees (Aragon, Spain). A two-stage calibration was performed to account for changes in the sediment deposition pattern caused by sediment management. The reservoir sedimentation model is then validated for another simulation period which confirms that the processes related to reservoir sedimentation are well represented by the model.
- An application is carried out on the 933-$km^2$ Benguê catchment, located in the

semi-arid region of Northeast Brazil. The catchment is characterized by a dense reservoir network, covering almost 45% of the catchment area, with a significant lack of data. Water and sediment balances of those reservoirs are computed using the simplified modelling approach. Three spatial configurations describing the cascade routing scheme are tested.

- The reservoir sedimentation model is applied again to the Barasona reservoir to evaluate the sediment release efficiency of sediment management strategies. Cost analysis is presented to help in the choice of the most promising sediment management technique for that situation. Thus, the model enables the assessment of technical features of the sediment management strategies.

Overall, simulation results are characterized by large uncertainties, partly due to low data availability and also due to uncertainties of the model structure to adequately represent the processes related to reservoir sedimentation. The uncertainties are summarized in the following:

- Use of regression models to estimate suspended sediment concentration of inflow discharges into the Barasona reservoir.
- Properties of sediment deposits (bed composition, dry bulk density, deposition thickness).
- Use of the Rouse equation for the assessment of vertical distribution of suspended sediment concentration immediately upstream of the dam. That equation was developed for equilibrium conditions in rivers.
- Use of area-volume relationship to estimate storage capacities of small reservoirs.

# Zusammenfassung

Semiaride Gebiete sind hauptsächlich durch geringe Wasserressourcen gekennzeichnet und unterliegen häufig dem Risiko der Wasserknappheit. In diesen Gebieten ist die Wasserbereitstellung für Bewässerung und Trinkwasserversorgung stark von der oberflächlichen Speicherung in Stauseen abhängig, deren Wasserverfügbarkeit nachteilig durch Sedimentablagerung beeinflusst wird.

Zur Wiedergabe des komplexen Sedimentablagerungsverhaltens in Stauseen von semiariden Gebieten und die Auswirkungen von Sedimentmanagementmaßnahmen wird ein Sedimentationsmodell entwickelt und mit dem WASA-SED Modell gekoppelt, das für die Modellierung der Abflussbildung und des Sedimenttransportes in Einzugsgebieten geeignet ist.

Das Sedimentationsmodell beinhaltet zwei Ansätze, die unter der Berücksichtigung verschiedener Stauseengrößenklassen und Datenverfügbarkeit eingesetzt werden können. Für die Stauseen mit verfügbaren Informationen über ihre geometrischen Eigenschaften (wie Stauseetopographie und Höhe-Fläche-Volumen-Beziehung) und weitere Kenngrößen wie Ablagerungsmächtigkeit, Korngrößenverteilung und Sedimentdichte, kann ein detaillierter Modellansatz für die Sedimentablagerung verwendet werden. Wo diese Informationen nicht verfügbar sind, wird auf einen vereinfachten Ansatz zurückgegriffen.

Der detaillierte Modellansatz ermöglicht die Betrachtung von Ablagerungsmustern im Stausee und Einschätzungen über die Effektivität von Sedimentmanagementmaßnahmen hinsichtlich der Sedimententlastung. Dieser Ansatz beruht auf der Simulation des Sedimenttransportes entlang eines Stauseelängsprofils. Für die Berechnung des Sedimenttransfers wird der Stauseekörper in einer Folge von Querprofilen repräsentiert. Der Sedimenttransport wird dabei korngrößenspezifisch entsprechend der Transportkapazität berechnet. Dafür stehen vier verschiedenen Sedimenttransportgleichungen zur Verfügung.

Der vereinfachte Modellansatz ist für die Simulation des Sedimenttransfers in Gebieten mit hoher Stauseedichte geeignet, jedoch können weder Sedimentmanagementmaßnahmen noch die räumliche Verteilung der Ablagerungen berücksichtigt werden. Dafür werden die Stauseen in Abhängigkeit von ihrer Größe und Position in *kleine* und *strategische* Stauseen unterteilt. Dabei sind strategische Stausseen solche mit mittlerem bis großem Volumen sowie einer Lage im Hauptgerinne oder solche mit sonstiger besonderer Bedeutung. Kleine Stauseen hingegen befinden sich an den Nebenflüssen und werden im Modell in aggregierter Form durch ihre Einteilung in Stauseegrößenklassen repräsentiert. Ein Kaskadenverfahren wird für den Wasser- und Sedimentlauf zwischen den Stauseeklassen verwendet. Dabei werden für jede Stauseeklasse der Wasser- sowie Sedimenthaushalt für einen hypothetischen repräsentativen Stausee mit mittleren Eigenschaften berechnet. Die Sedimentaufnahme und die Korngrößenverteilung des abgegebenen Sediments werden mit dem Überlaufanteil-Ansatz berechnet.

In dieser Studie werden drei Modellanwendungen vorgestellt:

- Für den 92,2 Mio.m³-großen Barasona-Stausee (Vorland der Zentralpyrenäen, Aragon, Spanien) wird die Modellierung der Sedimentablagerung mit dem detaillierten Modellansatz vorgenommen. Die Kalibrierung dafür wurde in zwei Schritten durchgeführt, um Änderungen im Stauseemanagement Rechnung zu tragen. Die Modell-Validierung wird schließlich für eine andere Simulationsperiode vorgenommen. Dabei wird ersichtlich, dass die Prozesse der Sedimentablagerung gut durch das Modell wiedergegeben werden.

- Das Modell wird auf das 933 km²-große Benguê-Einzugsgebiet, das sich im semiariden Nordosten Brasiliens befindet, angewendet. Dieses Einzugsgebiet ist durch eine hohe Dichte an kleinen Stauseen, charakterisiert, die fast 45% des Gebietes umfasst, wofür jedoch wenige Messdaten verfügbar sind. Deshalb werden der Wasser- und Sedimenttransport mit dem vereinfachten Modellansatz berechnet. Dabei werden drei Konfigurationen des Kaskadenverfahrens getestet.
- Die Modellanwendung erfolgt erneut für den Barasona-Stausee bezüglich der Effektivität der Sedimentmanagementmaßnahmen. Eine Kostenanalyse ermöglicht die Auswahl geeigneter Maßnahmen für den Stausee. Dadurch wird eine Beurteilung der verschiedenen Sedimentmanagementstrategien ermöglicht.

Im Allgemeinen unterliegen die Simulationsergebnisse großen Unsicherheiten, teilweise wegen der geringen Datenverfügbarkeit, andererseits durch die Unsicherheiten in der Modellstruktur zur korrekten Wiedergabe der Sedimentablagerungsprozesse. Die Unsicherheiten lassen sich wie folgt zusammenfassen:

- Unsicherheiten des Regressionsmodells zur Bestimmung der Sedimentkonzentration in den Zuflüssen des Barasona-Stausees.
- Eigenschaften der abgelagerten Sedimente (Korngrößenverteilung, Trockenrohdichte, Ablagerungsmächtigkeit).
- Verwendung der Rouse-Gleichung für die Bestimmung der vertikalen Verteilung der Schwebstofffracht unmittelbar vor der Staumauer, da diese Gleichung für Gleichgewichtsbedingungen in Flüssen entwickelt wurde.
- Verwendung der Fläche-Volumen-Beziehung für die Bestimmung der Speicherkapazitäten der kleinen Stauseen.

# CHAPTER 1

# 1. Introduction

## 1.1. Background

Dryland environments are often exposed to the hazard that the available freshwater resources fail to meet the water demand in the domestic, agricultural and industrial sectors. Water availability often relies on the retention of river runoff in reservoirs. However, the water storage in reservoirs is often adversely affected by sedimentation because of severe soil erosion in headwater catchments. Therefore, the assessment of sediment deposition processes in reservoirs becomes indispensable.

Reservoir sedimentation is the process of sediment deposition that occurs after a dam construction. A dam causes reduction in flow velocity and consequently in turbulence, which causes the settling process of sediments carried by the inflowing water. This mechanism ultimately causes the sedimentation in reservoirs, which is a severe problem for designers and users. Depending on the amount of material deposited, the shortening of the reservoir life time will bring several unpredicted consequences.

The consequences of reservoir sedimentation can have serious impacts on the local and regional economic situation related to drinking water supply, irrigation and power generation. Reduction of water availability is a major impact of reservoir silting for semi-arid regions (Araújo et al., 2006). Sedimentation also leads to the obstruction of water intakes, sediment deposition in the delta region and streambed aggradation. As a by-product of the human activities upstream of the dam, the fine fraction of the incoming suspended sediments may carry adsorbed pollutants. Its deposition may have negative environmental consequences, such as physical, chemical and biological pollution of the water body, low water transparency, growth of submerged and floating vegetation causing oxygen depletion and increasing fish mortality. Eutrophication is the key process, if nutrients are transported. Initially, “submerged vegetation” – algae mostly – will increase oxygen primary production. Nonetheless, turbidity (caused by sediment, e.g.) in reservoirs undergoing eutrophication reduces sun light entrainment. As a result, there will be oxygen over-concentration in the upper water layers and oxygen depletion in the lower layers.

Understanding the mechanisms and feedbacks of complex natural and human systems, together with the quantitative assessment of sediment production and sediment transport in catchments and, consequently, the reservoir sedimentation, are a prerequisite for sustainable water management.

For any dam or reservoir where sustainable long-term use is to be achieved, it will be necessary to manage sediment as well as water. Sedimentation needs to be controlled and kept at a minimum level to ensure continuous usage of the reservoir for water supply and power generation. However, the sustainable sediment management of reservoirs is not achieved without costs. Activities for maintaining the original storage capacity of reservoirs, such as temporary removal of the dam from service for sediment management activities, release of increased volumes of water downstream of the dam for sediment discharge and dredging will be not economically attractive to managers of existing reservoirs.

In order to simulate bed aggradation and degradation in reservoirs and to enhance sediment management strategies, a deterministic, process-based, one-dimensional modelling approach for a spatially semi-distributed reservoir sedimentation model has been developed.

## 1.2. Objectives

As sediment deposition is one of the most important problems affecting the useful life of reservoirs, knowledge of both rate and spatial pattern of sediment deposition is required to predict its impacts and to identify practicable management strategies. To achieve these aims, a reservoir sedimentation model has been developed which reproduces as closely as possible the complex behaviour of sediment deposition. The model has been designed to fulfil the following research objectives:

- to calculate non-equilibrium transport of non-uniform sediment along the longitudinal profile of a reservoir using different sediment-transport equations.
- to enable the assessment of reservoir bed elevation changes along a longitudinal profile and to include a simplified approach to simulate the lateral distribution of sediment deposition and bed degradation.
- to compute the temporal variability of the reservoir bed composition for several grain size classes.
- to simulate several sediment management alternatives and to analyse the technical and economic feasibility to identify the most promising alternative.
- to calculate the main parameters related to reservoir sedimentation, such as trapping efficiency, sedimentation rate, sediment release, reservoir life expectancy, among others.
- to include a simplified modelling approach for small reservoirs. It may be expected that the small reservoirs play an important role in the water and sediment retention upstream of the large ones.

The reservoir sedimentation model is coupled with the WASA model (Water Availability in Semi-Arid environments), an existing hydrological catchment model tailored for specific semi-arid characteristics and extended for the quantitative assessment of sediment mobilisation in catchments and sediment transport in the river system (Güntner, 2002).

## 1.3. Structure of this thesis

This PhD thesis is divided into six chapters. Chapter 2 contains the literature review of the processes related to reservoir sedimentation.

The structure of the reservoir sedimentation modelling and governing equations are presented in Chapter 3.

In Chapter 4, descriptions of the study areas in Brazil and Spain are presented, taking into account the general aspects of the catchments and the reservoir features. Data collection and monitoring campaigns that were carried out in the study areas are also described in Chapter 4.

Results of model applications for the study areas are presented, analysed and discussed in Chapter 5, including model uncertainties and sensitivity analysis to model input data and model structure. Additionally, sediment management scenarios are simulated for the prediction of reservoir sedimentation in the next decades.

Finally, Chapter 6 presents the conclusions and recommendations of this study.

# CHAPTER 2

# 2. State of the Art of Reservoir Sedimentation

## 2.1. Sediment properties

### 2.1.1. Introduction

Sediment properties define how each individual or aggregate particle behaves in flowing water. Size, shape and density affect the settling velocity, which in turn affects sediment transport rates and at what points particles deposit. These characteristics are important for reservoir sedimentation as the rate of entrainment, transport, deposition and compaction are functions of the properties of the sediment particles. The properties mentioned above are beyond the scope of this section.

### 2.1.2. Size of Sediment Grains

Grain size is the most important parameter describing sediment behaviour in water, and a variety of terms may be used to describe the size characteristics of individual grains and composite samples. Sediment particles are divided into different groups such as boulders, cobbles, gravels, sand, silt and clay, according to their sizes (Shen and Julien, 1992). Here, the size classification system recommended by American Geophysical Union is used, which is a geometric scale based on a ratio of 2 between successive sizes (see Table 2.1).

Sediment particles are never exactly spherical and the term "diameter" only approximates their sizes. Several methods are used to determine and express grain diameter. Grain may be measured along three mutually perpendicular axes of which there will be a longest, an intermediate and a shortest axis (Morris and Fan, 1997). The *mean diameter* or *triaxial diameter* of a sediment particle is the arithmetic average of the three axes. The *nominal diameter* is the diameter of a sphere having the same volume as the particle. The *fall diameter* or *sedimentation diameter* is the diameter of a sphere with specific density of 2.65 and having the same terminal fall velocity in quiescent distilled water at 24°C as the particle. The *sieve diameter* is defined as the square size opening in a sieve which a given sediment particle will just pass through. (Shen and Julien, 1992).

**Table 2.1 Grain size classes according to the American Geophysical Union.**

| Size Class | Dmin (mm) | Dmax (mm) |
|---|---|---|
| Very large Boulders | 2048 | 4096 |
| Large Boulders | 1024 | 2048 |
| Medium Boulders | 512 | 1024 |
| Small Boulders | 256 | 512 |
| Large Cobbles | 128 | 256 |
| Small Cobbles | 64 | 128 |
| Very coarse Gravel | 32 | 64 |
| Coarse Gravel | 16 | 32 |
| Medium Gravel | 8 | 16 |
| Fine Gravel | 4 | 8 |
| Very fine Gravel | 2 | 4 |
| Very coarse sand | 1.0 | 2.0 |
| Coarse sand | 0.5 | 1.0 |
| Medium sand | 0.25 | 0.50 |
| Fine sand | 0.125 | 0.250 |
| Very fine sand | 0.0625 | 0.125 |
| Coarse silt | 0.0313 | 0.0625 |
| Medium silt | 0.0156 | 0.0313 |
| Fine silt | 0.0078 | 0.0156 |
| Very fine silt | 0.0039 | 0.0078 |
| Coarse clay | 0.0020 | 0.0039 |
| Medium clay | 0.0010 | 0.0020 |
| Fine clay | 0.00049 | 0.00098 |
| Very fine clay | 0.00024 | 0.00049 |

### 2.1.3. Grain Size Distribution

Granulometric characteristics of deposited sediment may be described by a grain size distribution curve, which represents the cumulative dry weight of the sample in each

size fraction. Depending upon the soil texture and gradation, the shape of the particle size distribution can vary greatly. Some specific points in the particle size distribution are used to define sediment properties. The $d_{35}$ diameter is the maximum size for the smallest 35% of the sample, which was used by Einstein's method for partitioning fluid drag. The $d_{50}$ diameter is the maximum size for the smallest 50% of the sample and corresponds to the median diameter. The $d_{65}$ diameter is the maximum size for the smallest 65% of the sample and has been often used to indicate roughness of sediment mixtures. The $d_{16}$, $d_{84}$ and $d_{90}$ diameters are also frequently used to describe sediment mixtures.

### 2.1.4. Particle Shape

The shape of a particle affects the average velocity of the water flow, the fall velocity and bed load transport. Among the many coefficients found in the literature, two of them are presented here. The *sphericity* is the ratio between the surface area of a sphere with the same volume as the particle and the actual particle's area. The value of sphericity of a sphere is one, and it is less than one for the other shapes. This coefficient is not easily calculated because a single particle surface has a very small surface area which is difficult to measure. However, it represents the most suitable shape coefficient to represent the shape influence on the particle fall velocity. The *roughness* is defined as the ratio of the average radius of the corners and edges of a particle to the radius of a circle inscribed in the maximum projected area of the particle. It is geometrically independent of sphericity and has a relatively small effect on the hydraulic behaviour, but it is of primary importance in determining the abrasiveness of a particle to hydraulic equipment (Morris and Fan, 1997).

### 2.1.5. Bulk Properties of Sediment

Specific weight and bulk density are used to express the dry weight per unit of volume of a bulk sediment sample, including both solid grains and voids, after drying to a constant weight at 105°C. The volumetric unit or specific weight of the sediment determines the space occupied by deposits of sediment. The specific weight can be defined as the weight of the particle divided by its volume, whereas the bulk density of sediment deposited is defined as the dry weight of the sediment deposit divided by its bulk volume. The bulk density of clay and silt deposits can vary significantly over time owing to compaction. Therefore, it is an important factor in determining sediment accumulation in reservoirs (Shen and Julien, 1992).

### 2.1.6. Fall Velocity

Fall velocity or settling velocity is a primary determinant of sediment behaviour in a fluid. A sediment particle can be transported in suspension only if its settling velocity is less than the vertical component of hydraulic turbulence. Settling velocity is also a primary determinant of the percentage and grain size distribution of the inflowing load that becomes trapped in a reservoir, and the pattern of sediment distribution along the length of the reservoir (Morris and Fan, 1997). The settling velocity of a particle depends on the effects of size, shape and density of a sediment particle, the effects of fluid density and turbulence (Shen and Julien, 1992). Several researchers have proposed expressions for the particle fall velocity. Results of the estimation of settling velocities using six different equations are presented in Figure 2.1. Owing to the simplicity of the Zhang's equation, its good agreement with the other settling velocity equations, and its ability to compute settling velocities for a wide range of sediment sizes, it will be used here. The Zhang's formula (Zhang and Xie, 1993) can be written as follows:

$$\omega_j = \sqrt{\left(13.95.\frac{\nu}{d}\right)^2 + 1.09.\Delta.g.d} - 13.95.\frac{\nu}{d} \quad (2.1)$$

where $\omega j$ is the settling velocity for a particle size $j$; $d$ is the particle diameter (m); $g$ is the gravitational acceleration ($m^2.s^{-1}$); $\Delta$ is the relative density ($\gamma_s/\gamma-1$); $\gamma_s$ and $\gamma$ are the specific weights of sediment and fluid, respec-

tively; and $\nu$ is the kinematic viscosity ($m^2.s^{-1}$), computed as:

$$\nu = \frac{1.14 - 0.031.(T-15) + 0.00068(T-15)^2}{10^6} \qquad (2.2)$$

in which $T$ is the water temperature (°C).

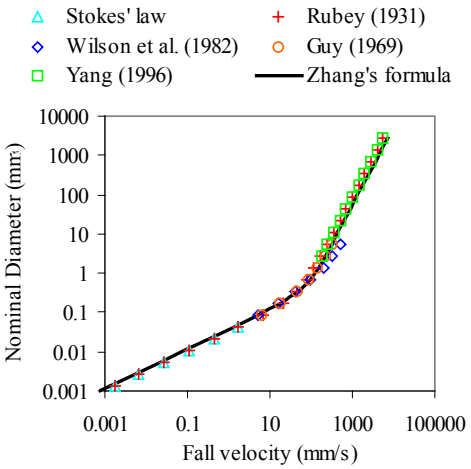


**Figure 2.1 Settling velocity estimation using six different equations from the literature: Stokes' law (Haan et al, 1994); Rubey (1931); Wilson et al. (1982); U.S. Unteragency Committee on Water Resources Subcommittee on Sedimentation (Guy, 1969); Yang (1996); and Zhang's formula (Zhang and Xie, 1993).**

## 2.2. Non-Uniform Sediment Transport in Rivers and Reservoirs

### 2.2.1. Introduction

The field of non-uniform sediment transport is very complex, but has received increasing attention in recent decades because nearly all stream beds consist of mixed-size sediment particles. The non-uniform sediment transport can be classified into cohesive and non-cohesive sediment transport, according to the characteristics of the transported material. For coarse non-cohesive sediments, characteristics such as settling velocity, condition of incipient sediment motion and erosion rate are determined by gravitational forces, which can be represented by the grain diameter. However, in fine-grain sediments (smaller than 0.01 mm) surface forces predominate, and the behaviour of cohesive sediments cannot be determined based on grain sizes alone (Morris and Fan, 1997). There is no clear boundary between cohesive sediment and non-cohesive sediment. The definition is usually site-specific. In general, finer sized grains are more cohesive. Sediment sizes smaller than 2 μm (clay) are generally considered cohesive sediment. Sediment of size greater than 60 μm is coarse non-cohesive sediment. Silt (2 μm - 60 μm) is considered to be between cohesive and non-cohesive sediment (Huang et al., 2006).

### 2.2.2. Sediment Transport Modes

According to the mechanisms of transport, the total sediment load can be subdivided by source or by mode of transport (see Fig. 2.2). For source, the total load is split between the bed material load and wash load. The bed material load is derived from the river bed and is typically sand-sized or gravel-sized. The wash load consists of sediment that has been flushed into the river from upland sources and is sufficiently fine-grained that the river is always able to carry it in suspension. For mode of transport, the total sediment transport is divided into suspended load transport and bed load transport. The suspended load transport is dispersed in the flow by turbulence and is carried for considerable distances without touching the bed. The bed load transport is typically coarse sediment moving in almost continuous contact with the bed by rolling, sliding, or saltating under the tractive force exerted by the water flow (Campos, 2001).

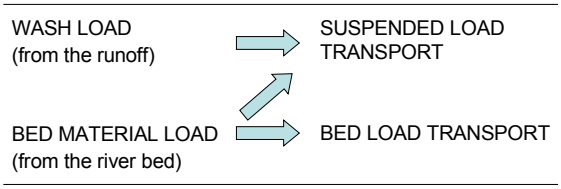


**Figure 2.2 Composition of the sediment transport (Campos, 2001).**

### 2.2.3. Non-Cohesive Sediment Transport

Several transport functions for cohesionless material have been developed with the aim of computing the rate and grain size distribution of the transported material, given the hydraulics and bed material gradation, such as Schoklitsch (1934), Kalinske (1947), Meyer-Peter and Müller (1948), Einsten (1950), Laursen (1958), Rottner (1959), Toffaleti (1969), Engelung and Hansen (1972), Ackers and White (1973), Yang (1973, 1979 and 1984), Rijn (1984a, 1984b), Parker (1990), Ribberink (1998), Gladkow and Söhngen (2000), Wu et al. (2000a), and Wilcock and Crowe (2003). Nevertheless, no universal function exists which can be applied with accuracy to all sediment and flow conditions. Computed results based on different transport formulas may differ significantly from each other and from measurements (Yang and Huang, 2001). Comparisons of accuracies of sediment transport formulas have been published by Schulits and Hill (1968), White et al. (1975), Yang (1976, 1979), Alonso (1980), Brownlie (1981), Yang and Molinas (1982), ASCE (1982), Yang (1984), Vetter (1989), Yang and Wan (1991), Yang and Huang (2001), Scheer et al (2002).

### 2.2.4. Cohesive Sediment Transport

Cohesive sediment, or mud, is a mixture of clay particles, silt, (fine) sand, organic material, sometimes gas, and, in general, a very large amount of water. This sediment has cohesive properties because of the electrochemical attraction of clay particles and the organic material. Thus, mud is encountered in the form of mud flocs, both in the water column and within the river or lake bed. As the composition of the sediment mixture varies in place and time (for instance because of seasonal effects), the mechanical properties of the mixture also vary in space and time. Moreover, the properties of mud flocs are affected by memory effects with respect to the history in physical, chemical and biological influences.

Cohesive sediments tend to aggregate to form large, low-density units. This process is strongly dependent on the type of sediment, the type and concentration of ions in the water and the flow condition (Mehta et al., 1989). As particle size decreases, the interparticle forces dominate gravitational force, and the settling velocity is no longer a function of only particle size. These forces, which may be several orders of magnitude larger than gravitational forces, give clay its stickiness and influence important phenomena such as flocculation, the rate of sedimentation and compaction, the angle of repose and erosion resistance. Flocculation produces particles aggregates having much larger effective diameter than discrete clay particles. Consequently, the settling rate of clay will initially increase as a function of concentration. However, at some higher concentration, the flocs create a structural lattice which greatly hinders fall velocity. Deposited cohesive sediments compact over time and the rate and extent of compaction will reflect the mechanical shear strength of the aggregates. Higher cohesive forces will form stronger and denser aggregates, and will in turn exhibit greater resistance to erosion by shear forces (Morris and Fan, 1997).

## 2.3. Reservoir Sedimentation

### 2.3.1. Introduction

Reservoirs are built to serve many functions that include storage facilities for domestic and irrigation water supply, power generation, enhanced navigation and flood attenuation. Discounting long-term damage to the structural integrity of the dam walls, the main factor influencing the operational life of a reservoir is the loss of effective water storage capacity due to sediment deposition. However, storage capacity loss is only one of many sediment-related problems such as: delta deposition (increasing flooding of infrastructure and agricultural lands, and reducing navigational clearance beneath bridges); navigation impairment due to sediment accumulation; air pollution due to erosion and transport by wind of desiccated deposits (creating a nuisance and

health hazard to nearby communities); earthquake hazard due to the presence of sediment against the dam (Chen and Hung, 1993); abrasion of hydraulic machinery (reducing its efficiency and increasing maintenance costs); obstruction of bottom outlets; reduction of energy generation; and ecological problems affecting species composition and both recreation and subsistence fishing (Morris and Fan, 1997).

Reservoir sedimentation is a complex process that varies with catchment sediment production, rate of transportation and mode of deposition. Reservoir sedimentation depends on the river regime, flood frequencies, reservoir geometry and operation, flocculation potential, sediment consolidation, density currents and possibly land use changes over the life expectancy of the reservoir. (Julien, 1995)

### 2.3.2. Generalized Deposition Patterns

As a natural stream enters an impounded reach and the flow depth increases, the flow velocity decreases and the sediment load begins to deposit. Sediments carried into a reservoir may deposit throughout its full length, thus raising the bed elevation in time and causing aggradation. The bed load and coarse fraction of the suspended load are deposited immediately to form the delta deposits, while fine sediments with lower settling velocities are transported deeper into the reservoir by either stratified or non-stratified flow (Julien, 1995).

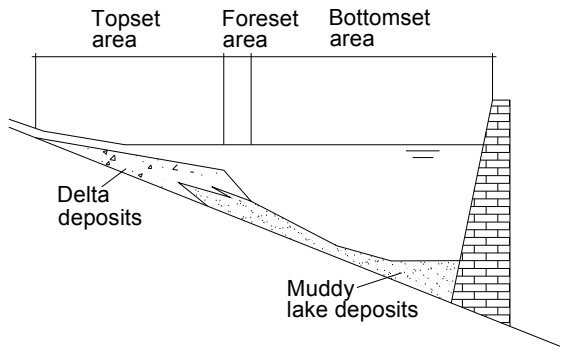


**Figure 2.3 Generalized depositional zones in reservoirs (Morris and Fan, 1997).**

Deltas are generally divided into a *topset area*, a *foreset area* constituting the delta front and a *bottomset area*, beyond the foreset slopes, as depicted in Figure 2.3. The topset deposits contain the coarsest fraction of the sediment load, which is rapidly deposited. The foreset deposits are characterised by an increase in slope and a decrease in grain size, as compared with those of the topset area. The bottomset deposits consist of fine sediment, which are deposited beyond the delta by turbidity currents or non-stratified flow (Morris and Fan, 1997).

### 2.3.3. Specific Weight of Reservoir Deposits

The density of deposited material in terms of dry mass per unit volume is used to convert total sediment inflow to a reservoir from a mass to a volume. Conversely, the volume of surveyed sediments in an existing reservoir must be converted into mass to estimate sediment yield from the catchment (Morris and Fan, 1997). The *unit weight of deposits* (also called *specific weight* or *dry bulk density*) is mainly determined by the initial unit weight, the operational mode of the reservoir and the consolidation rate of the deposits. For the calculation of the initial unit weight of a mixture ($W_o$), an empirical equation was developed by Lara and Pemberton (1963), based on 1,300 sediment samples of reservoir deposits in the United States, as follows:

$$W_o = W_c . P_c + W_{si} . P_{si} + W_{sa} . P_{sa} \qquad (2.3)$$

where $P_c$, $P_{si}$ and $P_{sa}$ are the ratios of clay, silt and sand in the mixture, respectively; and $W_c$, $W_{si}$ and $W_{sa}$ are the initial weights for clay, silt and sand, respectively (see Table 2.2).

Lane and Koelzer (1943) proposed an empirical formula to estimate the bulk density of sediment deposits based on observed data from American reservoirs (Eq. 2.4), taking into account the particle size and the reservoir operation.

$$W = W_o + B.\log(t) \quad (2.4)$$

where $t$ is the time in years; and $B$ is the compaction factor computed as a function of sediment size. The compaction factor $B$ is defined for four reservoir operational conditions, as presented in Table 2.2. A weighted value of the compaction factor $B$ can be computed using the following equation:

$$B = B_c.P_c + B_{si}.P_{si} + B_{sa}.P_{sa} \quad (2.5)$$

where $B_c$, $B_{si}$ and $B_{sa}$ are the compaction factors for clay, silt and sand, respectively.

**Table 2.2 Values of initial weight according to grain size and operation conditions (Lara and Pemberton, 1963).**

| Operation Condition | Initial Weight (kg/m$^3$) | | |
|---|---|---|---|
| | Clay | Silt | Sand |
| Continuously submerged | 416 | 1121 | 1554 |
| Periodic drawdown | 561 | 1137 | 1554 |
| Normally empty reservoir | 641 | 1153 | 1554 |
| Riverbed sediment | 961 | 1169 | 1554 |

**Table 2.3 Values of compaction factor K according to grain size and operation conditions (Lara and Pemberton, 1963).**

| Operation Condition | Compaction factor K (kg/m$^3$) | | |
|---|---|---|---|
| | Clay | Silt | Sand |
| Continuously submerged | 256 | 91 | 0 |
| Periodic drawdown | 135 | 29 | 0 |
| Normally empty reservoir | 0 | 0 | 0 |

Miller (1953) developed an approximate expression for determining the average unit weight ($W_t$) of a deposited mixture in t years, as follows:

$$W_t = W_o + 0.4343.K.\left[\frac{t}{t-1}\ln(t) - 1\right] \quad (2.6)$$

## 2.3.4. Reservoir Releasing and Trap Efficiency

The *sediment release efficiency* in a period of time is a function of the size of the incoming sediment load, the duration of the sediment particles in the reservoir, the characteristics of the reservoir and the ratio of the incoming water discharge to the outgoing water discharge. Sediment release efficiency of a reservoir is then computed as a ratio of the released sediment to the total sediment inflow over a specified time period, whereas *trap efficiency* is the ratio of the sediment retention in a reservoir to the total incoming. Trap efficiency is related to various parameters, such as the ratio of reservoir storage capacity to the average annual runoff; the ratio of retention period to the average flow velocity in the reservoir; and the specific storage of the reservoir, i.e. the ratio of the reservoir storage to the river basin area above the reservoir.

Churchill (1948) presented a method to estimate the trap efficiency of a reservoir, using the sedimentation index of the reservoir ($S_i$), which is defined as the ratio of the retention period ($t_r$) to the mean flow velocity through the reservoir ($v$). The minimum data required to use this method are storage volume, annual inflow and reservoir length. The sedimentation index of the reservoir is computed as follows:

$$S_i = \frac{t_r}{v} \quad (2.7)$$

$$t_r = \frac{C}{I} \quad (2.8)$$

$$v = \frac{I.L}{C} \quad (2.9)$$

where $C$ is the reservoir storage capacity at the mean pool level for the analysis period (m$^3$); $I$ is the average daily inflow rate during study period (m$^3$.s$^{-1}$); and $L$ is the reservoir length at mean operating pool level (m).

Probably, the most widely used method for the calculation of sediment trap efficiency was developed by Brune (1953). Brune determined an empirical relationship for estimating long-term trap efficiency in normally impounded reservoirs based on the correlation between the capacity to inflow ratio

(*C:I*) and trap efficiency ($t_e$) observed in Tennessee Valley Authority reservoirs in the southeastern United States (see Fig. 2.4).

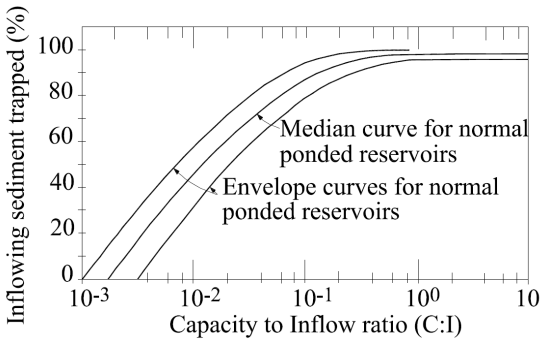


**Figure 2.4 Brune curve for estimating sediment trapping or release efficiency in conventional impounded reservoirs (Morris and Fan, 1997).**

According to Borland (1971), the Churchill method is more applicable for estimating sediment retention in desilting and semi-dry reservoirs. Both methods are based on the ratio of volume to inflow, disregarding features such as the grain size of the inflowing sediment load and the outlet configuration (Morris and Fan, 1997).

An experimental method for the prediction of sediment trapping efficiency was proposed by Einstein in 1965, as reported by Borland (1971). However, no other reference to Einstein's work was found in the literature to confirm whether his work was used or tested with real reservoir data (Campos, 2001).

In 1966, Karaushev proposed a method to predict sediment trapping efficiency, taking into account a sediment property, the fall velocity. None of the other methods mentioned previously consider any sediment characteristics (Campos, 2001).

### 2.3.5. Empirical Methods to Predict Reservoir Sedimentation

Several empirical methods have been developed to predict deposition patterns. The first method to be used is the classical method, which assumes simply that the trapped sediments settle in layers parallel to the horizontal line giving generally very unrealistic results (Campos, 2001).

The U.S. Bureau of Reclamation proposed another method, which uses the assumption that an equal volume of sediment will be deposited within each depth increment in the reservoir (Borland and Miller, 1958), called area-increment method. Nevertheless, the bureau found that the deposition pattern varied from one site to another in a somewhat predictable fashion. Sediment distribution within the impoundment is mainly affected by reservoir geometry, operation and sediment grain size, which led to the development of four different empirical curves based on these characteristics. The empirical area reduction method was described by Borland and Miller (1958) and revised by Lara (1962). Both methods are applied by performing the following steps (Morris and Fan, 1997):

- Determination of the sediment volume to be distributed within the reservoir.
- Selection of the appropriate type curve, according to the reservoir shape, reservoir operation and grain size distribution of the deposited material. The reservoir shape is defined using the parameter m, the inverse of the slope of the straight line of the reservoir depth versus its capacity in a log-log scale paper (see Table 2.4). The reservoir operation can be classified as stable pool (type I), moderate drawdown (type II), considerable drawdown (type III), or normally empty (type IV). Giving equal weight to reservoir shape and reservoir operation, the appropriate type curve can be determined (see Table 2.5). The predominant grain size can be classified as sand and coarser (type I), silt (type II) and clay (type III). The grain size distribution is considered the least important factor influencing sediment distribution. However, it has been used as an auxiliary variable to select the weighted type curve in those cases when there is a choice between two type numbers.
- Computation of the minimum reservoir elevation after sedimentation (also called zero-capacity elevation), using the dimensionless function $F$ at several different pool elevations:

$$F = \frac{S - V_h}{H.A_h} \quad (2.10)$$

where $S$ is the total sediment deposition; $V_h$ is the reservoir volume at each elevation $h$; $H$ is the original maximum depth of the reservoir below normal pool; and $A_h$ is the reservoir area at a given elevation $h$. Values for the relative reservoir depth $p$ are then computed as follows:

$$p = \frac{h - h_{min}}{H} \quad (2.11)$$

where $h_{min}$ is the original bottom elevation. Values of the dimensionless function F and relative depths are then plotted (see Fig. 2.5). The intersection point with the selected type curve gives the zero-capacity elevation $h_o$, defined by:

$$h_o = p_o.H + h_{min} \quad (2.12)$$

where $p_o$ is the relative depth at the new zero-capacity elevation $h_o$, obtained from Figure 2.5.

- Distribution of the trapped sediment within the reservoir according to the selected type curve is represented by the relative sediment area $a$. The relative sediment area $a$ is computed as a function of relative depth, as follows:

Type I: $$a = 5.047.p^{1.85}.(1-p)^{0.36} \quad (2.13)$$

Type II: $$a = 2.487.p^{1.57}.(1-p)^{0.41} \quad (2.14)$$

Type III: $$a = 16.967.p^{1.15}.(1-p)^{2.32} \quad (2.15)$$

Type IV: $$a = 1.486.p^{-0.25}.(1-p)^{1.34} \quad (2.16)$$

The area of sediment deposition at each pool elevation $A_s$ is then given by:

$$A_s = f_{cor}.a \quad (2.17)$$

where $f_{cor}$ is the area correction factor computed as a ratio between the original surface area $A_o$ corresponding to the new zero-capacity elevation and the relative sediment area $a$ at that elevation. The volume of sediment deposition $V_{s,k}$ is then computed for each pool elevation $h_k$, as follows:

$$V_{s,k} = \frac{A_{s,k} + A_{s,k+1}}{2}.(h_{k+1} - h_k) \quad (2.18)$$

where the index k indicates the pool elevation.

**Table 2.4 Classification of the reservoir shape using the parameter m (Morris and Fan, 1997).**

| Reservoir Shape | Type | m |
|---|---|---|
| Lake | I | 3.5 - 4.5 |
| Floodplain-foothill | II | 2.5 - 3.5 |
| Hill and gorge | III | 1.5 - 2.5 |
| Gorge | IV | 1.0 -2.0 |

**Table 2.5 Criteria for the determination of the reservoir type curve, using the reservoir shape, the reservoir operation and grain size distribution of the deposited material (Morris and Fan, 1997).**

| Operational class | Shape class | Weigthed class |
|---|---|---|
| I | I | I |
| | II | I or II |
| | III | II |
| II | I | I or II |
| | II | II |
| | III | II or III |
| III | I | II |
| | II | II or III |
| | III | III |
| IV | IV | IV |

Empirical methods are normally quicker and easier to use than numerical models and require less measured data. Nevertheless, empirical methods are not able to identify the specific locations in a reservoir which will be affected by sedimentation. Furthermore, they are not suitable to simulate changes on the sediment deposition pattern caused by shift of operating regime, such as implementation of sediment management (Morris and Fan, 1997). Therefore, empirical methods will not be considered in this study.

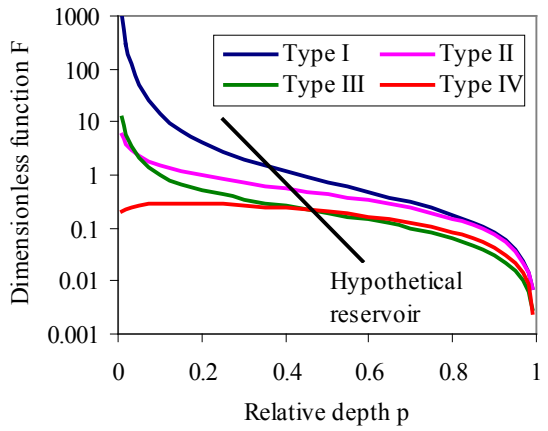


**Figure 2.5 Type curves for determining the new zero-capacity elevation for a hypothetical reservoir (adapted from Morris and Fan, 1997).**

### 2.3.6. Numerical Methods to Predict Reservoir Sedimentation

The use of numerical models has increased very fast in the past few decades, mainly due to the improvement of computing platforms. According to Simoes and Yang (2006), the advances have occurred particularly in the fields of sediment transport, water quality, and multidimensional fluid flow and turbulence. Furthermore, many numerical models are in the public domain and can be obtained free of charge. The implementation of graphical user interfaces, automatic grid generators, geographic information systems and improved data collection techniques promise to further expedite the use of numerical models as a popular tool for solving river engineering problems.

Numerical models can be one-, two-, or three-dimensional. However, one-dimensional models are considered far more applicable because they do not require extensive amounts of computer time and calibration data. Furthermore, the assumption of one-dimensional flow is appropriate for the analyses of many types of sediment problems in rivers and reservoirs that normally have elongated geometry (Morris and Fan, 1997).

**One-Dimensional Models**

Several 1D numerical models have been developed in recent decades for simulation of sediment behaviour in rivers and reservoirs, such as HEC-6 (U.S. Army, 1991), FLUVIAL-12 (Chang, 1998), CONCEPTS (Langendoen, 2000), GSTARS series, EFDC1D, (Hayter et al., 2001), CCHE1D (Wu and Vieira, 2002), etc.

- HEC-6 model is a movable-boundary open-channel flow model that computes sediment scour and deposition by simulating the interaction between the hydraulics of the flow and the rate of sediment transport (U.S. Army, 1991).
- FLUVIAL-12 model (Chang, 1998) is an erodible-boundary model that was formulated and developed for water and sediment routing in natural and man-made channels. It simulates inter-related changes in channel-bed profile, channel width and bed topography induced by the channel curvature.
- CONCEPTS model (Conservation Channel Evolution and Pollutant Transport System) simulates unsteady, one-dimensional flow, graded-sediment transport and bank-erosion processes in stream corridors (Langendoen, 2000).
- GSTARS model (General Stream Tube Model for Alluvial River Simulation) is a steady-, non-uniform-flow model which simulates certain aspects of two-dimensional flow by using the stream tube concept for hydraulics computation (Yang et al., 1989). GSTARS 2.0 (Yang et. al., 1998) significantly revised and expanded the capabilities of GSTARS for PC applications. With a new graphical interface, GSTARS 2.1(Yang and Simoes, 2000) replaced GSTARS 2.0 for cohesive and non-cohesive sediment transport in rivers. GSTARS 3.0 (Yang and Simoes, 2002) further expanded the capabilities of GSTARS 2.1 for cohesive and non-cohesive sediment transport in rivers and reservoirs. Recently, a new version of the GSTARS series was developed, the GSTAR-1D model (General Stream Tube Model for Alluvial River Simulation – One

Dimension), which emphasizes unsteady cohesive sediment transport (Yang et al., 2004).

- EFDC1D model (One-Dimensional Hydrodynamic/Sediment Transport Model for Stream Networks) can simulate bi-directional unsteady flows and has the ability to accommodate unsteady inflows and outflows associated with upstream inflows, lateral inflows and withdrawals, groundwater-surface water interaction, evaporation and direct rainfall. The model also includes representation of hydraulic structures such as dams and culverts. For sediment transport, the model includes settling, deposition and resuspension of multiple size classes of cohesive and noncohesive sediments (Hayter et al., 2001).
- CCHE1D model (One-Dimensional Channel Network Model) is able to calculate unsteady flow in channel networks using either the diffusive wave model or the dynamic wave model, taking into account the difference between the flows in the main channel and flood plains of a compound channel, and the influence of hydraulic structures such as culverts, measuring flumes, bridge crossing and drop structures (Wu and Vieira, 2002). It simulates non-uniform sediment transport in rivers and streams using a non-equilibrium transport model, including bank erosion and channel widening process.

The first 1D method developed exclusively for reservoir sedimentation is possibly the one proposed by Lopes in his PhD thesis in 1978. After Lopes, many 1D numerical models for reservoir sedimentation have been available such as those by White and Bettes (1984), Annandale (1984), Han and He (1990), Siddique (1991), Tang and Chen (1998), Huang (2001), Toniolo and Parker (2003) and González et al. (2006).

**Two-Dimensional Models**

Two-dimensional numerical models for flow and sediment transport are becoming widely used due to the advent of fast personal computers and to the existence of a significant number of commercially available models (Simoes and Yang, 2006). Several 2D numerical models have been found in the literature such as those proposed by Merrill (1974), McAnnally (1989), Evans et al. (1990), Hoggan and Twiss (1993), Sloff (1997), Greco and Molino (1997), Tarela and Menendez (1999), Letter et al. (2000), Choi and Garcia (2002), Shojaeefard et al. (2007).

**Three-Dimensional Models**

As all natural and man-built systems and phenomena are three-dimensional, such processes are better described by three-dimensional numerical models (Wang et al., 1989). Three-dimensional models are usually based on the Reynolds-averaged form of the Navier-Stokes equations, using additional equations of varied degree of complexity for the turbulence closure (Simoes and Yang, 2006).

Although not developed for reservoir sedimentation, the SSIIM model (Olsen, 1991) is a general sediment transport model, which has been applied to reservoirs (Olsen, 1994). The model uses a finite method to compute the Navier-Stokes equations in three dimensions on a general non-orthogonal grid. For the sediment calculations, the model uses the diffusion/advection equation and a bed load transport formula.

A three-dimensional numerical model of suspended sediment transport, taking into account the effects of cohesiveness between sediment, was proposed by Chen et al. (1999). The equations of mass conservation, momentum and suspended sediment transport are solved using an operator splitting scheme. Advection and Coriolis force equations are solved using the Eulerian-Lagrangian method. Horizontal diffusion is approximated by an implicit finite element method for each horizontal layer. Vertical diffusion and pressure gradient are discretized by implicit finite difference method.

Wu et al. (2000b) proposed a three-dimensional model for calculating flow and sediment transport in open channels. The flow is calculated by solving the full Reynolds-averaged Navier-Stokes equations with the k-e

turbulence model. Suspended load transport is simulated through the general convection-diffusion equation with an empirical settling-velocity term. Bed load transport is simulated with a non-equilibrium method and the bed variation is computed using an overall mass-balance equation.

In 2001, De Cesare et al. studied the impacts of turbidity currents on reservoir sedimentation using a three-dimensional numerical model. The governing equations for turbidity currents are the incompressible Navier-Stokes equations with an additional equation for the sediment concentration.

A general three-dimensional sediment transport model was developed by Fang and Wang (2000). The model computes the sediment laden flow in a non-orthogonal curvilinear coordinate system using equations derived from a tensor analysis of two-phase flow. The equations incorporate a natural variable-density turbulence model with non-equilibrium sediment transport.

An early three-dimensional model created purely to be used for reservoir sedimentation is that proposed by Campos (2001). The three-dimensional Advection-Diffusion equation is used to model suspended sediment transport through the reservoir. That equation is discretized and solved using a Cranck-Nicholson scheme. The system of equations resulting from the Cranck-Nicholson scheme is then solved using a line-by-line algorithm. Finally, bed variation and bed material transport are computed using a two-dimensional bed-load continuity equation.

After Campos, several three-dimensional numerical models have been developed to simulate density currents in lakes and reservoirs such as those proposed by Choi and Garcia (2002), Dallimore et al. (2004) and Huang et al. (2005).

## 2.4. Sediment Management Alternatives

### 2.4.1. Introduction

Sediment deposition is generally considered an undesirable but unavoidable consequence of water storage in reservoirs. Dam construction dramatically alters the natural water-sediment equilibrium, creating an impounded river reach characterized by extremely low flow velocities and high trap efficiency. The natural water-sediment equilibrium will eventually be achieved at all sites as a result of either management of natural phenomena or complete siltation of the reservoir. As the impounded reach is completely filled up with sediment, the dam will be overtopped by water and sediments. Therefore, sediment management strategies are extremely necessary to achieve a sustainable use of reservoirs (Palmieri et al., 2001).

### 2.4.2. Sediment Routing

Sediment routing is a sediment control measure that partially preserves the natural sediment-transport characteristics of the river. It focuses on either minimizing deposition or balancing deposition and scour during flood periods. Sediment routing techniques are classified into *sediment pass-through* and *sediment bypass*.

**Sediment Pass-Through**

Sediment pass-through is characterized by either maximizing flow velocity to pass sediment through the impounded reach without deposition (reservoir drawdown) or venting density currents. The main advantage of the drawdown techniques is the significant increase in sediment release and reduction of environmental impact on the downstream river system and other users. Drawdown techniques are employed only during flood events to release inflowing sediment into the impounded reach and may be classified into *seasonal drawdown* and *flood drawdown* (Morris and Fan, 1997).

***Seasonal Drawdown***

Under seasonal drawdown, the reservoir is operated either partially (*partial drawdown*) or completely (*seasonal emptying*) during a predetermined period of the flood season (Morris and Fan, 1997), as illustrated in Figures 2.6 and 2.7. Close to the end of the rainy season, the water inflow must be used to refill the reservoir and to ensure a regulated water supply during the dry

season. In the case of partial drawdown, the reservoir elevation is maintained at a lower pool elevation to increase flow velocity and decrease detention time and sediment trapping. However, the coarse material will continue to be trapped in the impounded reach. When the reservoir is completely emptied, the natural water-sediment equilibrium is achieved and the sediment release efficiency increases significantly. The bottom outlets remain open during the rainy season to enable a natural riverine flow through the reservoir.

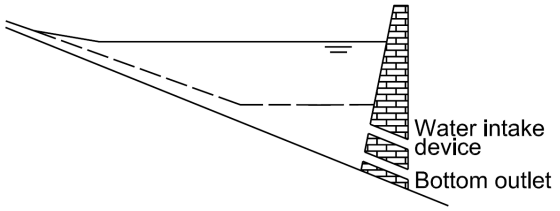


**Figure 2.6 Partial drawdown of a reservoir for sediment management purposes (adapted from Morris and Fan, 1997).**

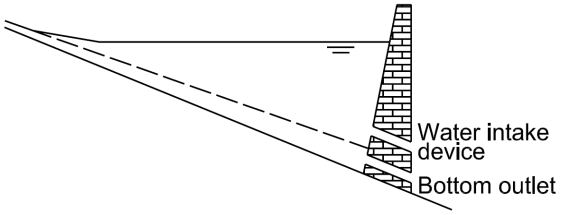


**Figure 2.7 Reservoir emptying for sediment management purposes (adapted from Morris and Fan, 1997).**

### *Flood Drawdown*

The main objective of flood drawdown is to release as much sediment as possible from a reservoir during individual flood events. Flood drawdown can be performed either by *rule curve* or by *hydrograph prediction* (Morris and Fan, 1997). The rule curve technique is only applied for small reservoirs with large gate capacity controlled by a rule curve. It consists of lowering the reservoir level during a flood event to increase flow velocities and to decrease sediment trapping efficiency. Flood drawdown by hydrograph prediction is generally applied to reservoirs with significant storage and limited discharge capacity. The water level is also lowered before arrival of the flood to enable the passage of the sediment-laden flow through the impounded reach during the rising limb of the flood hydrograph and the refill of the reservoir during the hydrograph recession. However, real-time hydrologic data and calibration datasets are vitally important for hydrograph prediction.

### *Venting of turbidity currents*

Turbidity currents are sediment-laden underflows that are driven by density differences caused by suspension of fine sediment. They belong to a larger class of flows known as gravity or density currents. Turbid density currents are important because they can significantly influence the distribution of sediments within a reservoir. As depicted in Figure 2.8, the turbidity density currents can be vented by opening low-level outlets, allowing the removal of sediments without significant drawdown of the pool level (De Cesare et al., 2001). The duration of the turbidity current should be known to increase the venting efficiency. For that, measurement of turbidity currents along the main channel of the reservoir must be performed using sensors such as turbidimeters. Factors affecting the venting of density currents are the incoming flow and sediment conditions, the topography of the reservoir, and outlet facilities such as elevation, location, discharge and capacity.

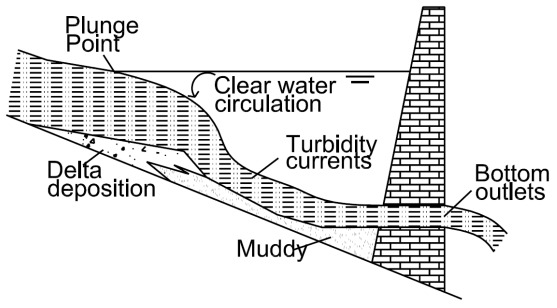


**Figure 2.8 Venting of turbidity currents (adapted from Morris and Fan, 1997).**

**Sediment Bypass**

Sediment bypass is performed either to divert sediment-laden flow around a reservoir (*on-channel storage*) or to divert water of low sediment concentration from the main channel to a reservoir located off it (*off-channel storage*). Sediment bypass around an on-stream impoundment is controlled by flood gates located upstream of the reservoir, which are normally closed, allowing only overflow to the reservoir with significantly less sediment (Fig. 2.9). In off-stream reservoirs, intake structure is used to appropriately select water inflow from the main stream, excluding either partially or completely sediment-laden flow from large floods (Morris and Fan, 1997), as presented in Figure 2.10.

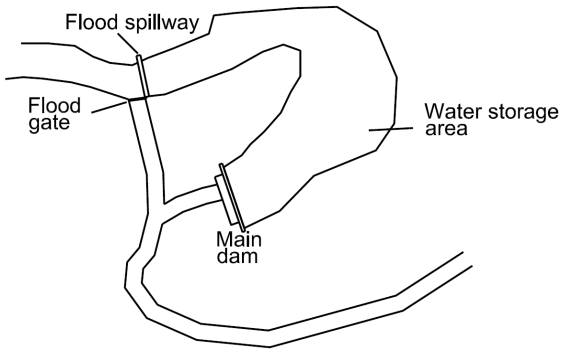


**Figure 2.9 Sediment bypass around an on-stream impoundment (adapted from Morris and Fan, 1997).**

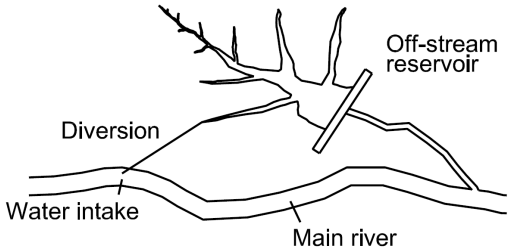


**Figure 2.10 Sediment bypass around an off-stream impoundment (adapted from Morris and Fan, 1997).**

### 2.4.3. Flushing

Although flushing involves reservoir drawdown by opening low-level outlets to temporarily establish riverine flow, it should not be confused with sediment routing (Morris and Fan, 1997). Flushing focuses on the removal of sediment previously deposited in the reservoir, whereas sediment routing aims at minimizing deposition of incoming sediment during flood events. The flushing operation is characterized by a very high sediment release efficiency and, consequently, very high sediment concentration downstream of the dam, causing a strong environmental impact on the downstream river system. Sediment concentrations downstream of the dam during flushing operations differ significantly from sediment inflow due to the large volume of accumulated sediment released during a short period of time by erosion of the main channel along the impounded reach (Timothy and Blair, 2006).

### 2.4.4. Sediment Excavation and Dredging

Sediment deposits may be removed by either *conventional excavation* or *dredging*. The main criteria for selecting a removal method are the grain size and geometry of the deposit, available disposal site and whether the sediment is to be removed under wet or dry conditions (Morris and Fan, 1997). Conventional excavation requires that the reservoir be dewatered, so that sediment excavation and removal can be accomplished in dry conditions. The dewatered sediment is then excavated by conventional land equipment and hauled to an appropriate disposal site. The viability of this approach depends upon the volume of the material, the amount of time required to dry the sediment, the elevation difference between the points of excavation and disposal, and the haul distance to the disposal site. For small sediment volume and non-hazardous sediments, the disposal process can be done economically (Timothy and Blair, 2006).

Sediment removal by dredging can be performed either mechanically (*mechanical dredging*) or hydraulically (*hydraulic dredging*). The advantages of sediment removal by dredging are high efficiency (less water consumption), maintenance of normal operations of the project, execution at any place, wide use of the removed material for farmland (fine sediment) and construction (coarse material), and unlimited recovery of storage capacity. Mechanical dredging consists of using buckets to dig and lift sediment to the surface with minimal water entrainment and without dewatering the site. However, it is still necessary that the excavated material be dewatered prior to truck transport to the disposal facility. In hydraulic dredging, the sediment is removed as a sediment-water slurry of approximately 15 to 20 percent solids, by weight, by mixing sediment and water. It is often the preferred approach to removing large amounts of sediment because of the ability to pump long distances and efficiently handle material from fine sediment through coarse sand. Hydraulic dredging is normally conducted from a barge accessing most shallow areas of the reservoir and also deeper areas as the reservoir is drawn down. With normal impoundment operation, submersible dredges can be used to dredge deep areas of the reservoir. Bulking of fine sediment and limitations of dredging coarse material are disadvantages of the hydraulic dredging (Timothy and Blair, 2006).

## 2.5. Closure

The literature review showed that several empirical and numerical models were developed to evaluate reservoir sedimentation. However, few reservoir sedimentation models enable the simulation of changes to the sediment deposition pattern caused by sediment management. The reservoir sedimentation model proposed in this study accounts for these effects and differs from the others in its ability to assess sediment retention in dense reservoir networks.

# CHAPTER 3

# 3. Modelling Approaches

## 3.1. Model Structure

### 3.1.1. General Aspects

In the context of this study, a deterministic, process-based, one-dimensional sedimentation model has been developed for reservoirs in dryland environments. The reservoir sedimentation model enables the calculation of non-equilibrium transport of non-uniform sediment along the longitudinal profile of a reservoir, referring to the lowermost point of each cross-section. The model computes sediment scour and deposition by simulating the interaction between the hydraulics of the flow and the rate of sediment transport. Additionally, it enables the simulation of sediment management alternatives in order to evaluate their efficiency in reducing sediment accumulation in reservoirs.

The reservoir sedimentation model has been implemented as a module in the WASA model (Model of Water Availability in Semi-Arid environments), which was developed by Güntner (2002). The WASA model is a deterministic, spatially semi-distributed model, which simulates in detail the rainfall-runoff processes for the quantification of water availability and has been extended to model sediment transport processes at the hillslope, river and reservoir scale. The hillslope component was extended to include sediment-transport processes using the MUSLE approach. The river routing module was modified to include a spatially distributed, semi-process-based approach for the transport of water and sediment through the river network. The current version of this hydro-sedimentological model is named WASA-SED.

As the WASA-SED model is used within this study for the estimation of water and sediment yield from catchments, an overview of the model structure and process representation is given in the following.

### 3.1.2. Temporal and Spatial Structure

The temporal resolution of the proposed modelling system (WASA-SED model) is one day. However, a shorter time step (a minimum of one hour) can be employed to simulate certain storm events, depending on the resolution of available input data. This modelling system comprises three conceptual levels: *hillslopes*, *rivers* and *reservoirs*.

**Hillslopes**

At the hillslope scale, a hierarchical top-down disaggregation scheme is applied in order to represent the influence of spatially variable land-surface properties on soil moisture pattern and runoff generation (Güntner and Bronstert, 2004a; Güntner et al., 2004b). The following spatial modelling units may be identified for the characterisation of the hillslope components (Fig. 3.1):

- *Sub-basins* are basic units for water resources management defined according to the location of reservoirs and gauging stations of river discharges.
- *Landscape units* are modelling units with similar characteristics in terms of lateral processes and variability in vertical processes. The delineation of landscape units is based on the Soil and Terrain digital Database - SOTER concept (Oldeman and van Engelen, 1993), which characterises the landscapes according to geological, topographical and soil characteristics.
- *Terrain components* are spatial units obtained from the sub-division of landscape units according to the topography of the terrain in order to describe the structured variability within the landscapes units.

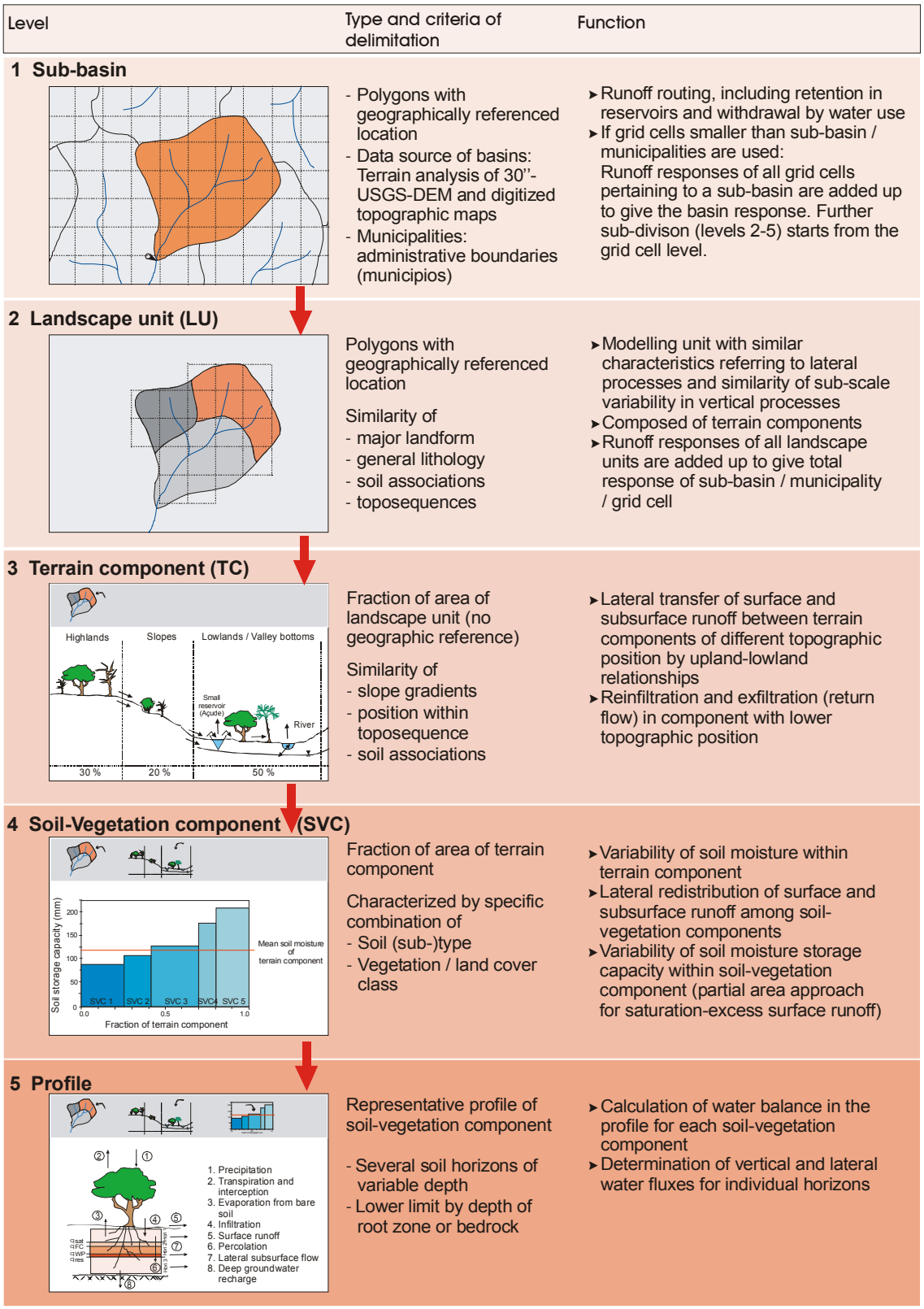


**Figure 3.1 Hierarchical multi-scale disaggregation scheme for structuring river basins into modelling units in WASA-SED (made by Güntner, 2002).**

- *Soil-vegetation components* are modelling units that describe the heterogeneity of soil moisture within terrain components. They are characterized by a specific combination of soil type and land cover.
- *Soil profile* is the smallest spatial scale of the hierarchy, characterized by a predefined number of horizons according to the soil type. The lower boundary of the profile is set either to the depth of bedrock or to the depth of the root zone whenever the depth of bedrock is assumed to be too deep below the surface.

**River network**

The river network is the spatial component that connects hillslope and reservoir processes. Channel reaches are mainly characterised by their gradient and plan geometry, defining streamflow characteristics such as flow velocity, travel time and sediment transport capacity.

**Reservoirs**

For the description of water storage and sediment retention, the reservoirs are classified into *strategic reservoirs* and *small reservoirs*, according to their location and size. Strategic reservoirs are medium and large-sized reservoirs located on main rivers at the sub-basin's outlet. Therefore, the strategic reservoirs may obtain inflow from upstream sub-basin via the river network and generated runoff within the sub-basin where they are located. The small reservoirs are located on tributary streams and are represented in the model in an aggregated manner by grouping them into size classes according to their storage capacity.

## 3.2. Modelling Approach for Hillslopes

### 3.2.1. Introduction

The hillslope module comprises the modelling of the hydrological and sediment-transport processes taking place on the hillslopes. Its output, consisting of water and sediment fluxes, is passed to the river module for further processing. The hydrological modelling accounts for interception, evaporation, infiltration, surface and subsurface runoff, transpiration and ground water recharge. The sediment-transport module for the hillslopes is based on the MUSLE approach (Williams, 1975), which is applied at the level of terrain components to account for spatial variability of hydraulic properties of soil and vegetation.

### 3.2.2. Hydrological Processes

In the following section, the hydrological processes considered in the WASA-SED model are briefly described according to Güntner (2002).

**Interception**

For the representation of interception processes, a simple bucket approach is applied as follows (Güntner, 2002):

$$I_t = I_{t-1} + P_i - E_i \qquad (3.1)$$

with:

$$P_i = \min\left(P,\ \left(I_c - I_{t-1}\right)\right) \qquad (3.2)$$

$$E_i = \min\left(E_{pot}\ ,\ I_t\right) \qquad (3.3)$$

where $I_t$ is the water in the interception storage at time step $t$ (mm); $I_c$ is the capacity of the canopy interception storage (mm); $P$ is the precipitation (mm); $P_i$ is the intercepted precipitation (mm); $E_i$ is the evaporation from the interception storage (mm); and $E_{pot}$ is the potential evaporation (mm).

**Evapotranspiration**

A two-layer evapotranspiration model is applied to account for energy transfer at the soil surface, including soil evaporation. Evaporation from the interception storage and from open water bodies $E$ is calculated using the classical Penman-Monteith approach (Penman, 1948; Monteith, 1965). For the calculation of the total evapotranspiration $E_{pm}$ of land surface, the two-layer approach of Shuttleworth and Wallace (1985) is used.

$$E = \frac{t}{\lambda}\left[\frac{\Delta A + \rho c_p \frac{D}{r_a^a}}{\Delta + \gamma\left(1 + \frac{r_s^c}{r_a^a}\right)}\right] \quad (3.4)$$

where $E$ is the evaporation from the interception storage and from open water bodies (mm per time step); $t$ is the number of seconds in time step (-); $\lambda$ is the latent heat of vaporization of water (J.Kg$^{-1}$); $\Delta$ is the gradient of the saturated vapour pressure curve (hPa.K$^{-1}$); $A$ is the available energy (W.m$^{-2}$); $\rho$ is the density of air (Kg.m$^{-3}$); $c_p$ is the specific heat of moist air (J.kg$^{-1}$.K$^{-1}$); $D$ is the vapour pressure deficit at reference level (hPa); $r_a^a$ is the aerodynamic resistance(s.m$^{-1}$); $r_s^c$ is the canopy resistance (s.m$^{-1}$); and $\gamma$ is the psychometric constant (hPa.K$^{-1}$).

$$E_{pm} = E_p + E_s \quad (3.5)$$

with:

$$E_p = \frac{t}{\lambda}\left[\frac{\Delta(A - A_s) + \rho c_p \frac{D_m}{r_a^c}}{\Delta + \gamma\left(1 + \frac{r_s^c}{r_a^c}\right)}\right] \quad (3.6)$$

$$E_s = \frac{t}{\lambda}\left[\frac{\Delta A_s + \rho c_p \frac{D_m}{r_a^s}}{\Delta + \gamma\left(1 + \frac{r_s^s}{r_a^s}\right)}\right] \quad (3.7)$$

where $E_p$ is the plant transpiration; $E_s$ is the soil evaporation; $A_s$ is the available energy at the soil surface (W.m$^{-2}$); $D_m$ is the vapour pressure deficit inside the canopy (hPa); $r_a^c$ is the bulk boundary layer resistance which controls the transfer between the leaf surfaces and a hypothetical mean canopy airstream at height $z_m$; $r_a^s$ is the aerodynamic resistance which controls the transfer between the soil surface and $z_m$; and $r_s^s$ is the soil surface of the substrate.

**Infiltration**

Infiltration processes are simulated in the hydrological model on the basis of the Green-Ampt approach adapted by Peschke (1977 and 1987) and Schulla (1997). The calculation of infiltration is performed for each soil-vegetation component. The total water input into the soil-vegetation component ($R_f$) is computed as:

$$R_f = P - P_i + R_{s,tc} + R_{s,svc} \quad (3.8)$$

where $P$ is the precipitation (mm.$\Delta$t$^{-1}$); $P_i$ is the intercepted precipitation (mm.$\Delta$t$^{-1}$); $R_{s,tc}$ is the lateral surface inflow from a terrain component of a higher topographic position (mm.$\Delta$t$^{-1}$); and $R_{s,svc}$ is the lateral surface inflow from other soil-vegetation components within the same terrain component (mm.$\Delta$t$^{-1}$). The moment in time $t_{s,i}$, when saturation of the surface of the horizon occurs, is given by:

$$t_{s,i} = \frac{F_{s,i}}{R_f} \quad (3.9)$$

with:

$$F_{s,i} = d_{s,i}.n_{a,i} \quad (3.10)$$

$$d_{s,i} = \frac{\psi_{f,i}}{\frac{R_f}{k_{s,i}/s_f} - 1} \quad (3.11)$$

$$n_{a,i} = n_{t,i} - \theta_i \quad (3.12)$$

where $F_{s,i}$ is the infiltration volume until time $t_{s,i}$ (mm); $d_{s,i}$ is the depth of wetting front below top of the horizon $i$ at time $t_{s,i}$ (mm); $n_{a,i}$ is the refillable porosity of the horizon $i$ (-); $n_{t,i}$ is the total porosity of the horizon $i$ (-); $\theta_i$ is the initial water content of the horizon $i$ (-); $\psi_{f,i}$ is the suction at the wetting front of the horizon $i$ (mm); $k_{s,i}$ is the saturated hydraulic conductivity (mm.$\Delta$t$^{-1}$); and $s_f$ is a scaling factor introduced to balance the underestimation of rainfall intensities by daily rainfall data. The cumulative infiltration amount $F_i$ of the entire

time step is solved iteratively using the following equation, taking into account that the infiltration rate decreases from $t_{s,i}$ until the end of the time step.

$$F_i = F_{s,i}\left(t - t_{s,i}\right) + c.\ln\left(\frac{F_i + c}{F_{s,i} + c}\right) + F_{s,i} \qquad (3.13)$$

with:

$$c = n_{a,i} \cdot \psi_{f,i} \qquad (3.14)$$

For the uppermost horizon, infiltration-excess surface runoff takes place whenever the total water input at the soil surface exceeds the total infiltration of the entire time step. In the case of the deeper horizons, infiltration excess takes place when either $d_{s,i}$ is larger than the total depth of the horizon i or the total water input into that horizon exceeds its total refillable volume. Therefore, $t_{s,i}$ can be computed for lower horizons as follows:

$$t_{s,i} = \frac{d_{h,i} \cdot n_{a,i}}{R_f} \qquad (3.15)$$

**Percolation**

In the WASA model, a temporal delay in percolation is assumed to depend on the travel time through the layer, as proposed by Arnold et al. (1990).

$$Q_{v,i} = \begin{cases} 0 \Leftrightarrow \theta_i \le \theta_{fc,i} \\ \left(\theta_i - \theta_{fc,i}\right)\left(1 - \exp\left(-\frac{1}{t_{d,i}}\right)\right) \Leftrightarrow \theta_i > \theta_{fc,i} \end{cases} \qquad (3.16)$$

with:

$$t_{d,i} = \frac{\theta_i - \theta_{fc,i}}{k_{u,i}} \qquad (3.17)$$

where $Q_{v,i}$ is the percolation from one horizon $i$ to the next horizon below; $\theta_i$ is the actual soil moisture of the horizon $i$ (mm); $\theta_{fc,i}$ is the soil moisture at field capacity in the horizon $i$ (mm); $t_{d,i}$ is the travel time in the horizon $i$ (hours or days); and $k_{u,i}$ the unsaturated hydraulic conductivity (mm.$\Delta t^{-1}$).

**Lateral Subsurface Flow**

The quantification of lateral subsurface flow to terrain components of downslope position or to the river and to adjacent soil-vegetation component of the same terrain component is performed using the Darcy equation.

$$Q_{l,i} = A_q . k_{s,i} . s_{tc} \qquad (3.18)$$

with:

$$A_q = \frac{a_{svc} A_{lu}}{l_{lu}} . d_{s,i} \qquad (3.19)$$

$$d_{s,i} = d_i \cdot \frac{\theta_i - \theta_{fc,i}}{\theta_{sat,i} - \theta_{fc,i}} \qquad (3.20)$$

where $Q_{l,i}$ is the lateral outflow from the horizon $i$ ($m^3.\Delta t^{-1}$); $k_{s,i}$ is the saturated hydraulic conductivity ($m.\Delta t^{-1}$); $A_q$ is the cross-section of the soil-vegetation component ($m^2$); $s_{tc}$ is the slope gradient of the terrain component (-); $a_{svc}$ is the fraction of area of soil-vegetation component in landscape unit (-); $A_{lu}$ is the area of landscape unit ($m^2$); $l_{lu}$ is the slope length of landscape unit (m); $d_{s,i}$ is the saturated depth of the horizon $i$ (m); $d_i$ is the total depth of the horizon $i$ (m); and $\theta_{sat,i}$ is the soil moisture at saturation in the horizon $i$ (mm).

**Deep Groundwater**

Deep groundwater is modelled using conceptual groundwater storage with two outflow components (Güntner, 2002). Percolation to deep groundwater can be lost by evaporation, defined as a constant fraction of percolation, or return to the river network in the form of a simple linear storage approach.

$$Q_{gw} = \frac{V_{gw}}{k_{gw}} \qquad (3.21)$$

where $Q_{gw}$ is the outflow from deep groundwater storage ($m^3.\Delta t^{-1}$); $V_{gw}$ is the actual stored

volume in the groundwater storage ($m^3$); and $k_{gw}$ is a storage constant, which can be derived from recession analysis or by calibration. Only the fraction $f_{gwd}$ of the ground water outflow $Q_{gw}$ is routed directly to the river, while the remaining fraction of $1\text{-}f_{gwd}$ contributes to lateral subsurface inflow into the lowermost terrain component.

### 3.2.3. Sedimentological Processes

Sediment generation on the hillslopes is modelled using the MUSLE approach (Modified Universal Soil Loss Equation) as proposed by Williams (1975).

$$Q_{sed} = 11.8.\left(Q_{surf}.q_p.A_{tc}\right)^{0.56}.K.C.P.LSf_{cf} \quad (3.22)$$

where $Q_{sed}$ is the sediment yield (t); $Q_{surf}$ is the surface runoff volume (m); $q_p$ is the peak runoff rate ($m^3.s^{-1}$); $A_{tc}$ is the area of the terrain component ($m^2$); $K$ is the USLE soil erodibility factor ($0.01.t.acre.hr.acre^{-1}.ft^{-1}.tf^{-1}.in^{-1}$); $C$ is the USLE cover and management factor (-); $P$ is the USLE support practice factor (-); $LS$ is the USLE topographic factor (-); and $f_{cf}$ is the coarse fragment factor (-). The soil erosion routine is applied to each terrain component using the concept of transport capacity. The transport capacity is estimated in the WASA-SED model using either the maximum value that is predicted by MUSLE assuming unrestricted erodibility (K = 0.5), or using the unit-stream-power-based equation of Govers (1990) can be used, as follows:

$$T_{cap} = c\left(\omega - \omega_{cr}\right)^{\eta} \quad (3.23)$$

where $T_{cap}$ is the transport capacity ($m^3.m^{-3}$); $c$ and $\eta$ are particle size-dependent coefficients experimentally derived (-); $\omega$ is the unit stream power ($cm.s^{-1}$); and $\omega_{cr}$ is the critical value of the unit stream power ($cm.s^{-1}$).

## 3.3. Modelling Approach for River Stretches

### 3.3.1. Introduction

The river module of the WASA-SED model is a spatially distributed, semi-process-based modelling approach that enables the simulation of water and sediment fluxes through the river network.

### 3.3.2. Hydrological Processes

The proposed water routing model is based on the kinematic wave approximation after Muskingum (Chow et al., 1988). The Manning's equation is used for the calculation of flow rate, velocity and flow depth of the river stretches. A trapezoidal channel dimension is used to approximate the river cross-sections.

$$Q_{out,2} = c_1.Q_{in,2} + c_2.Q_{in,1} + c_3.Q_{out,1} \quad (3.24)$$

with:

$$c_1 = \frac{\Delta t - 2.K.X}{2K\left(1 - X\right) + \Delta t} \quad (3.25)$$

$$c_2 = \frac{\Delta t + 2.K.X}{2K\left(1 - X\right) + \Delta t} \quad (3.26)$$

$$c_3 = \frac{2K\left(1 - X\right) - \Delta t}{2K\left(1 - X\right) + \Delta t} \quad (3.27)$$

where $Q_{in,1}$ is the inflow rate at the beginning of the time step ($m^3.s^{-1}$); $Q_{in,2}$ is the inflow rate at the end of the time step ($m^3.s^{-1}$); $Q_{out,1}$ is the outflow rate at the beginning of the time step ($m^3.s^{-1}$); $Q_{out,2}$ is the outflow rate at the end of the time step ($m^3.s^{-1}$); $\Delta t$ is the time increment (h); $K$ is the storage time constant for each segment (-); and $X$ is a weighting factor having the range $0 \leq X < 0.5$.

### 3.3.3. Sedimentological Processes

**Suspended Load Transport**

Suspended load transport is modelled using the transport capacity concept, computed as a function of the peak flow velocity. For each time step the final amount of sediment for each river stretch is calculated as follows:

$$Q_{sed,2} = Q_{sed,1} - Q_{dep} + Q_{deg} \quad (3.28)$$

where $Q_{sed,1}$ is the amount of suspended sediment in the reach at the beginning of the time step (t); $Q_{sed,2}$ is the amount of suspended sediment in the reach at the end of the time step (t); $Q_{dep}$ is the amount of sediment deposited in the reach segment (t); and $Q_{deg}$ is the amount of sediment re-entrained in the reach segment (t).

**Bed Load Transport**

Bed load transport can be computed in the river module of the WASA-SED model using five different bed load transport formulas: Meyer-Peter & Müller (1948); Schoklitsch (1950); Smart & Jaeggi (1983); Bagnold (1956); and Rickenmann (1991, 2001).

## 3.4. Detailed Modelling Approach for Reservoirs

### 3.4.1. Introduction

As reservoir sedimentation plays an important role in the sediment transport processes at the catchment scale, a new modelling approach has been specifically developed for the assessment of sediment retention in reservoirs (Mamede et al., 2006). The modelling approach enables the calculation of reservoir life expectancy, the trapping efficiency of the reservoir, the amount of released sediments downstream of the reservoir and the simulation of several reservoir sediment management scenarios.

For the simulation of sediment transport in reservoirs, four aspects are considered: water balance of the reservoir, hydraulic transfer through the reservoir, sediment transport in the reservoir and reservoir bed elevation changes. The water balance is computed based on the continuity equation, considering all inflows, outflows and changes in storage of the reservoir. For the calculation of the hydraulic properties, two spatial components are identified: the *river sub-reach component* and the *reservoir sub-reach component*. Hydraulic calculations in the river sub-reach are based on the standard step method for a gradually varied flow (Graf & Altinakar, 1998), whereas a modelling approach adapted from the GSTARS model is used for the reservoir sub-reach (Yang and Simoes, 2002). The sediment transport within the reservoir is computed using a one-dimensional equation of non-equilibrium transport of non-uniform sediment, adapted from Han and He (1990). For the calculation of reservoir bed elevation changes, the sediment balance is performed for each cross-section, considering three conceptual layers above the original bed material.

### 3.4.2. Reservoir Water Balance

The water-balance module of the reservoir sedimentation model accounts for the interactions between water fluxes going into and out of the reservoir for daily or hourly simulation intervals. In general, the reservoir water mass balance can be written as shown in the following equation assuming that the fluid specific density is constant:

$$\Delta V = Q_{in} + Q_{prec} + Q_{gr} - (Q_{evap} + Q_{inf} + Q_{over} + Q_{ws} + Q_{sm}) \quad (3.29)$$

where $Q_{in}$ is the direct runoff from the tributary rivers; $Q_{prec}$ is the direct rainfall on the reservoir water surface; $Q_{gr}$ is the groundwater inflow; $Q_{evap}$ is the direct evaporation from the water surface of the reservoir; $Q_{inf}$ is the groundwater outflow by infiltration; $Q_{over}$ is the overflow discharges through the spillway; $Q_{ws}$ is the outflow discharge for water supply; and $Q_{sm}$ is the outflow discharge for sediment management. Groundwater inflow and outflow are assumed negligible relative to other inflow and outflow components. For the Brazilian semi-arid region, this assumption has been generally accepted since early studies from DNOCS and SUDENE/ORSTON. Nonetheless, recent studies have shown that this assumption is not always acceptable (see Costa, 2007; and Pereira, 2006). The reservoir water balance is then computed for each time step as follows:

- Determination of overflow discharges in the case that the storage capacity of the

reservoir is exceeded by the actual storage volume after inflows provided by the river module of the WASA model.

- Assessment of storage volume reduction in the reservoir by evaporation. Evaporation values are calculated in the climate module of the WASA model as described in Güntner (2002).
- Computation of the increased storage volume through rainfall directly on the reservoir. If storage capacity of the reservoir is exceeded by the actual storage volume after precipitation, overflow discharge is updated.
- Calculation of water volume withdrawn from the reservoir for water supply. The outflow discharge is a fraction of the target reservoir yield ($Q_{90}$), which is defined as a mean annual discharge that can be withdrawn in 90% of all years (reliability level of 90%). The target reservoir yield is based on simple hydrological modelling for dryland environments (Güntner et al., 2004b).
- Computation of water volume withdrawn from the reservoir for sediment management purposes. It depends on the selected sediment management alternative.
- Calculation of reservoir volume at the end of the time step. Reservoir level and surface area are computed using the stage-area-volume curves of the reservoir.

### 3.4.3. Hydraulic Calculations

The determination of hydraulic properties is a pre-requisite for sediment transport modelling in general. As presented in Figure 3.2, the reservoir is divided into the river sub-reach component and the reservoir sub-reach component, considering the variation of the reservoir level. The length of the river sub-reach becomes longer for lower reservoir levels, whereas the length of the reservoir sub-reach decreases.

The limits between the two spatial components are obtained from the comparison of the normal depth of each cross-section, not taking into account the existence of the reservoir and the depth related to water stage of the reservoir at the same cross-section. The normal depth is the maximum water depth for a uniform flow, computed by the Manning formula. If the value of normal depth is greater than the depth of the reservoir at the same cross-section, it belongs to the river sub-reach.

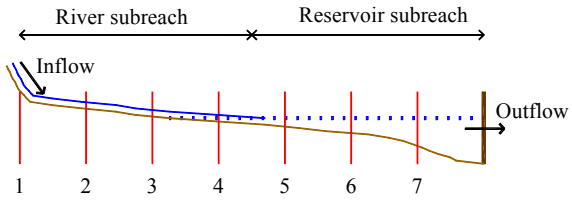


**Figure 3.2 Longitudinal profile of the reservoir (division into river and reservoir sub-reaches).**

**Reservoir Routing**

The reservoir routing is performed using a modelling approach as proposed by Yang and Simoes (2002) in the GSTARS model, with some modifications. The water discharge is computed for each cross-section from upstream towards downstream using a weighting factor, which represents the influence of input discharges and output discharges on that cross-section. In the proposed reservoir sedimentation model, the weighting factor is the volume represented by the respective cross-section, as shown in Figure 3.3, whereas in the GSTARS model, the weighting factor is calculated from the reservoir's surface area represented by each cross-section. The water discharge of each cross-section is calculated as follows:

$$Q_j = Q_{in} - (Q_{in} - Q_{out}) \cdot \sum_{k=m}^{j} v_k \qquad (3.30)$$

where $Q_j$ is the water discharge at the cross-section $j$; $v_k$ is the fraction of reservoir volume represented by that cross-section ($v_k = V_k/V_{res}$); $V_k$ is the volume represented by cross-section $k$ ($m^3$); $V_{res}$ is the reservoir volume ($m^3$); $m$ is the index for the first cross-section belonging to the reservoir sub-reach; $Q_{in}$ is the inflow discharge into the reservoir ($m^3.s^{-1}$); and $Q_{out}$ is the reservoir outflow discharge ($m^3.s^{-1}$). From the definition of $v_k$, one has:

$$\sum_{k=m}^{r} v_k = 1 \qquad (3.31)$$

where $r$ is the index for the most downstream cross-section, located close to the dam. The water discharge at the cross-section $r$ is equal to the reservoir outflow discharge ($Q_r = Q_{out}$).

The reservoir water level is assumed to be horizontal for the computation of the geometric elements of each cross-section. The average flow velocity of the cross-section $j$ ($V_j$) is then computed using the following equation:

$$Q_j = V_j A_j \qquad (3.32)$$

where $A_j$ is the wetted surface at the cross-section $j$ ($m^2$).

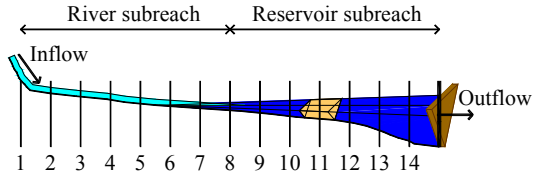


**Figure 3.3 Fraction of the reservoir volume represented by the cross-section 11.**

**River Routing**

The standard step method for a gradually varied flow (Graf & Altinakar, 1998) is applied for the calculation of the hydraulic properties at the river sub-reach. This method is able to compute the water-surface profile for subcritical or supercritical flow regimes. However, a constant for integration must be supplied. For subcritical flow regimes, the cross-section of control is the first section at the reservoir sub-reach, which has known physical properties. In the case of supercritical flow regime, the water surface profile is computed from known upstream boundary conditions. No mixed flow is computed. Calculations must begin at the control section and proceed in the direction in which the control operates, i.e. upstream for subcritical flow and downstream for supercritical flow.

For gradually varied flows, the profile of water surface can be computed using the equation of energy:

$$\frac{V^2}{2g} + h + z = H \qquad (3.33)$$

where $h$ is the water depth (m); z is the elevation of the bed (m); $H$ is the elevation of the energy-grade line (m); $V$ is the average flow velocity ($m.s^{-1}$); and $g$ is the gravitational acceleration ($m^2.s^{-1}$). Differentiating the equation of energy with respect to the position $x$, one may write:

$$\frac{d}{dx}\frac{(Q/A)^2}{2g} + \frac{dh}{dx} - S_f = -S_e \qquad (3.34)$$

where $S_f$ is the slope of the bed given by $dz/dx$ (-); $S_e$ is the slope of energy-grade line given by $dH/dx$ (-); and $Q/A$ is the average flow velocity obtained from equation of continuity ($Q=V.A$).

The dynamic Equation 3.34 is rewritten below for the calculation of the water surface profile at the river sub-reach between the running section $i$ and the preceding section $i$-$1$ as follows (Graf & Altinakar, 1998):

$$H_i - H_{i-1} = S_f . L_i + K_{ss}\frac{Q^2}{2g}\left|\frac{1}{A_i^2} - \frac{1}{A_{i-1}^2}\right| \qquad (3.35)$$

where; $L_i$ is the distance between the running section $i$ and the preceding section $i$-$1$; $Q$ is the water discharge at the river sub-reach, assumed to be constant at gradually varied flows; $A_i$ and $A_{i-1}$ are the wetted areas of the running section $i$ and the preceding section $i$-$1$, respectively; $S_f$ is the representative friction slope between two sections; and $K_{ss}$ is for a singularity as caused by a change between two consecutive sections or other possible irregularities. For subcritical flow regime, the head-loss coefficient $K_{ss}$ is internally set to 0.1 for contractions and to 0.3 for expansions. Typical values for gradual transitions in supercritical flow are around 0.05

for the contraction coefficient and 0.1 for the expansion coefficient (Brunner, 2002).

Three different equations are available for the calculation of the friction slope $S_f$: average friction slope equation (Eq. 3.36); geometric mean friction slope equation (Eq. 3.37); and average conveyance equation (Eq. 3.38).

$$S_f = \frac{S'_{f,i} + S'_{f,i-1}}{2} \quad (3.36)$$

$$S_f = \sqrt{S'_{f,i} . S'_{f,i-1}} \quad (3.37)$$

$$S_f = \left( \frac{2Q}{K_i + K_{i-1}} \right)^2 \quad (3.38)$$

where $K_i$ and $K_{i-1}$ are values of conveyance at the running section $i$ and the preceding section $i$-$1$, respectively; and $S'_{f,i}$ and $S'_{f,i-1}$ are the average slopes of the energy-grade line with respect to the horizontal at the running section $i$ and at the preceding section $i$-$1$, respectively. The average slope can be computed by:

$$S'_{f,i} = \frac{V_i^2 . n_i^2}{R_{h,i}^{4/3}} \quad (3.39)$$

where $n$ is the Manning's friction coefficient for the running section; $R_h$ is the hydraulic radius of the running section.

**Table 3.1 Criteria utilized to select friction equation at mild slopes (M) and steep slopes(S).**

| Profile Type | Conditions | Flow Regime | Equation |
|---|---|---|---|
| M1 | $h > h_n > h_c$ | subcritical | 3.38 |
| M2 | $h_n > h > h_c$ | subcritical | 3.37 |
| M3 | $h_n > h_c > h$ | supercritical | 3.36 |
| S1 | $h > h_c > h_n$ | subcritical | 3.37 |
| S2 | $h_c > h > h_n$ | supercritical | 3.38 |
| S3 | $h_c > h_n > h$ | supercritical | 3.36 |

The selection of the appropriate equation for the calculation of the friction slope $S_f$ is performed automatically in the reservoir sedimentation model, according to the forms of water surface encountered in gradually varied flow, as presented in Table 3.1. The parameters $h$, $h_n$ and $h_c$ are the water depth, the normal water depth and the critical water depth, respectively.

### 3.4.4. Reservoir Sediment Transport

Many of the computational methods applied in engineering practice are based on simplifying assumptions such as equilibrium sediment-transport approach using the concept of sediment carrying capacity. However, the sediment carrying capacity and the actual sediment concentration may differ a lot, particularly for the case of reservoir sedimentation and scouring process of river channel below impounding reservoirs. Han and He (1990) proposed the following equation for non-equilibrium sediment transport:

$$\frac{dS}{dx} = \frac{\alpha\omega}{q}(S^* - S) \quad (3.40)$$

where $S$ is the sediment concentration; $S^*$ is the sediment carrying capacity; $q$ is the discharge per unit width; $\omega$ is the settling velocity; and $\alpha$ is the coefficient of saturation recovery. According to Han and He (1990), the parameter $\alpha$ can be taken as 0.25 for reservoir sedimentation and 1.0 for scouring during flushing of the reservoir and in the river channel with fine bed material. Integrating Equation 3.40, it can be expressed as:

$$S_j = S_j^* + (S_{j-1} - S_j^*).e^{-\left(\frac{\alpha.\omega.L}{q}\right)} \quad (3.41)$$

where L is the reach length. Equation 3.41 is applied to each of the particle size fractions in the non-cohesive range.

Four different sediment transport equations selected from the literature are available in

the reservoir sedimentation model for the calculation of the sediment carrying capacity S*, as presented in Table 3.2. They were selected based on the fact that all four equations enable the calculation of both bed load transport and suspended load transport. The application of different sediment transport equations to the same dataset may generate estimates of transport rates ranging over more than two orders of magnitude (Schulits and Hill, 1968; White et al., 1975; Yang, 1976; Yang, 1979; Alonso, 1980; Brownlie, 1981; Yang and Molinas, 1982; ASCE, 1982; Yang, 1984; Vetter, 1989; Yang and Wan, 1991; Yang and Huang, 2001; Scheer et al, 2002). Therefore, the following measures can be taken to find the most appropriate sediment transport function (Morris and Fan, 1997):

- Comparison of measured long-term bed load and suspended load data and computed data using different sediment transport equations.
- Simulation of historical depositional and scour processes in existing reservoirs with appreciable sediment accumulation or a suitable calibration event using different sediment transport equations.
- Comparison of conditions in the study area against the dataset used in the development of each sediment transport equation.
- Evaluation of applicability indexes to each sediment transport equation. Williams and Julien (1989) proposed an applicability index based on the relative roughness, Shield parameter and dimensionless grain size.
- Measurements at other sites and engineering judgment in the case of new reservoirs without historical depositional pattern and in those places, where field data on transport rates are not available.

**Table 3.2 Sediment-transport formulae for the calculation of sediment transport through the reservoir and their limits of applicability within the reservoir sedimentation model, referring to sediment particle sizes.**

| Formulas | Limits (mm) |
|---|---|
| Wu et al. (2000a) | 0.004 to 100 |
| Ashida and Michiue (1973) | 0.040 to 100 |
| Tsinghua University (1985, IRTCES) | 0.001 to 100 |
| Ackers and White (1973) | 0.040 to 100 |

**Wu et al. (2000a)**

Wu et al. (2000a) developed a fractional formula for bed load transport and a fractional formula for suspended load. These formulas have been calibrated and tested for a wide range of laboratory and field data. A particular feature of the sediment transport equation proposed by Wu et al. (2000a) is its ability to simulate hiding and exposure effects of non-uniform sediment transport. The transport rate of the *k-th* fraction of bed load per unit width ($q_{b,q}$) can be calculated as follows:

$$q_{b,k} = P_k . \phi_{b,k} \sqrt{\Delta . g . d_k^{\,3}} \qquad (3.42)$$

where $P_k$ is the ratio of material of size fraction $k$ available in the bed; $\Delta$ is the relative density ($\gamma_s/\gamma-1$); $\gamma$ and $\gamma_s$ are the specific weights of fluid and sediment, respectively; $g$ is the gravitational acceleration; $d_k$ is the diameter of the particles in size class $k$; and $\phi_{b,k}$ is the dimensionless transport parameter for fractional bed load yields. The parameter $\phi_{b,k}$ can be computed as follows:

$$\phi_{b,k} = 0.0053 . \left[ \left( \frac{n'}{n} \right)^{3/2} \frac{\tau_b}{\tau_{c,k}} \right]^{2.2} \qquad (3.43)$$

where $\tau_{c,k}$ is the critical shear stress; $\tau_b$ is bed shear stress; $n$ is the Manning's roughness; and $n'$ is the Manning's roughness related to grains. The parameters n and n' can be obtained from:

$$n = \frac{R_h^{\,2/3} . S_f^{\,1/2}}{V} \qquad (3.44)$$

$$n' = \frac{\sqrt[6]{d_{50}}}{20} \qquad (3.45)$$

where $R_h$ is the hydraulic radius; $S_f$ is the energy slope; $V$ is the average flow velocity; and $d_{50}$ is the median diameter computed as the maximum size for the smallest 50% of the sample.

The critical shear stress $\tau_{c,k}$ can be calculated with:

$$\tau_{c,k} = (\gamma_s - \gamma).d_k.\theta_c.\xi_k \quad (3.46)$$

where $\theta_c$ is the critical Shields parameter, assumed to be 0.03; and $\xi_k$ is the hiding and exposure factor, which is defined as:

$$\xi_k = \left(\frac{P_{e,k}}{P_{h,k}}\right)^{\chi} \quad (3.47)$$

where $\chi$ is a empirical parameter determined using laboratory and field data ($\chi$ = -0.6); $P_{e,k}$ and $P_{h,k}$ are the total exposed and hidden probabilities of the particles in size class $k$, respectively. They can be expressed as:

$$P_{e,k} = \sum_{j=1}^{q} P_{b,j}\frac{d_k}{d_k + d_j} \quad (3.48)$$

$$P_{h,k} = \sum_{j=1}^{q} P_{b,j}\frac{d_j}{d_k + d_j} \quad (3.49)$$

where $P_{b,j}$ is the probability of particles in size class $j$ staying in the front of particles in size class $k$ and it is assumed to be the ratio of particles $d_j$ in the bed material.

The average bed shear stress can be calculated with:

$$\tau_b = \gamma.R_h.S_f \quad (3.50)$$

Wu et al. (2000a) also proposed a suspended load transport rate related to the rate of energy available to the channel. The fractional transport rate of non-uniform suspended load can be written as:

$$q_{s,k} = P_k.\phi_{s,k}\sqrt{\Delta.g.d_k^{\,3}} \quad (3.51)$$

where $\phi_{s,k}$ is the dimensionless transport parameter for fractional suspended load yields. The parameter $\phi_{s,k}$ is calculated as follow:

$$\phi_{s,k} = 0.0000262.\left[\left(\frac{\tau}{\tau_{c,k}} - 1\right)\frac{V}{\omega_k}\right]^{1.74} \quad (3.52)$$

where $\tau$ is the shear stress on the entire cross-section; and $\omega$ is the settling velocity computed with the Zhang's formula (Eq. 2.1).

The fractional sediment transport capacity for total sediment load ($Q_{t,k}$) can be calculated as the sum of the bed load transport rate and the suspended load transport rate.

$$Q_{t,k} = (q_{b,k} + q_{s,k}).B \quad (3.53)$$

where $B$ is the top width of the section.

**Ashida and Michiue (1973)**

Ashida and Michiue (1973) proposed a fractional bed load transport equation, as written below:

$$q_{b,k} = 17.P_k.u_{e,k}.d_k.\tau_{e,k}\left(1 - \frac{\tau_{c,k}}{\tau_k}\right)\left(1 - \sqrt{\frac{\tau_{c,k}}{\tau_k}}\right) \quad (3.54)$$

where $P_k$ is the ratio of material of size fraction $k$; $d_k$ is the diameter of the particles in size class $k$; $u_{e,k}$ is the effective shear velocity (m.s$^{-1}$); $\tau_k$ is the shear stress of the particles in size class $k$; $\tau_{e,k}$ is the effective shear stress; and $\tau_{c,k}$ is the critical shear stress. The parameters $\tau_k$, $\tau_{e,k}$ and $\tau_{c,k}$ are calculated as follows:

$$\tau_k = \frac{u_*^2}{\Delta.g.d_k} \quad (3.55)$$

$$\tau_{e,k} = \frac{u_{e,k}^{\,2}}{\Delta.g.d_k} \quad (3.56)$$

$$\tau_{c,k} = \frac{u_{c,k}^{2}}{\Delta . g . d_k} \quad (3.57)$$

where $\Delta$ is the relative density ($\gamma_s/\gamma - 1$); $\gamma$ and $\gamma_s$ are the specific weights of fluid and sediment, respectively; $g$ is the gravitational acceleration; $u^*$ is the shear velocity; and $u_{c,k}$ is the critical shear velocity. The parameters $u^*$, $u_{e,k}$ and $u_{c,k}$ are computed from:

$$u^* = \sqrt{g . R_h . S_f} \quad (3.58)$$

$$u_{e,k} = \frac{V}{5.75 \log\left(\frac{R_h / d_{50}}{1 + 2\tau_k}\right)} \quad (3.59)$$

$$u_{c,k} = \begin{cases} \sqrt{0.85} . u_{c,50} \Leftrightarrow \frac{d_k}{d_{50}} < 0.4 \\ \frac{\log 19}{\log\left(\frac{19 d_k}{d_{50}}\right)} . u_{c,50} \Leftrightarrow \frac{d_k}{d_{50}} \geq 0.4 \end{cases} \quad (3.60)$$

where $R_h$ is the hydraulic radius; $S_f$ is the energy slope; $V$ is the average flow velocity; $d_{50}$ is the median diameter computed as the maximum size for the smallest 50% of the sample; and $u_{c,50}$ is the dimensionless critical shear velocity for the $d_{50}$, which is calculated as:

$$u_{c,50} = \Delta . g . d_{50} . \tau_{c,50} \quad (3.61)$$

where $\tau_{c,50}$ is the critical shear stress for the $d_{50}$, assumed to be 0.05.

The suspended load transport is adapted from the method of Ashida & Michiue (1970), as proposed by Yang and Simoes (2002) in the GSTARS Model.

$$q_{s,k} = C^* V (e^{-p.a} - e^{-p.h}) . \frac{e^{p.a}}{p} \quad (3.62)$$

where $C^*$ is the concentration at a reference level $a$ ($a = 0.05h$); $h$ is the water depth; and $p$ is an empirical parameter computed as:

$$p = \frac{6 . \omega_k}{\kappa . u^* . h} \quad (3.63)$$

where $\kappa$ is the von Kàrmàn constant, taken as equal to 0.412.

The concentration at the reference level can be calculated as follows:

$$C^* = 0.025 . p_k . \left[\frac{f(\varepsilon_o)}{\varepsilon_o} - F(\varepsilon_o)\right] \quad (3.64)$$

in which:

$$f(\varepsilon_o) = \frac{1}{\sqrt{2\pi}} e^{\left(-0.5 . \varepsilon_o^2\right)} \quad (3.65)$$

$$F(\varepsilon_o) = \frac{1}{\sqrt{2\pi}} \int_{\varepsilon_o}^{\infty} e^{\left(-0.5 . \varepsilon^2\right)} d\varepsilon \quad (3.66)$$

where $\varepsilon_o$ is a empirical parameter computed as:

$$\varepsilon_o = \frac{\omega_k}{0.75 . u^*} \quad (3.67)$$

The fractional sediment transport capacity for total sediment load is calculated as in Equation 3.53.

**Tsinghua University**

The empirical Tsinghua University Method (IRTCES, 1985) was developed to calculate the transport capacity of flushing flows in reservoirs. No distinction was made between bed load and suspended load. The method is based on observations of flushing in reservoirs in China, where the predominant practice is annual flushing and so relatively little consolidation occurs between flushing operations. Extrapolation to other reservoirs and conditions should be done with caution.

$$Q_s = \Omega \frac{Q^{1.6} S^{1.2}}{B^{0.6}} \quad (3.68)$$

where $Q_s$ is the sediment transport capacity at the current section ($t.s^{-1}$); $Q$ is the water discharge ($m^3.s^{-1}$); $S$ is the bed slope; $B$ is the channel width; and $\Omega$ is a constant set from the sediment type. Recommended values of the parameter $\Omega$ are as follows: 1600 for loess sediments; 650 for other sediments with median size finer than 0.1 mm; 300 for sediments with median size larger than 0.1 mm; and 180 for flushing with a low discharge.

**Ackers and White (1973)**

Ackers and White (1973) proposed a formula to estimate the total load transport, under the assumption that fine sediment transport is best related to the turbulent fluctuations in the water column and coarse sediment transport is best related to the net grain shear with the mean velocity used as the representative variable. This empirical formula is based on 925 sets of data from flume experiments with a grain size ranging from 0.04 to 4 mm. The general transport equation for the Ackers & White function for a single grain size class $k$ is represented by:

$$q_{t,k} = P_k.\psi.V.d_k.\left(\frac{V}{u*}\right)^{n_o}.\left(\frac{F_{gr}}{F_{gr,cr}.\xi_k}-1\right)^{m_o} \quad (3.69)$$

where $P_k$ is the ratio of material of size fraction $k$; $d_k$ is the diameter of the particles in size class $k$; $V$ is the average flow velocity; $u*$ is the shear velocity computed as in Equation 3.58; $\xi_k$ is the hiding and exposure factor, computed as in Equation 3.47; $F_{gr}$ is the sediment mobility number; and $n_o$, $m_o$, $\psi$ and $F_{gr,cr}$ are dimensionless coefficients. These coefficients depend on the dimensionless particle size $d*$, calculated as follows:

$$d*_k = d_k\left\{\frac{\Delta.g}{\nu^2}\right\}^{1/3} \quad (3.70)$$

where $\Delta$ is the relative density ($\gamma_s/\gamma-1$); $\gamma$ and $\gamma_s$ are the specific weights of fluid and sediment, respectively; and $\nu$ is the kinematic viscosity computed as in Equation 2.2.

Ackers & White (1973) make a distinction between particles with $1 < d* < 60$ and particles with $d* \geq 60$. Later revisions were made for the $\psi$ and $m_o$ coefficients (Wallingford, 1990), because there were uncertainties in the original formula in the sediment transport for relatively fine and coarse sediments. Nevertheless, Scheer (2000) showed that the results of the Ackers & White-formula with the modified parameters are slightly worse than the predictions of the original formula. Therefore, the original formula was included in the reservoir sedimentation model. The parameters of that formula can be found in Table 3.3.

The fractional sediment transport capacity for total sediment load can be computed as:

$$Q_{t,k} = q_{t,k}.B \quad (3.71)$$

where B is the top width of the section.

**Table 3.3 Coefficients of the formula proposed by Ackers and White (1973).**

| Coefficients | $1 < d* < 60$ | $d* \geq 60$ |
|---|---|---|
| $n_o$ | $1 - 0.56.\log(d*)$ | 0 |
| $m_o$ | $\frac{9.66}{d*} + 1.34$ | 1.5 |
| $\psi$ | $10^{-3.53+2.86.\log(d*)-\log^2(d*)}$ | 0.025 |
| $F_{gr,cr}$ | $\frac{0.23}{\sqrt{d*}} + 0.14$ | 0.17 |

## 3.4.5. Reservoir Bed Elevation Changes

The bed elevation changes are computed for each cross-section taking into account three conceptual layers above the original bed material as illustrated schematically in Figure 3.4. The *lowest layer* is used for storage. There, the sediment is compacted and protected against erosion. In the *intermediate layer*, the sediment can be deposited or resuspended. In the *top layer*, sediment-laden flow occurs. The time-

dependent mobile bed variation is calculated using the sediment balance equation proposed by Han (1980) as follows:

$$\frac{\partial(Q.S)}{\partial x}+\frac{\partial M}{\partial t}+\frac{\partial(\rho_d.A_d)}{\partial t}=0 \qquad (3.72)$$

where $Q$ is the water discharge; $S$ is the sediment concentration; $M$ is the sediment mass in water column with unit length in longitudinal direction; $A_d$ is the total area of deposition; and $\rho_d$ is density of deposited material. If the time span for deposition in a reservoir is not too large, the consolidation of deposits can be neglected and the initial density of deposits may be used. The mass of deposits $W$ can be computed for each grain size $k$ and each cross-section $j$ from

$$W_{j,k}=Q_{j-1}.P_{j-1,k}.S_{j-1,k}-Q_j.P_{j,k}.S_{j,k} \qquad (3.73)$$

where $P_{j,k}$ and $P_{j-1,k}$ are the ratios of material of size fraction $k$ at the running section $j$ and preceding section $j-1$, respectively.

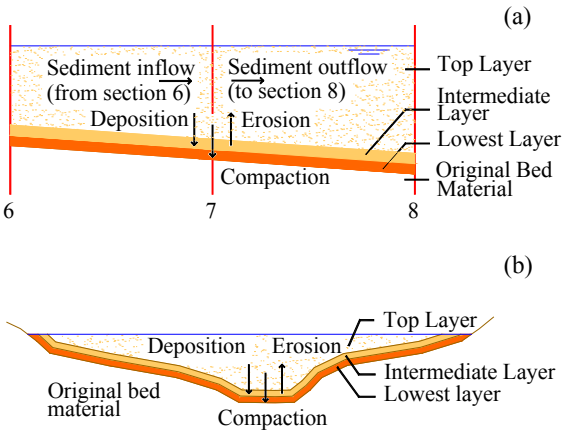


**Figure 3.4 Schematic description of sediment balance at the cross-section considering three conceptual layers: longitudinal view (a) and cross-section (b).**

Values for incoming sediment in the reach as represented by the first cross-section of the reservoir are provided by the river module of the WASA model, described previously in Section 3.3. When the sediment transport capacity at the current cross-section exceeds the incoming load into the reach, the bed material can be eroded, constrained by its availability at the bed. Deposition takes place whenever the sediment transport capacity is exceeded by sediment inflow. In the calculation of the sediment transport capacity for each grain size, one of the four available sediment transport equations is used, assuming that the entire bed is composed of that size fraction alone. According to Yang and Simoes (2002), the fractional sediment transport capacity can be written for each grain size as:

$$S^*_{j,k}=\sum_{k=1}^{N}[c.P_{j,k}-(1-c).P'_{j,k}].Q_{t,k} \qquad (3.74)$$

where: $N$ is the total number of sediment classes; $P'_{j,k}$ is the ratio of material of size fraction $k$ incoming into the reach represented by the cross-section $j$; $P_{j,k}$ is the ratio of material of size fraction $k$ available in the bed; $c$ is a weighting factor that enables the inclusion of incoming sediment into the reach ($0 \le c \le 1$); and $Q_{t,k}$ is the fractional sediment transport capacity for total sediment load obtained from the sediment transport equations presented previously.

For each time step, the sediment balance is performed for each size fraction and cross-section, from upstream towards downstream. The amount of sediment transported out of the reach represented by a cross-section is constrained by the sediment transport capacity. The transported material flows into the next downstream reach in the same time step, with no time delay. The total amount of sediment deposited at the reach $V_{dep}$ corresponds to the amount of sediment inflow exceeding the sediment transport capacity. On the other hand, the total amount of sediment eroded at the reach $V_{ero}$ corresponds to the total amount of sediment that can still be transported by the water flux, whenever the sediment transport capacity exceeds the incoming load into the reach. Nevertheless, erosion is constrained by sediment availability at the bed of the reach.

The geometry of the cross-section is updated whenever deposition or entrainment occurs at the intermediate layer. The decrement of the cross-section area due to sediment deposition

($A_{dep}$) and the increment of the cross-section area caused by sediment remobilisation ($A_{ero}$) are computed as follows:

$$A_{dep,j} = \frac{V_{dep,j}}{L'_j} \tag{3.75}$$

$$A_{ero,j} = \frac{V_{ero,j}}{L'_j} \tag{3.76}$$

where $L'_j$ is the length of the reach represented by the cross-section j, computed as the arithmetic mean of the distances $L_j$ and $L_{j-1}$. A schematic description of the surface area and lengths represented by a cross-section can be seen in Figure 3.5, specifically for cross-section 7.

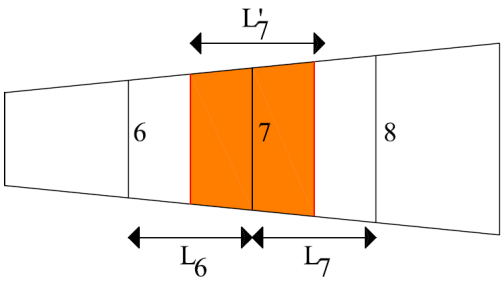


**Figure 3.5 Schematic plan view of the surface area and lengths represented by cross-section 7.**

The bed geometry of the cross-section is then adjusted using either the area of deposition ($A_{dep}$) or the area of entrainment ($A_{ero}$). As suspended sediment is assumed to be uniformly distributed throughout the cross-section and settles vertically, the cross-section bed elevation will change proportionally to water depth:

$$e_m = e_{dep} \cdot f_{d,m} \tag{3.77}$$

where $e_m$ is the bed elevation change at the point $m$ of the cross-section $j$; $f_{d,m}$ is a weighting factor for deposition; and $e_{dep}$ is the maximum bed elevation change at the deepest point of the cross-section caused by deposition ($f_{d,m} = 1$). The weighting factor ($f_{d,m}$) is computed as a ratio between the water depth at the point $m$ and the maximum depth of the cross-section $j$:

$$f_{d,m} = \frac{h_m}{h_{max}} \tag{3.78}$$

For a given section, the following relation can be given:

$$A_{dep} = \sum_{m=1}^{n_w} A_{dep,m} \tag{3.79}$$

where $n_w$ is the total number of points below water level; and $A_{dep,m}$ is the sub-area of deposition represented by the point $m$, as presented in Figure 3.6. The sub-area of deposition represented by the point $m$ is then computed as:

$$A_{dep,m} = A'_m + A''_m \tag{3.80}$$

in which:

$$A'_m = \frac{\left[\frac{(e_{m-1} + e_m)}{2} + e_m\right]}{2} . d'_m \tag{3.81}$$

$$A''_m = \frac{\left[e_m + \frac{(e_m + e_{m+1})}{2}\right]}{2} . d''_m \tag{3.82}$$

where $d'_m$ and $d''_m$ are the widths of the sub-areas $A'_m$ and $A''_m$, respectively (see Fig. 3.6). Upon substitution of Equation 3.77 into Equation 3.79, one obtains:

$$e_{dep} = \frac{A_{dep}}{\sum_{m=1}^{n_w} w^*_m} \tag{3.83}$$

with:

$$w^*_m = \frac{(f_{d,m-1} + 3f_{d,m})d'_m}{4} + \frac{(3f_{d,m} + f_{d,m+1})d''_m}{4} \tag{3.84}$$

In the case of entrainment, a symmetrical distribution of bed thickness at the intermediate layer is assumed, adapted from the equilibrium channel width model proposed by Foster & Lane (1983) which considers a symmetrical distribution of shear stress

$$e_m = e_{ero} . f_{e,m} \quad (3.85)$$

where $f_{e,m}$ is a weighting factor for erosion adapted from Foster and Lane and applied here to describe the symmetrical distribution of bed thickness (see Eq. 3.86); and $e_{ero}$ is the maximum bed elevation change at the deepest point of the cross-section caused by erosion ($f_{e,m}$ = 1). The weighting factor ($f_{e,m}$) is computed as follows:

$$f_{e,m} = 1 - (1 - X^*)^{2.9} \quad (3.86)$$

where $X^*$ is the normalized distance along the wetted perimeter, starting at the water surface.

The maximum bed elevation change $e_{ero}$ is then calculated in the same way by solving Equations 3.79 to 3.84 for erosion. The bed variation at each point $m$ is constrained by the maximum thickness of the intermediate layer $f_{act}$. $f_{act}$ has been often expressed in terms of sediment diameters (Parker and Sutherland, 1990; Hoyter et al., 2001; Yang et al., 2004). In

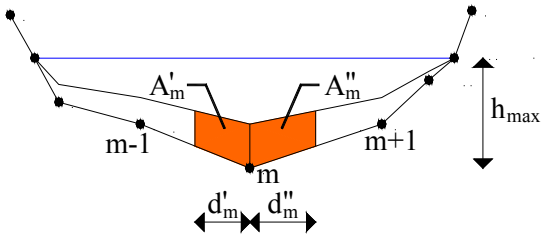


**Figure 3.6 Schematic description of the sub-area of deposition represented by each point of the cross-section.**

### 3.4.6. Vertical Profiles of Suspended Sediment Concentrations

When the sediment reaches the dam, it could be either trapped or released by the outlet devices (bottom outlet, intake device and weir). Therefore, the vertical distribution of suspended sediment concentrations immediately upstream of the dam should be evaluated. In the proposed reservoir sedimentation model, the Rouse equation is used for that purpose (Eq. 3.87), as described by Morris and Fan (1997).

$$\frac{S_y}{S_a} = \left( \frac{h - y}{y} . \frac{a}{h - a} \right)^z \quad (3.87)$$

where $S_y$ and $S_a$ are the concentrations of sediment having fall velocity $\omega$ at vertical distances $y$ and $a$ ($a = 2d$) above the bed; d is the sediment diameter; $h$ is the total water depth; and $z$ is a coefficient computed as follows:

$$z = \frac{\omega}{\kappa . u^*} \quad (3.88)$$

where $\omega$ is the settling velocity computed with the Zhang's formula (Eq. 2.1); $\kappa$ is the von Kàrmàn constant, taken equal to 0.412; and $u^*$ is the shear velocity computed as in Equation 3.58. The value of the coefficient $z$ decreases as the fall velocity $\omega$ decreases, producing a more uniform vertical distribution of sediment concentration for finer sediment. The sediment concentration $S_a$ at the vertical distance $a$ above the bed is assumed to be equal to the sediment carrying capacity at the cross-section computed using the equation proposed by Han and He (1990) for non-equilibrium sediment transport (Eq. 3.41).

## 3.5. Simplified Modelling Approach for Reservoir Network

### 3.5.1. Introduction

The original WASA model (Güntner, 2002) enabled the assessment of water storage

volumes in small reservoirs using a simplified approach for different reservoir size classes, which has been updated in the context of this study to account for sedimentation processes. A cascade routing scheme is applied to describe the upstream-downstream position of the reservoir classes and the redistribution of water and sediment yield among the reservoir classes, adapted from Güntner et al. (2004b). For the strategic reservoirs, which are medium and large-sized reservoirs located on main rivers at the sub-basin's outlet, the water and sediment balances are calculated explicitly in the model.

### 3.5.2. Water Balance

To represent the small reservoirs in an aggregated manner, they are grouped into size classes according to their storage capacity. The water balance of these reservoirs is performed using a cascade routing scheme, after making some assumptions. The small reservoirs are assumed to be located on tributary streams. For each class, the water balance is calculated for one hypothetical representative reservoir with mean characteristics. The total actual water storage volume $V_r$ is then given by the multiplication of the water storage volume of the representative reservoir $V_{rm}$ and the total number of reservoirs from that class $n$.

$$V_{rm} = V_{o,rm} + \frac{Q_{in,r} - U_r}{n} - Q_{out,rm} + \\ + (P_{rm} - E_{rm})A_{rm} - I_{rm} \quad (3.89)$$

where $V_{o,rm}$ is the water storage volume of the mean reservoir *rm* in the class *r* at the beginning of the time step ($m^3$); $Q_{in,r}$ is the water inflow to the reservoir class *r* within the time step ($m^3$); $U_r$ is the withdrawal water use from the class *r* ($m^3$); $Q_{out,rm}$ is the water outflow from reservoir *rm* within the time step ($m^3$); $P_{rm}$ is the precipitation directly on the reservoir surface (m); $E_{rm}$ is the evaporation from the reservoir surface (m); $A_{rm}$ is the surface area of the reservoir *rm* ($m^2$); and $I_{rm}$ is the infiltration loss to alluvium and bedrock ($m^3$).

Water inflow into the small reservoirs is provided by runoff generated within the sub-basin where the reservoirs are located. Runoff contribution from upstream sub-basins flows through the main river without retention in the reservoir classes. For the quantification of water inflow into the reservoir class *r*, a weighting factor ($f_{in,r}$) is computed as a ratio between the runoff contributing area of that reservoir class ($A_r$) and the total runoff contributing area of the sub-basin ($A_{sub}$), as proposed by Vries (2006). In the original runoff distribution algorithm (Güntner, 2002), the generated runoff within the sub-basin is distributed equally to each reservoir class, i.e, one sixth of the total sub-basin runoff is attributed as direct inflow to each reservoir class and another one sixth part of the generated runoff is attributed to the water discharge at the sub-basin outlet without retention.

$$f_{in,r} = \frac{A_r}{A_{sub}} \quad (3.90)$$

Smaller reservoirs are assumed to be located upstream of larger reservoirs. Additional water inflow to a reservoir class *r* may be provided from outflow of reservoir classes *x* of smaller storage capacity, whenever their storage capacity is surpassed (Fig. 3.7). This is valid for small reservoirs, which are usually provided with neither bottom outlets nor with intake devices. Water inflow into a reservoir class *r* is calculated in the same time step, without time delay.

$$Q_{in,r} = f_{in,r} \cdot Q_{gen} + \sum_{x=1}^{r-1} k_{x,r} \cdot Q_{out,x} \quad (3.91)$$

with:

$$Q_{out,r} = Q_{out,rm} \cdot n \quad (3.92)$$

$$k_{x,r} = \frac{f_{in,r}}{1 - \sum_{x=1}^{r-1} f_{in,x}} \quad (3.93)$$

where $Q_{gen}$ is the total sub-basin runoff within the time step ($m^3$); $k_{x,r}$ is the fraction of outflow discharge from the reservoir class $x$ that flows into the reservoir class $r$ of larger storage volume (-).

After the passage of the reservoir cascade, the effective water yield from the sub-basin $Q_{sub}$ is calculated as follows:

$$Q_{sub} = f_{sub} \cdot Q_{gen} + \sum_{r=1}^{5} p_r \cdot Q_{out,r} \qquad (3.94)$$

with:

$$p_r = \frac{f_{sub}}{f_{sub} + \sum_{x=r+1}^{5} f_{in,x}} \qquad (3.95)$$

where $f_{sub}$ is the fraction of the total sub-basin area not controlled by small reservoirs.

For the calculation of the reservoir water surface $A_{rm}$, the equation proposed by Molle (1989) is used, which correlates reservoir area and reservoir volumes, given in $m^2$ and $m^3$, respectively. The Molle equation was developed based on data from 416 reservoirs located in the Brazilian semi-arid region.

$$A_{rm} = c.d. \cdot \left( \frac{V_{rm}}{d} \right)^{(c-1)/c} \qquad (3.96)$$

where $c$ and $d$ are empirical constants that describe the reservoir geometry. Molle found average values of 2.7 and 1500 for the parameters $c$ and $d$, respectively.

Infiltration losses $I_{rm}$ were found to be 34% of evaporation losses in reservoirs with storage capacity smaller than 2 $Mm^3$ (Molle, 1989). For larger reservoirs, percolation losses are assumed negligible.

The water balance of strategic reservoirs is computed as in Equation 3.29. Inflow discharges into a strategic reservoir $Q_{in}$ may be obtained from an upstream sub-basin via the river network and runoff generated within the sub-basin, where they are located, without retention in the reservoir classes (Eq. 3.94).

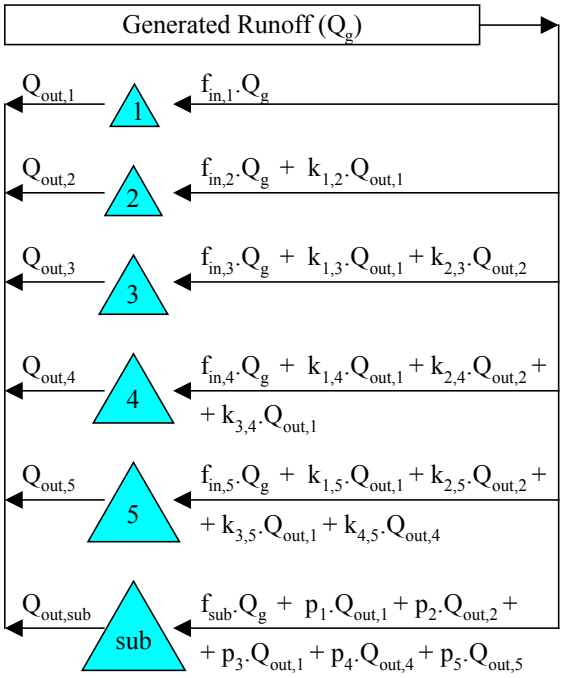


**Figure 3.7 Cascade routing scheme for small reservoirs from five size classes (class 1 to 5).**

### 3.5.3. Sediment Budget

The sediment budget in the small reservoirs is performed using a pond performance modelling as proposed by Haan et al. (1994). It consists of using the overflow rate concept for a rectangular reservoir with steady-state inflows and outflows, without resuspension of sediment.

In Figure 3.8, the sediment flow trajectories in an idealized rectangular reservoir are presented. The critical settling velocity $V_c$ is defined as the minimum settling velocity that will just allow a particle to settle to the bottom in its trajectory through the reservoir. Particles with settling velocity $V_c$ greater than the critical settling velocity will be trapped. The critical settling velocity is given by the ratio of reservoir depth $D$ and flow through time $T$. For a rectangular-shaped reservoir, the critical settling velocity can be calculated as a ratio of overflow discharges and reservoir surface area, known as overflow rate.

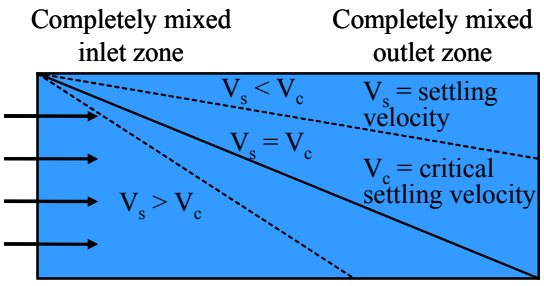


**Figure 3.8 Sediment flow trajectories in an idealized rectangular sediment pond (Haan et al., 1994).**

The total trapping efficiency (TE) can be computed using the overflow rate concept, taking into account the grain size distribution of the sediment that flows into the reservoir, as presented below:

$$TE = (1 - X_c) + \int_0^{X_c} \frac{V_s}{V_c} . dx \qquad (3.97)$$

After some rearrangements, one can write:

$$TE \cong (1 - X_c) + \sum_{i=1}^{n} \frac{V_{s,i}}{V_c} . \Delta X_i \qquad (3.98)$$

where $X_c$ is the fraction of particles with settling velocity less than $V_c$; and $n$ is the number of intervals $\Delta X$ used to calculate the integral of the previous equation.

The effluent grain size distribution can be also estimated with the overflow rate concept, expressed by the following equation:

$$F_i = \sum_{i=1}^{j} \Delta F_i \qquad (3.99)$$

where $F_i$ is the fraction of effluent smaller than particle size $i$; $j$ is the number of particles size smaller than $i$; and $\Delta F_i$ is the fraction of effluent for each particle size $i$, as follows:

$$\Delta F_i = \frac{\frac{1 - V_{s,i}}{V_c} . \Delta X_i}{\sum \frac{1 - V_{s,i}}{V_c} . \Delta X_i} \qquad (3.100)$$

Given the trapping efficiency and the effluent grain size distribution of each reservoir class, the sediment budget of small reservoirs at the sub-basin scale is performed using the same cascade routing scheme, as explained previously (see Fig. 3.7). Erosion and deposition processes at tributaries are assumed negligible. Sediment inflow into the reservoir class $r$ is given by Equation 3.101, whereas Equation 3.102 calculates the sediment discharges at the outlet point of each sub-basin after the passage of the cascade routing scheme. The index $s$ refers to sediment discharges.

$$Q^s_{in,r} = f_{in,r} . Q^s_{gen} + \sum_{x=1}^{r-1} k_{x,r} . Q^s_{out,x} \qquad (3.101)$$

$$Q^s_{sub} = f_{sub} . Q^s_{gen} + \sum_{r=1}^{5} p_r . Q^s_{out,r} \qquad (3.102)$$

The grain size distribution of incoming sediment into the reservoir class $r$ ($\%P_{k,in,r}$) and that related to water discharges at the outlet point of sub-basin ($\%P_{k,sub}$) can be calculated using Equations 3.103 and 3.104 derived from Equations 3.101 and 3.102, respectively.

$$\%P_{k,in,r} = \frac{\%P_{k,gen} . f_{in,r} . Q^s_{gen}}{Q^s_{in,r}} + \frac{\sum_{x=1}^{r-1} \%P_{k,out,x} . k_{x,r} . Q^s_{out,x}}{Q^s_{in,r}} \qquad (3.103)$$

$$\%P_{k,sub} = \frac{\%P_{k,gen} . f_{sub} . Q^s_{gen}}{Q^s_{sub}} + \frac{\sum_{r=1}^{5} \%P_{k,out,r} . p_r . Q^s_{out,r}}{Q^s_{sub}} \qquad (3.104)$$

where $\%P_{k,gen}$ is the ratio of the size class $k$ of the sediment yield from the sub-basin; $\%P_{k,out,x}$ is the ratio of the size class $k$ of sediment released by reservoir classes $x$ of smaller water storage capacity; and $\%P_{k,out,r}$ is the ratio of the size class $k$ of sediment released by the reservoir class $r$. $\%P_{k,out,r}$ is obtained from the pond performance modelling presented previously by interpolation of the effluent grain size distribution of each class $r$.

For strategic reservoirs, the sediment budget may be computed either using the simplified modelling approach proposed by Haan et al. (1994) or using the detailed modelling approach explained in Sections 3.4.4 to 3.4.6, depending on reservoir size and data availability.

# CHAPTER 4

# 4. Study Areas and Monitoring Campaigns

## 4.1. Benguê Catchment in Brazil

### 4.1.1. Area Description

The semi-arid region of north-east Brazil has an area of a one million square kilometres and hosts about 15 million inhabitants, where conflicts regarding water use are already very evident. The water supply in this region relies mostly on surface water stored in reservoirs. In the state of Ceará 93% of the water delivered with minimum confidence (90%) comes from these reservoirs.

The maximal available water capacity in the state of Ceará will be soon reached. Therefore, it is fundamental for a sustainable development of this region to maintain the quality and quantity of the water resources. Sediment deposition in the dams due to sediment production, sediment transport and reservoir sedimentation presents a great risk for the conservation of these resources.

The Benguê reservoir is located in the municipality of Aiuaba in the driest region of the Federal State of Ceará (Fig. 4.1). The contributing basin area is about 933 km$^2$. This area is inside the uppermost Jaguaribe catchment with a size of approximately 25,000 km$^2$ (about 1/6 of the State area), being controlled by the Oros dam, which is the second largest reservoir in Ceará, with a storage capacity of about 1,940 Mm$^3$.

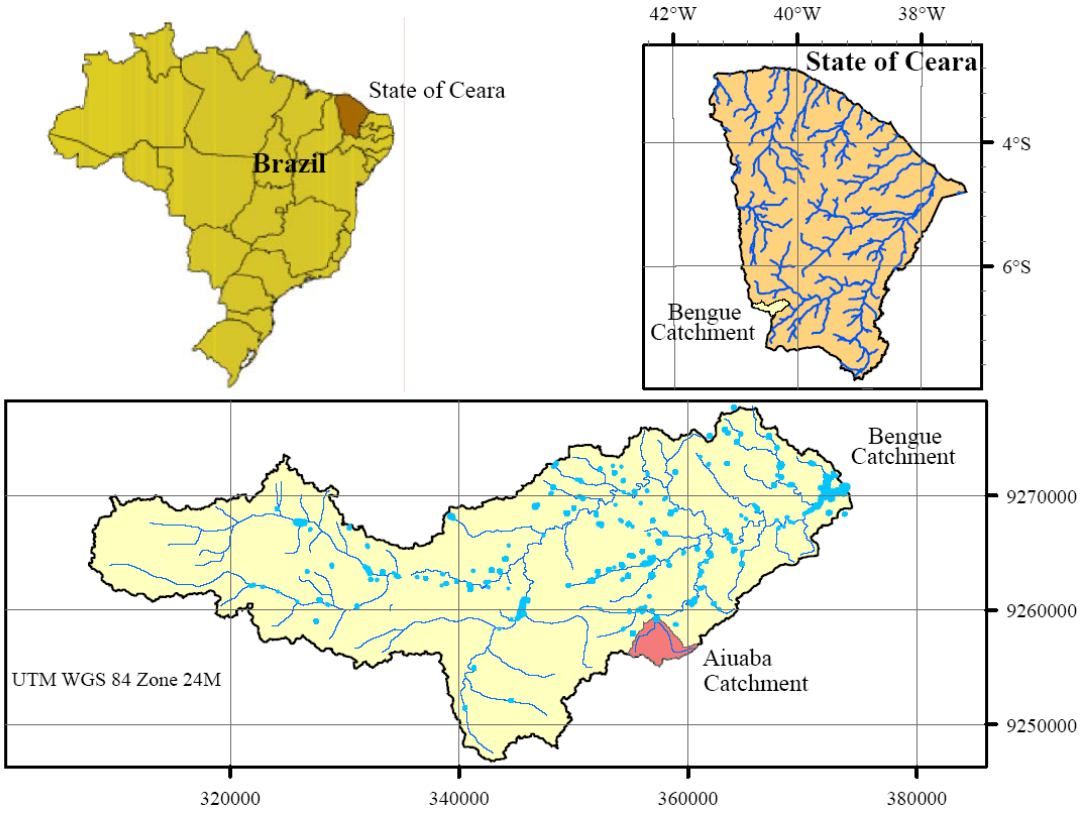


**Figure 4.1 Location of the 933-km$^2$ Benguê catchment and the 12-km$^2$ Aiuaba experimental catchment.**

The Benguê catchment is subdivided into several, partially nested sub-basins. One of them, the Aiuaba experimental catchment, has been monitored since 2003. It is a headwater catchment located in the southern part of the Benguê catchment (see Fig 4.1). The Aiuaba experimental catchment has a size of 12 km² and is controlled by a reservoir with a present storage capacity of about 0.1 $Mm^3$.

The predominant vegetation type of the Benguê catchment is the *Caatinga*. It is a deciduous vegetation type, consisting of a more or less dense mixture of trees, bushes and cacti, with ramified and thorn-bearing branches and heights varying from 3 to 7 m. Two different classes of *Caatinga* have been identified in the Benguê catchment according to its degree of conservation: a *Preserved Tree-Shrub Caatinga* (eastern part of the Bengué catchment between 330 and 650 m); and a *Degraded Tree-Shrub Caatinga* (eastern area of the catchment on undulated relief). *Dry Deciduous Forest* covers the south-eastern part of the Benguê catchment, mainly in the area with dissected plateaus. It is mainly characterised by its more or less dense tree layer: a dense, partly impenetrable bush layer; and an herbaceous layer where sufficient daylight penetrates. Another vegetation class identified in the Benguê catchment is the *Carrasco*. It is a dense vegetation type composed of a tree layer (5 to 6 m), with nearly 100% coverage and several trees reaching more than 10 m, a dense bush layer and virtually no herbaceous layer. According to the degree of conservation, *Carrasco* can be classified as: *Preserved Carrasco* which occurs on steep slopes, but also covers the plateau area; *Degraded Carrasco* covering the plateau regions with a relatively flat relief and altitudes ranging from 520 and 730 m; and *Regenerated Carrasco* which occurs in the western part of the catchment on areas regenerated after clear-cutting, 15 to 20 years ago (Creutzfeldt, 2006).

The most important economic activity in the region is agriculture. The main agricultural crops are cotton, maize and beans. Agricultural crops occur mainly around urban areas and at the southern plateaus of the Benguê catchment.

The Benguê catchment is located in a transition zone of geological and geomorphological conditions: the *Sertões* (Hinterland) in the eastern part and *Altos Planaltos Sedimentares* (high sedimentary plateaus) in the western and southern part (Creutzfeldt, 2006). The geology of the Sertoes is characterised by the crystalline complex, consisting of *Granite*, *Migmatitic Gneiss* and *Banded Gneiss* with fascis of *Mica Schist*. The Altos Planaltos Sedimentares are composed of *Plateaus*, *Mesas* and *Distinctive Valley Systems*.

Soils on the crystalline basement tend to be shallow, clayey and often contain a significant amount of rock fragments. According to the RADAMBRASIL Project (1981), the dominating soil types in the Benguê catchment are *Latossolo Vermelho-Amarelo Alico*, *Bruno nao Calcico*, *Podzolico Vermelho-Amarelo Eutrofico*, *Planossolo Solodico*, *Solos Litolicos Distroficos* and *Solos Litolicos Eutroficos*.

The climate of Benguê catchment is Tropical Semi-arid, with a mean annual evaporation of approximately 2,500 mm and the mean annual rainfall of around 560 mm. Rainfall occurs in a rainy season with a duration of about five months between January and June and maximal rainfall in March (Fig. 4.2). The mean annual temperature in the area is approximately 25$^0$C and elevation reaches from 400 to 800 m above sea level.

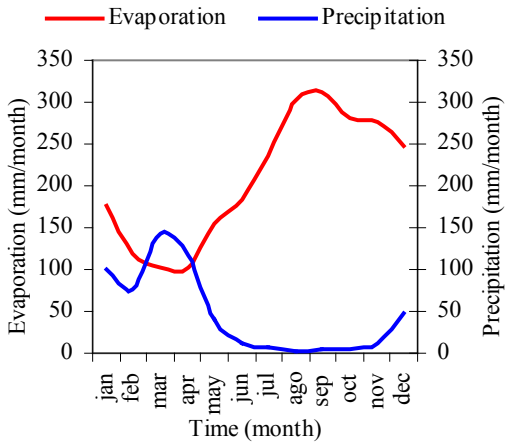


**Figure 4.2 Potential evaporation-precipitation relationship.**

The Horton overland flow is the predominant runoff type. The effective runoff generation is mainly concentrated on single, intense rainstorm events causing, in combination with high rates and a rapid initiation of overland flow, runoff flash floods with sharply peaked hydrographs (Creutzfeldt, 2006).

The Benguê dam was constructed by COGERH (Water Management Company in the Federal State of Ceará) in 2000. The dam impounds the ephemeral Umbuzeiro River, which dries out during the dry season from July to December. The Benguê Reservoir is able to supply 200 $L.s^{-1}$ for the cities downstream of the dam with a reliability level of 90%, but only 15 $L.s^{-1}$ has been released for water supply in the Aiuaba city, with approximately 2,000 inhabitants. A view of the reservoir area is presented in Figure 4.3.

The Benguê reservoir floods a surface area of 348 ha. The dam has a height of 23.6 m and is about 522 m long. The Creager spillway is 150 m long, with a maximum overflow of about 913 $m^3.s^{-1}$. The original storage capacity of the Benguê reservoir is 19.6 $Mm^3$. Its stage-area and stage-volume curves can be seen in Figure 4.4.

The reservoir level had been below the intake elevation (438 m) until January 2002 and the impoundment reached its maximum storage capacity the first time in the rainy season in 2004. The temporal evolution of water level and rainfall directly on the reservoir are presented in Figure 4.5. The average water inflow into the reservoir is about 30 $Mm^3.year^{-1}$. Nevertheless, the reservoir yields only 6.5 $Mm^3.year^{-1}$, with a reliability level of 90%. According to Araújo et al. (2003), the sedimentation rate in Ceará for similar catchments varies from 130 to 690 $t.km^{-2}.yr^{-1}$, depending on land use. Therefore, the sedimentation expectation for the Benguê dam ranges from 1.4 to 7.3 million tons per decade, or from 1.2 to 5.6 $Mm^3$ per decade, which means that, if erosion is not controlled, the dam will become filled up with sediment in less than 40 years.

Using satellite imageries, 121 reservoirs have been identified in the Benguê catchment, with a wide range of surface areas (from 150 to 830,000 $m^2$). The water stored in those reservoirs is used for irrigation and water supply. In total, the reservoirs are able to store approximately 10 $Mm^3$ (51% of the storage capacity of the Benguê reservoir).

**Figure 4.3 View of the Benguê reservoir in 2002.**

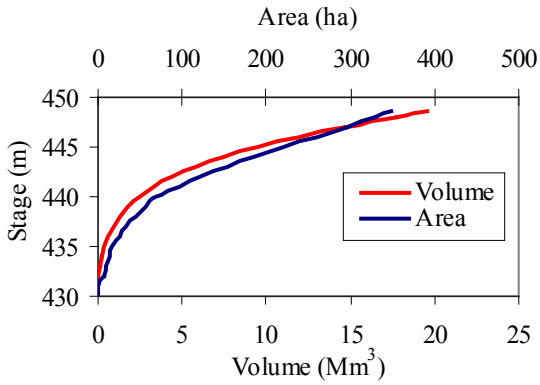


**Figure 4.4 Stage-area and stage-volume curves.**

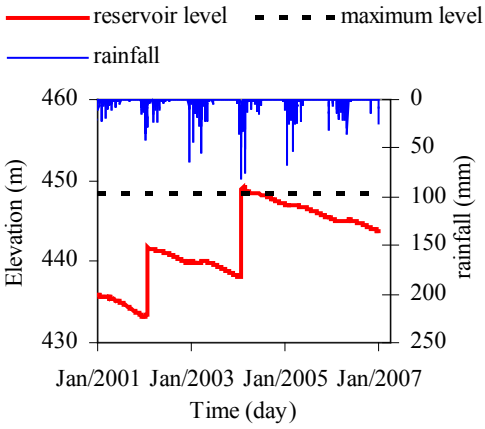


**Figure 4.5 Temporal evolution of water level and precipitation in the Benguê reservoir.**

### 4.1.2. Data Collection and Monitoring Campaigns

For the model development and application, extensive data collection programmes in the Benguê catchment are being carried out since 2004. Additionally, fieldwork campaigns were carried out to supplement the hydrological and sedimentological data and to gain an enhanced understanding of the sedimentation processes in the small reservoirs. Table 4.1 gives an overview of the monitoring scheme for the Benguê catchment.

**Table 4.1 Overview of the monitoring scheme for the Benguê catchment.**

| Data | Location | Devices | Sampling scheme | Observation time | Source |
|---|---|---|---|---|---|
| Rainfall | within and around the Bengue catchment | rainfall gauges | daily | since 1978 | FUNCEME |
| | Aiuaba catchment | | 5-min | since 2003 | UFC |
| Rainfall interceptation | Aiuaba catchment | Ville de Paris pluviometers | daily | since 2003 | UFC |
| Potential evaporation | Aiuaba catchment | class A pan | hourly | since 2003 | UFC |
| Soil moisture | Aiuaba catchment | soil humidity sensors | hourly | since 2003 | UFC |
| Reservoir water level | Bengue reservoir | limnimetric rulers | daily | since 2000 | COGERH |
| | Boqueirao reservoir | automatic water level sensor | 15-min | since 2003 | UFC |
| | five small reservoirs of the Cavaco catchment | limnimetric rulers | daily | rainy season of 2007 | - |
| Water discharges | Bengue reservoir | water balance | daily | since 2000 | - |
| | Boqueirao reservoir | Parshall flume | 15-min | since 2003 | UFC |
| Overflow discharges | Bengue reservoir | rating curve of the spillway | daily | since 2000 | COGERH |
| | Boqueirao reservoir | water balance | 15-min | since 2003 | UFC |
| Sediment fluxes into reservoirs | Bengue reservoir | water-stage sediment samplers and manual samples | events | since 2005 | - |
| | Boqueirao reservoir | | | since 2004 | UFC |
| Reservoir topography | Bengue reservoir | bathymetric surveys | twice | 2005 and 2007 | - |
| Sediment cores | Bengue reservoir during low water level | sediment corer | three months | fieldwork campaign of 2005 | - |
| Vertical profiles of suspended sediment concentration | Bengue reservoir | Van Dorn bottle | three months | fieldwork campaign of 2005 | - |
| Water quality parameters | Bengue reservoir | multi-parameter water quality meter | three months | fieldwork campaign of 2005 | - |
| Geometric data of small reservoirs (depth, area, volume) | Small reservoirs of the Bengue catchment | GPS, echo sounder and satellite imageries | six months | fieldwork campaign of 2005 and 2006 | - |

Within the Benguê catchment, there are ten rainfall gauges operated by FUNCEME (Water Resources and Meteorology Foundation in the Federal State of Ceará) on a daily basis. Water level is measured inside the Benguê reservoir with a set of limnimetric rulers and daily resolution by COGERH. In addition, data on overflow discharges and water withdrawal to supply the municipality of Aiuaba are provided by COGERH. Inflow discharges to the Benguê reservoir are estimated through the water balance in the reservoir (Figure 4.6). To account for sedi-

ment inflow into the Benguê reservoir, two water-stage sediment samplers were installed upstream of the Benguê reservoir on the main river and on a tributary stream. The sampler enables the measurement of suspended sediments in the river water with sediment concentration being measured at different depths of water flow within the river. Figure 4.7 shows the location of the measuring instruments within the Benguê catchment.

The 12-km² Aiuaba experimental catchment located within the Benguê catchment has been also monitored since 2003 by the Brazilian partners within the SESAM project and other research projects carried out by the Federal University of Ceará (UFC). An extensive database has been compiled on climate and hydrological data such as rainfall intensities, evaporation rates, interception rates and reservoir level data for the Boqueirao reservoir at the outlet of the catchment (Figure 4.12). Additionally, daily water level of five other reservoirs located within the 50-km$^2$ Cavaco catchment was monitored during the rainy season of 2007 to evaluate water retention in those reservoirs. Suspended sediment concentration has been measured during storm events using a water-stage sediment sampler installed upstream of the Boqueirao reservoir.

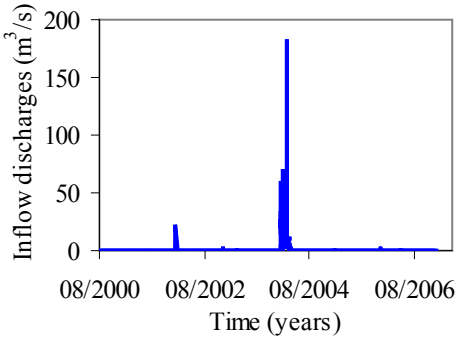


**Figure 4.6 Water inflow discharges into the Benguê reservoir estimated through the water balance.**

As part of this study, fieldwork campaigns were performed to obtain additional hydrological and sedimentological data. Two bathymetric surveys were carried out in 2005 and 2007. Unfortunately, it was observed that the interpolation uncertainties are higher than the total sediment deposition during the period, which made it difficult to compare the two maps. Furthermore, the maps derived from the bathymetric surveys differ from the original topographic map, as shown in Figure 4.8. This may be explained by the fact that the topographic survey of 2000 was performed before the dam construction merely to estimate the maximum storage capacity of the Benguê reservoir and, therefore, the resolution of the map is not as high as those carried out in 2005 and 2007 within this study.

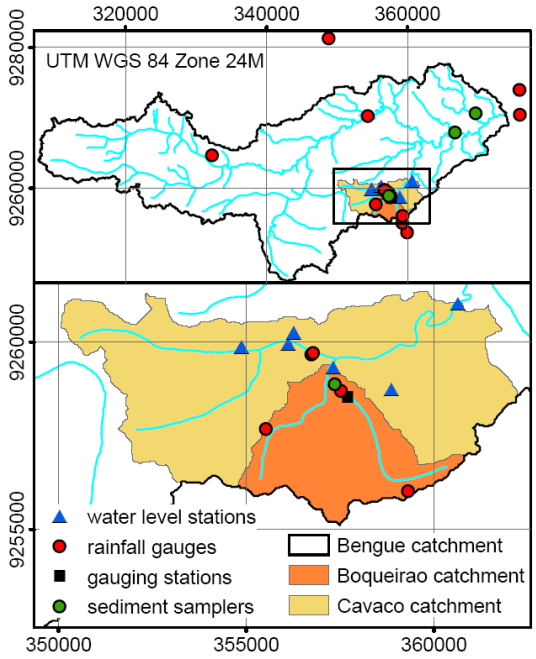


**Figure 4.7 Location of the measuring instruments within the Benguê catchment.**

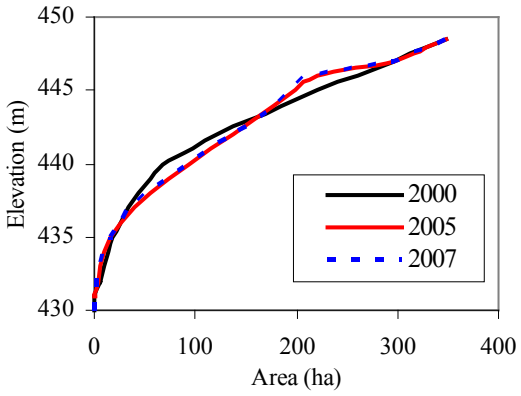


**Figure 4.8 Stage-area curves of the Benguê reservoir.**

Twenty-nine sediment samples were collected from each tributary stream upstream of the Benguê reservoir to characterize the deposited material in terms of their physical properties, such as, grain size distribution, soil permeability, wet and dry bulk density. The location of the samples is presented in Figure 4.9. The results on grain size distribution analysis show that the collected material is predominantly sand, with an average percentage of about 87%, as presented in Figure 4.10. Dry and wet bulk densities are, on average, 1.6 and 1.67 g.cm$^{-3}$, respectively.

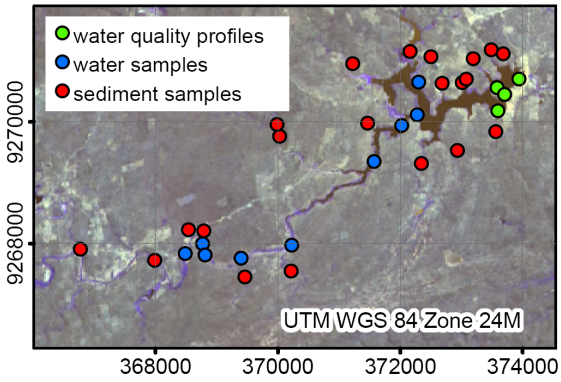


**Figure 4.9 Location of the water samples and sediment samples collected in the Benguê Reservoir (spring, 2005).**

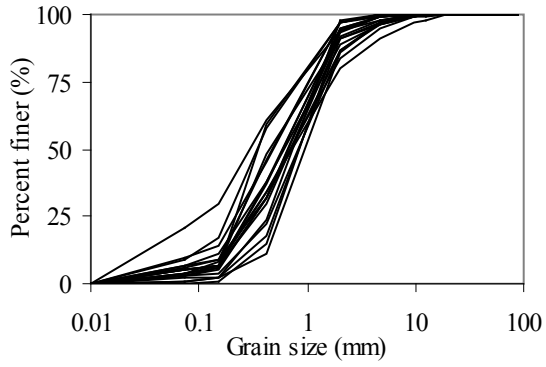


**Figure 4.10 Grain size distribution of the deposited sediment in the Benguê Reservoir (spring, 2005).**

Measurements of suspended sediment concentration of eight vertical profiles within the Benguê reservoir were carried out by sampling the water-sediment mixture using a Van Dorn bottle (Figure 4.9). Values of suspended sediment concentration vary from 10 mg.L$^{-1}$ at the water surface to 70 mg.L$^{-1}$ close to the reservoir bottom. Additionally, a multi-parameter water quality meter was used to measure some physical properties of water such as pH and temperature. The results, summarized in Figure 4.11 and Figure 4.12, show a very low variation in temperature and pH, respectively, from the water surface to the reservoir bottom for the four vertical profiles depicted in Figure 4.9.

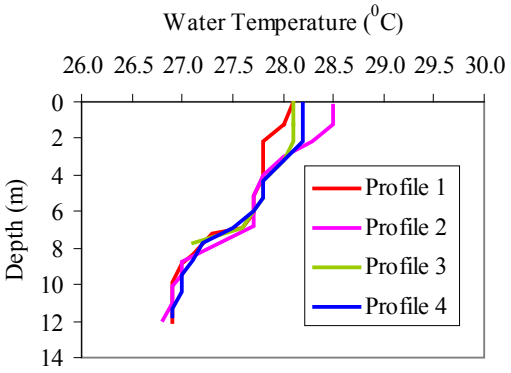


**Figure 4.11 Vertical variation of water temperature in the Benguê Reservoir (spring, 2005)**

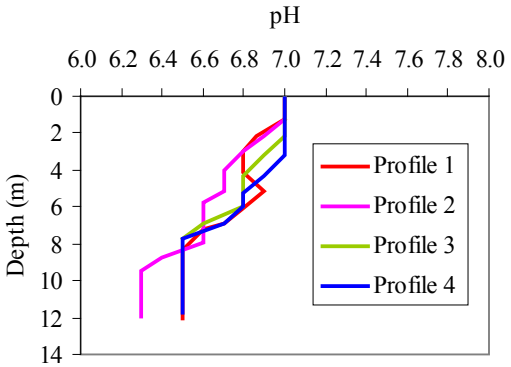


**Figure 4.12 Vertical variation of pH values in the Benguê Reservoir (spring, 2005).**

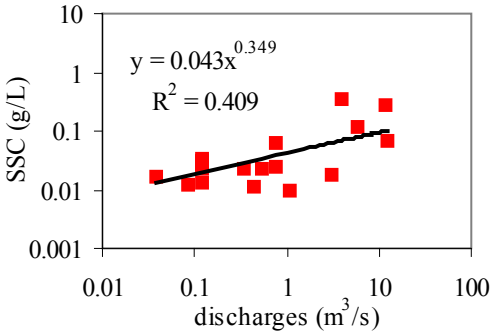


**Figure 4.13 Water inflow discharges and suspensed sediment concentrations (SSC) measured upstream of the Benguê reservoir during the rainy season of 2007.**

As no previous data on sediment load were available in the study area, intensive fieldwork campaigns were carried out to monitor sediment fluxes into the Benguê reservoir from 2005 to 2007 during the rainy season. Unfortunately, only very small flood events were observed in the rainy seasons of 2005 and 2006. In the rainy season of 2007, larger flood events occurred, enabling the collection of some water samples to estimate sediment fluxes into the Benguê reservoir, as presented in Figure 4.13. SSC values varying from 0.01 to 0.34 $g.L^{-1}$ were found, depending on the event.

Geometric data on several small reservoirs within the Benguê catchment, such as surface areas, water volumes and reservoir depths, were surveyed during the fieldwork campaigns of 2006 and 2007. The collected data were used to parameterize the WASA-SED model and to test the equation proposed by Molle (1989), which relates reservoir areas to volumes.

## 4.2. Barasona Catchment in Spain

### 4.2.1. Area Description

The Pre-Pyrenean Mediterranean zone of Spain, such as that where the Barasona reservoir is located, is characterized by high sediment yields and a high degree of impoundment of the natural river flow. The loss of retention volume in surface reservoirs due to sediment deposition often leads to a significant reduction in water availability within a period of few decades. Representative surveys indicate that almost 10% of reservoirs in Spain have experienced a reduction in capacity of 50% or more (Avendaño et al., 1997).

The Barasona dam controls 1,224 $km^2$ of the Esera catchment (see Figure 4.14). Its catchment is drained by two main rivers: the Esera River and the Isábena River.

The Barasona Reservoir has been heavily affected by the sedimentation of suspended sediments that reach the reservoir via the Esera and Isábena rivers. The badlands located in the upper part of both catchments are thought to be the major cause for the sedimentation of the Barasona Reservoir (Fargas et al., 1996). Most of the sediments are delivered to the Barasona Reservoir during flood events (Valero-Garces et al., 1999). The sedimentation of the reservoir is a severe problem for the region as it is a long-lasting threat for the water outlets to the canal of Aragon and Catalunya.

Until the early 1950s the deposited sediments were flushed out yearly through the bottom outlets. After that time, the bottom outlets were not opened every year, resulting in a higher effective sedimentation rate. A bathymetric survey of the reservoir in 1993 indicated that its original storage capacity had been reduced by 24.8 $Mm^3$. Finally, flushing operations were performed after the irrigation season for the three consecutive years 1995-1997 (Valero-Garcés et al., 1999).

The total annual reservoir inflow is largely contributed by the Esera River, which drains an area of 789 $km^2$ (65% of the whole area). The Esera and Isábena rivers have a transitional hydrologic regime characterized by two maxima, as presented in Figure 4.15. The highest flows are associated with late spring-early summer snow melt and heavy rains, summer thunderstorms and with late autumn heavy rains (Valero-Garces et al., 1999). The major rivers in the catchment never dry up, although flows are low during the summer and some of the tributaries of the Isábena and Esera Rivers exhibit ephemeral behaviour with no flow at the end of the dry season.

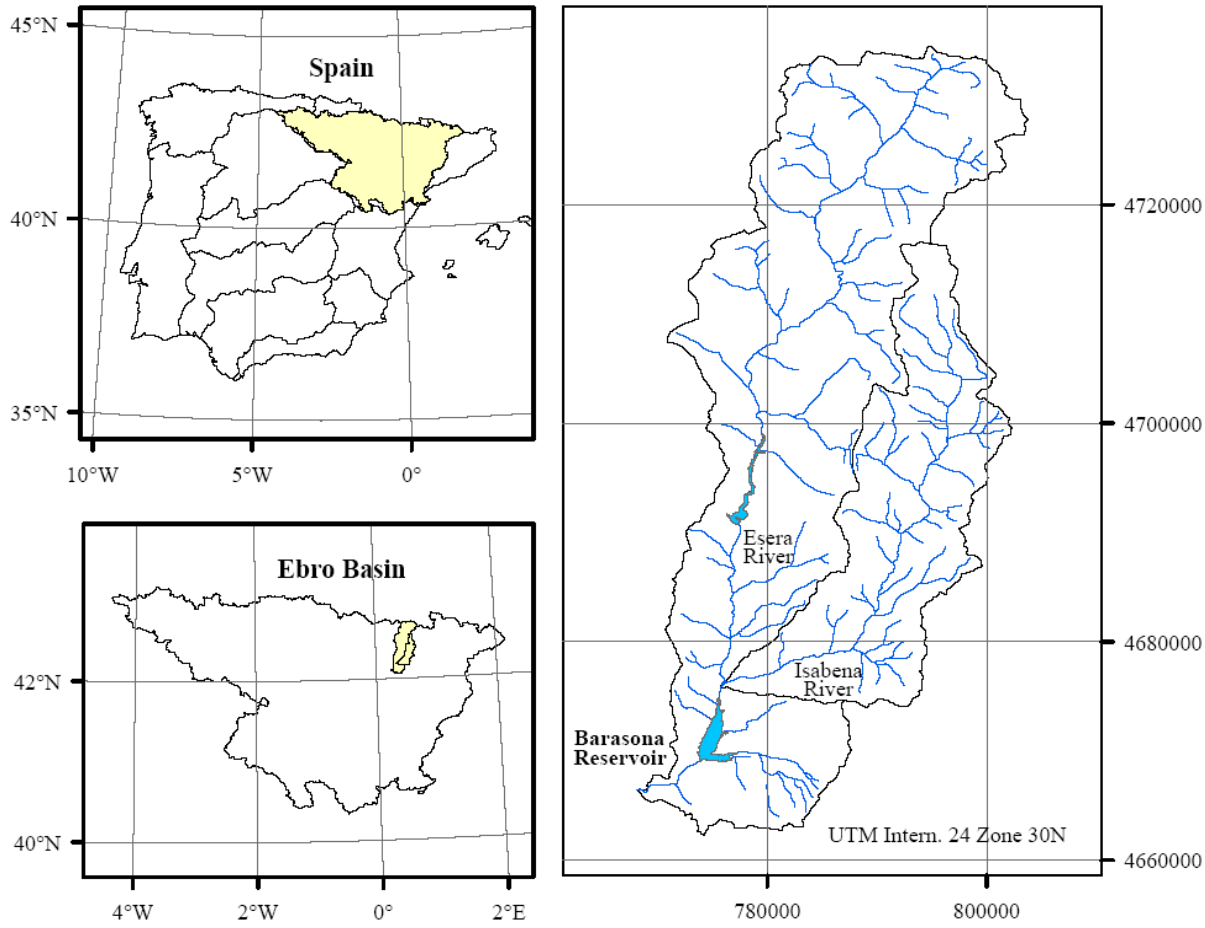


**Figure 4.14 Location of the Barasona reservoir and the two main contributing areas: the Esera catchment and the Isábena catchment.**

The climate of the Barasona catchments is a typical Mediterranean mountainous type with mean annual precipitation rates of 600 to 1200 mm and an average potential evaporation rate of 550 to 750 mm. Both rates show a strong south-north gradient, which can be related to the strong topographical difference in altitude within the catchments ranging from 400 to 2020 m. The vegetation includes evergreen oaks and pines in the valley bottoms and deciduous oaks in the upper areas.

The Barasona Catchment is characterized by an heterogeneous topography and lithology, containing the following geologic units: the axial Pyrenees composed of Palaeozoic rocks; the Internal Ranges composed of Cretaceous and Palaeogene sediments; several Internal Depressions formed upon more erodible materials; the Intermediate Depression, a relatively lowland area north of the reservoir composed of Miocene continental sediment and; the External Ranges that bound the basin to the south (Valero-Garces et al., 1999).

The middle part of the Barasona catchment is characterized by intense erosion processes, even under normal precipitation conditions. A significant part of the erosion processes occurs on badlands. Badlands are a typical landform of this region within the upper middle part of the catchments, dominated by Mesozoic carbonate rocks and marls. Badlands are heavily dissected barren terrains that

are composed of poorly cemented debris and marls lacking any vegetation cover. Badlands are vulnerable to flash flood erosion and produce large amounts of eroded material, that are then transported downstream as suspended sediments in the Esera and Isábena rivers. The large amount of suspended sediments in the river system creates severe problems of sedimentation at the Barasona reservoir (see Fig. 4.16).

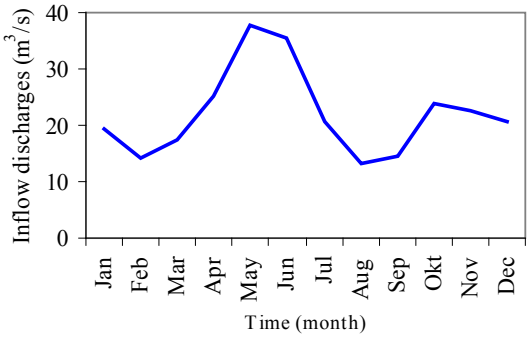


**Figure 4.15 Mean monthly inflow discharges into the Barasona Reservoir (1986-2005).**

The Barasona reservoir floods a surface area of about 700 ha, with a maximum width of over 1.5 km, a length of about 9 km and a maximum depth of approximately 50 m close to the dam. The dam was constructed on the Esera River in Spain in 1932 for irrigation purposes and power generation. In 1972, the crest elevation of the Barasona dam was increased and the storage capacity reached 92.2 $Mm^3$. The temporal evolution of its storage capacity is presented in Figure 4.17. Values of storage capacity were derived from bathymetric surveys (see Section 4.2.2)

The Barasona dam is a concrete gravity structure with four 10m-tall radial crest gates and a spillway design of 1738 $m^3s^{-1}$ (see Fig. 4.18). There are six bottom sluices used to drain the reservoir and release sediments. In total 146.84 $m^3.s^{-1}$ of water may be released through the bottom outlets. Furthermore, there is a water intake device with a capacity of 30 $m^3.s^{-1}$ to supply water to the Aragon and Catalunya canal.

**Figure 4.16 Delta deposition at the Barasona reservoir.**

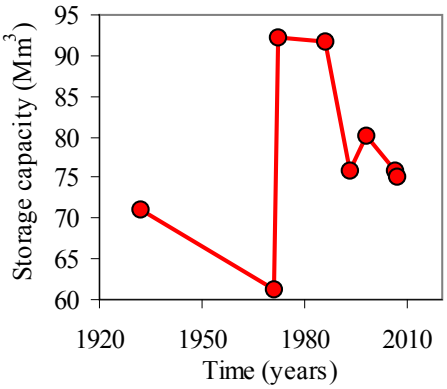


**Figure 4.17 Temporal evolution of the storage capacity of the Barasona reservoir.**

**Figure 4.18 View of the Barasona dam and its radial crest gates.**

### 4.2.2. Data Collection and Monitoring Campaigns

The existing monitoring scheme in the Barasona catchment comprises two gauging stations (Isábena station and Esera station) with a record of almost 65 years of daily water discharges provided by the CHEBRO (Hydrological Confederation of the Ebro Basin); daily measurements of water level and outflow discharges at the Barasona reservoir since 1940 (CHEBRO); and 15-min record of suspended sediment concentration at the Isábena station since 2005 using a turbidimeter and an ISCO-3700 Sampler (Figure 4.19) provided by the University of Lleida. The gauging stations are located immediately upstream of the Barasona reservoir on the Esera river and Isábena river, respectively (see Figure 4.20).

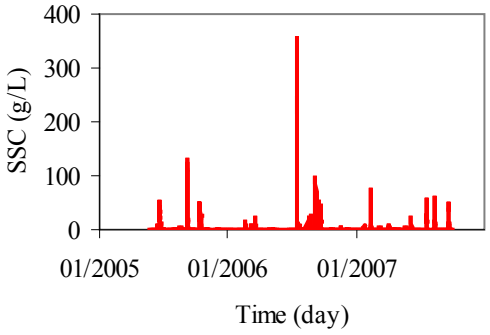


**Figure 4.19 15-min data on suspended sediment concentration (SSC) at the Isábena gauging station.**

**Table 4.2 Overview of the monitoring scheme for the Barasona catchment.**

| Data | Location | Devices | Sampling scheme | Observation time | Source |
|---|---|---|---|---|---|
| Rainfall | within and around the Barasona catchment | rainfall gauges | daily<br>15-min | since 1961<br>since 2005 | CHEBRO |
| Reservoir water level | Barasona reservoir | limnimetric rulers<br>water level sensors | daily<br>15-min | since 1940<br>since 2002 | CHEBRO |
| Inflow discharges | Isábena station<br>Esera station | rating curve | daily<br>15-min<br>daily | since 1940<br>since 1998<br>since 1940 | CHEBRO |
| Outflow discharges | Barasona reservoir | rating curve | daily | since 1940 | CHEBRO |
| Sediment fluxes into the reservoir | Upstream the Barasona reservoir at the Isábena station | turbidimeter<br>automatic and manual sampler | 15-min<br>events | since 2005 | University of Lleida |
| Reservoir topography | Barasona reservoir | bathymetric surveys | three times<br>twice | 1986, 1993 and 1998<br>2006 and 2007 | CHEBRO<br>University of Lleida |
| Sediment cores | Delta of the Barasona reservoir | sediment corer | 15 days | fieldwork campaign of 2006 | - |
| Longitudinal variation of SSC within the reservoir | Barasona reservoir | depth integrating sampler | 15 days | fieldwork campaign of 2006 | - |
| Vertical profiles of suspended sediment concentration | Barasona reservoir | point integrating sampler | one month | fieldwork campaign of 2006 and 2007 | - |
| Sediment release from the reservoir | Downstream the Barasona reservoir at the Aragon and Catalunya canal | depth integrating sampler | 15 days | fieldwork campaign of 2006 | - |

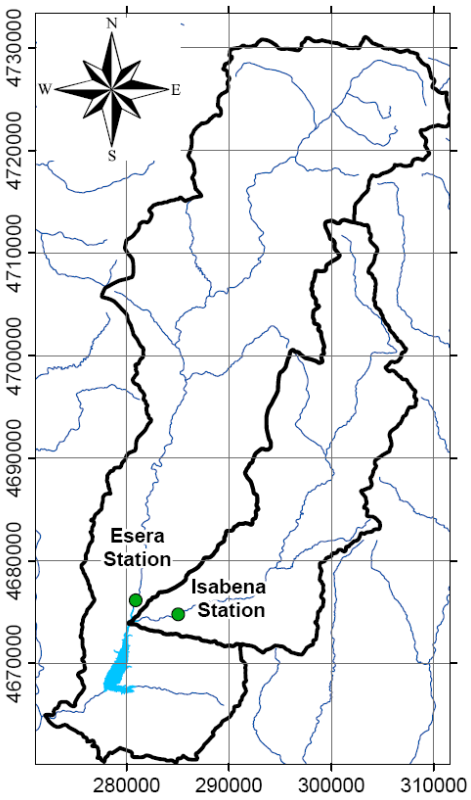


**Figure 4.20 Location of the gauging stations Esera and Isábena in the Barasona cacthment.**

For the assessment of sedimentation rates and deposition patterns, there exist five high-resolution bathymetric surveys (see Figure 4.21). Two of them were carried out within this research project in 2006 and 2007. Furthermore, sediment cores were extracted after emptying of the Barasona reservoir (1995-1997) by the Spanish Water Authorities in order to obtain physical and chemical features of the deposited material. The analysis of the collected material enabled the reconstruction of depositional history of the reservoir; the evaluation of deposition thickness and spatial variation in grain size distribution due to deposition and remobilization of material previously deposited; and the identification of sediment sources and areas of high sediment yield risks in the basin by comparative mineralogical analysis (Valero-Garces et al., 1999). According to Valero-Garces et al. (1999), sediment deposition has been dominated by settling of fine suspended sediment and most of the sediment has been transported to the Barasona reservoir during flood events.

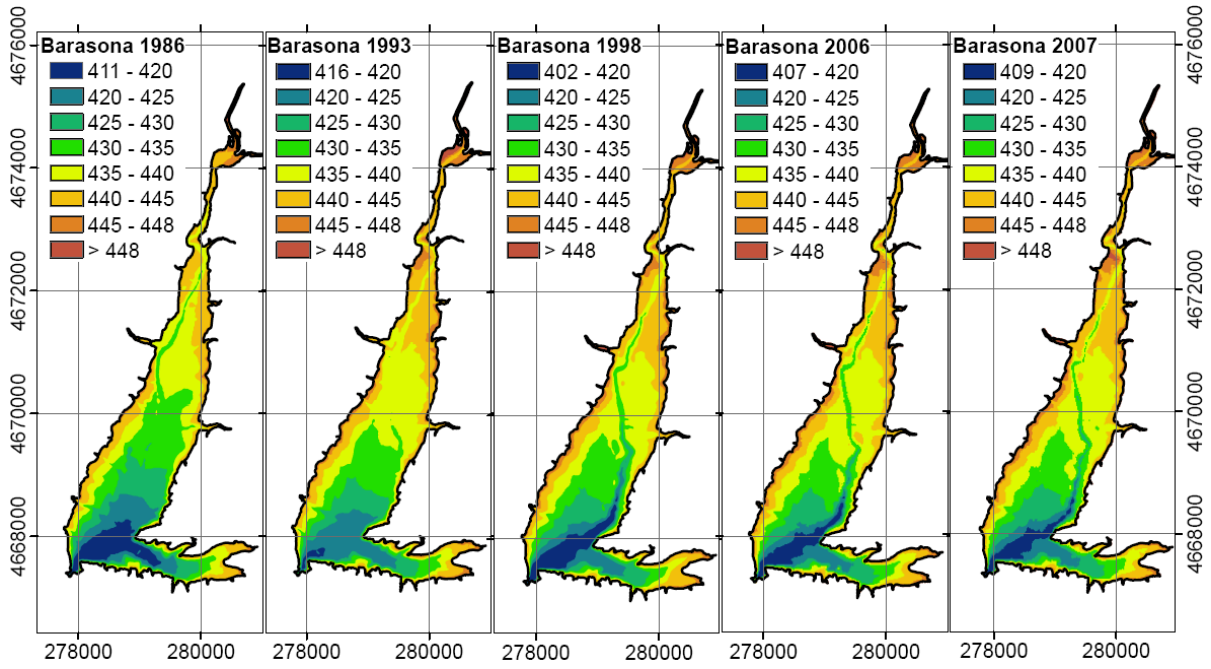


**Figure 4.21 Topographic maps derived from bathymetric surveys of the Barasona reservoir.**

Additional data were obtained from fieldwork campaigns in the Barasona catchment. Several sediment samples were collected from the reservoir delta to analyse the spatial variability of physical properties of the material, such as grain size distribution, wet and dry densities and porosity. The locations of the sediment samples are depicted in Figure 4.22. Results of the laboratory analysis show that the collected material is predominantly silt, with an average percentage of about 70%, according to the German soil classification (Figure 4.23). The sediment samples have a mean wet bulk density of 1.89 g.cm$^{-3}$ and a mean dry bulk density of 1.52 g.cm$^{-3}$, as presented in Table 4.1.

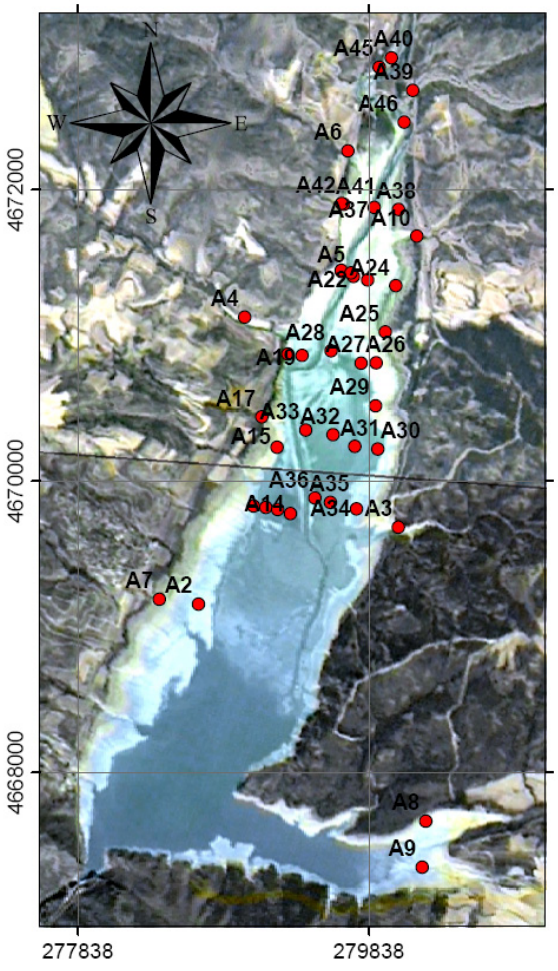


**Figure 4.22 Location of the sediment sampling points at the Barasona (autumn, 2005).**

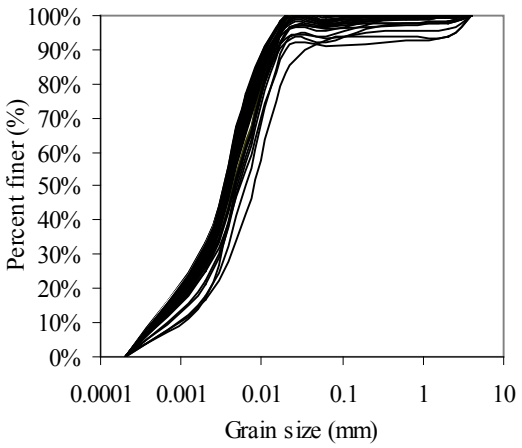


**Figure 4.23 Grain size distribution of the deposited sediment in the Barasona Reservoir, collected during the fieldwork (autumn, 2005).**

**Table 4.1 Physical properties of sediment samples collected upstream of the Barasona Reservoir (autumn, 2005).**

| Sample | Porosity (%) | Wet bulk density (g/cm3) | Dry bulk density (g/cm3) |
|---|---|---|---|
| A40 | 42.05% | 2.06 | 1.54 |
| A45 | 45.84% | 1.94 | 1.44 |
| A46 | 44.08% | 1.95 | 1.48 |
| A10 | 37.30% | 2.04 | 1.66 |
| A41 | 43.04% | 1.90 | 1.51 |
| A7 | 48.98% | 1.80 | 1.35 |
| A39 | 40.21% | 1.85 | 1.58 |
| A6 | 40.21% | 1.88 | 1.58 |
| A3 | 46.57% | 1.53 | 1.42 |
| A25 | 43.20% | 1.91 | 1.51 |
| A2 | 45.88% | 1.81 | 1.43 |
| A26 | 30.40% | 2.14 | 1.84 |
| A37 | 48.33% | 1.89 | 1.37 |
| A34 | 39.71% | 1.97 | 1.60 |
| A29 | 37.83% | 1.95 | 1.65 |
| A4 | 44.77% | 1.62 | 1.46 |
| A9 | 45.07% | 1.87 | 1.46 |
| A8 | 42.09% | 1.92 | 1.53 |
| mean | 42.53% | 1.89 | 1.52 |
| deviation | 4.50% | 0.14 | 0.12 |

For the assessment of the longitudinal variation of suspended sediment concentration (SSC), eleven water samples were collected in the Barasona reservoir during a single event (Figure 4.24). The results, summarized in Figure 4.25, show explicitly the variation in SSC from upstream towards downstream, with about

14 g.L$^{-1}$ at the inlet point, approximately 5 km away from the dam, and a mere 0.32 g.L$^{-1}$ very close to the dam. Additional water samples were collected upstream and downstream of the Barasona reservoir to estimate sediment trapping efficiency at the event scale. Table 4.2 shows that the sediment trapping ratio varies from 93 to 99% for flood events with high sediment concentration. For events with SSC lower than that in the reservoir, the sediment releasing ratio should be over 100%, i.e. sediment outflow exceeds sediment inflow within the time interval.

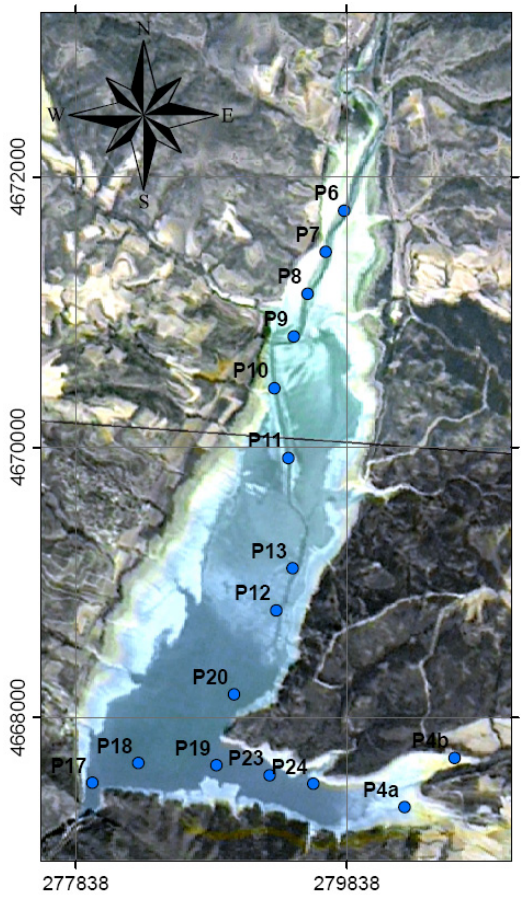


**Figure 4.24 Location of the sampling points for suspended sediments at the Barasona Reservoir (autumn, 2005).**

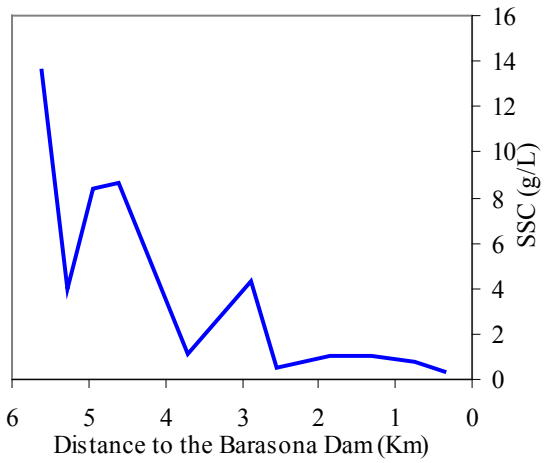


**Figure 4.25 Variation of suspended sediment concentration along a longitudinal profile of the Barasona Reservoir, measured during the field study (autumn, 2005).**

**Table 4.2 Sediment trapping ratio based on measured data of SSC of inflow and outflow discharges (autumn, 2005).**

| Event | SSC of inflow discharges (g/l) | SSC of outflow discharges (g/l) | Trapping ratio (%) |
|---|---|---|---|
| 06/09/2005 | 10.812 | 0.101 | 99.36% |
| 07/09/2005 | 13.584 | 0.225 | 93.43% |
| 08/09/2005 | 0.132 | 0.401 | - |
| 09/09/2005 | 5.325 | 0.039 | 98.17% |
| 10/09/2005 | 0.322 | 0.058 | 52.77% |
| 11/09/2005 | 0.056 | 0.078 | - |
| 12/09/2005 | 0.046 | 0.032 | - |

To account for stratification processes, water temperature was measured from ten vertical profiles in the Barasona Reservoir. Values of water temperature measured from the water surface to the reservoir bed varied gradually from approximately 24ºC at the water surface to circa 19ºC at a depth of 23 m very close to the dam.

# CHAPTER 5

# 5. Model Application

## 5.1. Model Application to the Barasona Reservoir in Spain

### 5.1.1. Model Parameterization

The reservoir sedimentation model was applied to the Barasona reservoir for the periods 1986-1997 (calibration) and 1998-2006 (validation). Table 5.1 gives an overview on the required parameters. The longitudinal profile of the Barasona reservoir was divided into 53 cross-sections, taking into account some selection rules:

- Ratio of the areas between two adjacent cross-sections should lie between 2/3 and 3/2.
- At least one cross-section at the river sub-reach.
- The most downstream cross-section should be located very close to the dam.
- Cross-section a maximum 5*B* apart, where *B* is the top width of the section
- All sites of key interest.
- Perpendicular to the flow direction.

The bed geometry of the cross-sections at the beginning of the simulation period ($x_i$,$y_i$) and at the year of dam construction ($x_o$,$y_o$) were derived from high-resolution bathymetric surveys of the Barasona reservoir. The initial bed composition $P_i$ at the beginning of the simulation period was estimated for each cross-section using data from sediment cores collected in the Barasona reservoir after emptying for flushing operations in the years 1995, 1996 and 1997 (Valero-Garces et al., 1999). On average, the deposited material is composed of almost 80% of silt.

For the longitudinal profile, the distance between adjacent cross-sections $L$ was defined following the selection rules presented previously. The Manning's coefficient $n$ along the longitudinal profile was estimated using reference values available in the literature (Chow, 1959; Graf, 1984; Barnes, 1967). The active layer thickness $f_{act}$ was derived by calibration (see Section 5.1.2). The parameter $f_{act}$ represents the maximum thickness of the active layer exposed to erosion at daily time step.

**Table 5.1 Required parameters at the different scale levels.**

| Parameters at the spatial scale levels | Unit |
|---|---|
| Cross section | |
| - initial bed geometry ($x_i$,$y_i$) | m |
| - original bed geometry ($x_o$,$y_o$) | m |
| - initial bed composition ($P_i$) | % |
| Longitudinal profile | |
| - distance between cross sections (L) | m |
| - Manning's coefficient (n) | - |
| - active layer thickness ($f_{act}$) | $m.day^{-1}$ |
| Reservoir | |
| - minimum reservoir level ($H_{min}$) | m |
| - maximum reservoir level ($H_{max}$) | m |
| - initial reservoir volume ($V_o$) | $1000.m^3$ |
| - maximum storage capacity ($V_{max}$) | $1000.m^3$ |
| - maximum reservoir area ($A_{max}$) | ha |
| - maximum water withdrawal ($Q_{max}$) | $m^3.s^{-1}$ |
| - year of dam construction ($t_o$) | - |
| - volume-area coefficients (a,b) | - |
| - spillway coefficients (c,d) | - |
| - dry bulk density ($\rho_d$) | $t.m^{-3}$ |

The parameters related to the reservoir body were provided by the CHEBRO (Hydrological Confederation of the Ebro Basin). Volume-area coefficients were derived from measurements of area and volume of the Barasona reservoir at different levels, as presented in Figure 5.1, specifically for the year 1986. Dry bulk density of the material deposited $\rho_d$ at the Barasona reservoir was determined by

laboratory analysis of sediment cores collected during fieldwork campaigns. An average value of 1.5 t.m$^{-3}$ was found (see Table 4.1).

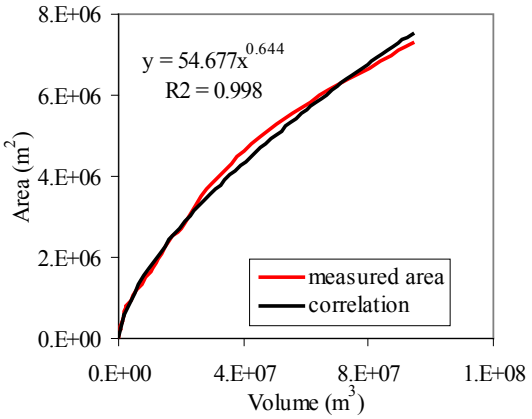


**Figure 5.1 Area-volume relationship of the Barasona reservoir.**

In order to minimize the uncertainties of using rainfall-runoff models, measurements of water discharges upstream from the reservoir at the gauging stations Isábena and Esera were used as inflow discharges into the reservoir. Measurements of suspended sediment concentration SSC were analysed and compared to water discharges in order to obtain a simple sediment rating curve. Nevertheless, SSC displayed only a weak correlation ($R^2$ = 0.0053) with water discharge (Figure 5.2). Instead, ancillary variables acting as driving forces or proxies for the processes (rainfall, cumulative discharge, rising/falling limb data) were included in a Quantile Regression Forests model (QRF model) to explain the variability in SSC, as proposed by Francke et al. (submitted). Measurements of SSC were recorded at a 15-min time interval at the Isábena gauging stations. Additionally, water samples were collected either automatically using an ISCO sampler or manually. The ancillary data used included 15-min rainfall data from 4 Spanish stations (Capella, Las Paules, Casa Llera and Castigaleu stations) and 15-min water discharge (Capella gauging station). To account for transmission times, rainfall from Las Paules was lagged by 5 hours, Castigaleu and Casa Llera by 1 hour. From these predictors, additional variables were derived: cumulated rainfall and discharge, each for 6, 24 and 48 hours. Discharge was also cumulated for 1 hour and its rate of change in a time window of +-2.5 hours was computed. Using the QRF model, a sedigraph was produced derived from the ancillary data. The results, depicted in Figure 5.3, showed that the QRF model worked adequately in the prediction of SSC using ancillary data, with a $R^2$ of 0.92.

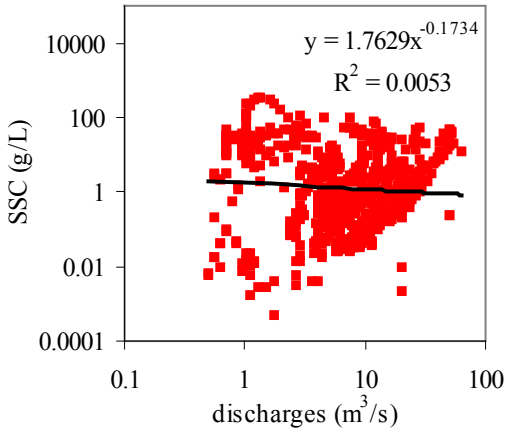


**Figure 5.2 Correlation between water discharges and suspended sediment concentration SSC at the Isábena gauging station.**

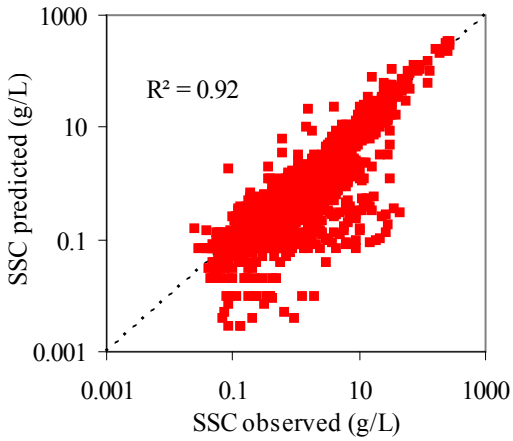


**Figure 5.3 Comparison of observed SSC with predicted SSC (QRF model) at the Isábena gauging station for the 15-min time scale.**

The QRF model resulting from training data of SSC during the observation period (2005-2007) was applied to the period 1998-2006, allowing the computation of mean daily SSC. A comparison of mean daily SSC derived from observed 15-min data with mean daily SSC obtained from the calculation using the QRF model is presented in Figure 5.4. The results indicated that the proposed approach was able to predict SSC using ancillary data despite the considerable decrease in temporal resolution, even with a lower correlation ($R^2 = 0.38$). In a second step, another QRF model for the prediction of mean daily SSC was trained using the results obtained from the previous step, based on ancillary data that are available on the daily time scale (discharge at Esera and Isábena gauging stations, daily rainfall from the Serraduy station, and derived data such as cumulative and rate-of-change as in the 15-min-model). The resulting model was then applied to the entire period of interest (1986-2006). SSC values at the Esera gauging station were assumed to be equal to those predicted for the Isábena gauging station. The total sediment inflow into the Barasona reservoir derived from the QRF models for the period 1986-1993 was compared to that estimated using a sediment trapping efficiency of 85% according to Brune (1953), volume changes between high-resolution bathymetric surveys and a dry bulk density of 1.5 $t.m^{-3}$. The comparison led to the application of a correction factor of 0.7 to approximate the SSC values derived from the QRF models to those obtained according to the above mentioned method.

The grain size distribution of the incoming sediment was obtained from granulometric analysis of sediment derived from 21 water samples collected at the Isábena gauging station since 2004. The results are shown in Figure 5.5. All model simulations for the Barasona reservoir used ten sediment classes, with grain size distribution derived from mean measured values. A sensitivity analysis of the model performance for different number of sediment classes is presented in Section 5.1.4.

Precipitation and evaporation time series used for the calculation of the water balance at the Barasona reservoir were derived from climate stations located close to the reservoir. Time series of outflow discharges, which include spillway overflow, water withdrawal to supply the Aragon and Catalunya Canal, and water discharges through the bottom, were provided by CHEBRO. Measured data of water inflow and outflow discharges were used as input files to calibrate the sediment balance model.

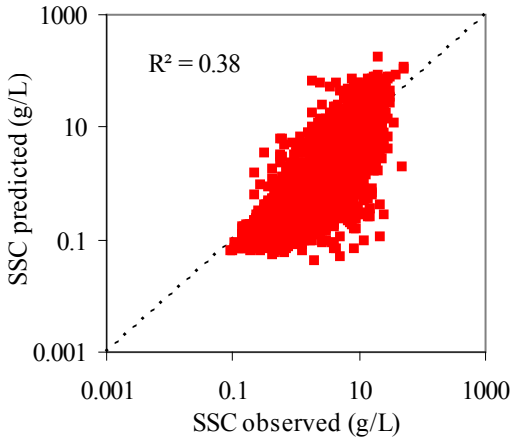


**Figure 5.4 Comparison of observed SSC with predicted SSC at the Isábena gauging station for daily time scale.**

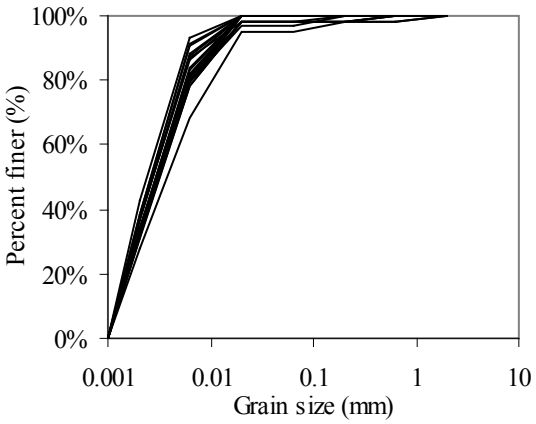


**Figure 5.5 Grain size distribution of the incoming sediment into the Barasona Reservoir.**

For the calculation of the sediment carrying capacity at the cross-sections of the Barasona reservoir during the calibration and validation stages, the equation proposed by Wu et al. (2000a) was selected. According to Mamede et al. (2006), the sediment transport equation after Wu yielded the best results in the simulation of

sediment deposition in the Barasona reservoir as compared with that proposed by Tsinghua University (IRTCES, 1985). The sediment transport equations proposed by Ackers and White (1973) and Ashida and Michiue (1973) could not be applied to the Barasona reservoir because they do not work appropriately within the reservoir sedimentation model for grain sizes below 0.04 mm. A sensitivity analysis for the application of different sediment transport equations is presented in Section 5.1.4.

### 5.1.2. Calibration

The calibration of the reservoir sedimentation model for the Barasona reservoir consisted of two stages: an application for the period 1986-1993 without sediment management operations, i.e. the bottom outlets remained closed during this period; and an application for the period 1995-1997, which is characterized by yearly flushing operation.

In the simulation for the period 1986-1993, a sensitivity analysis was performed to test the effect of changes in parameters values on model results According to the sensitivity analysis, the performance of the reservoir sedimentation model to assess bed elevation variation along the longitudinal profile of the reservoir is quite sensitive to changes on the parameter $f_{act}$ (see Section 3.4.5), which accounts for the maximum thickness of the active layer available for erosion, as presented in Figure 5.6. Nevertheless, close to the dam, bed elevations do not change significantly, which may be explained by the fact that deposition processes are dominant there. The best model performance for the assessment of bed elevation changes along the longitudinal profile of the reservoir and cross-sections, and distribution of sediment deposition was obtained using a $f_{act}$ of 3 cm.day$^{-1}$ (Fig. 5.6b). The blue points plotted in Figure 5.6b show the location of the cross-sections analysed in detail in terms of bed elevation changes.

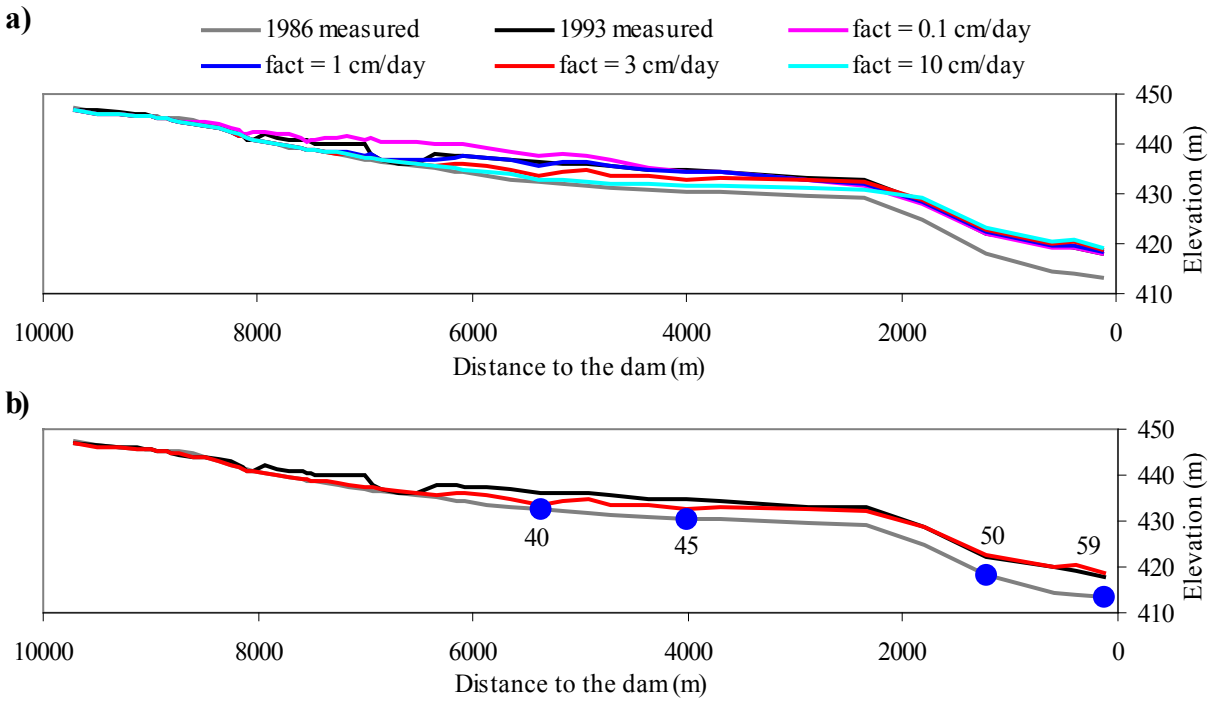


**Figure 5.6 Bed elevation changes along the longitudinal profile of the Barasona Reservoir (1986-1993) computed: a) for different values of the parameter $f_{act}$; and b) for a $f_{act}$ of 3 cm.day$^{-1}$, which resulted in the best model performance (blue points show the location of the cross-sections analysed in detail).**

Other model results after the calibration of $f_{act}$, such as sediment volume changes caused by either deposition or erosion along the longitudinal profile of the Barasona reservoir and bed elevation changes at four different cross-sections, were evaluated for the simulation period 1986-1993 (Figs. 5.7 and 5.8, respectively). The location of the four cross-sections is shown in Figure 5.6. The model results plotted in Figures 5.7 and 5.8 were compared to observed data derived from the high-resolution bathymetric survey of 1998 performed in the Barasona reservoir. The results showed that the calibration of a single parameter ($f_{act}$) enabled the reproduction of the sediment deposition pattern of the Barasona reservoir in that period. Considerable deviation close to the reservoir inlet may be explained by singularities of the reservoir morphology (lateral constrictions and sharp bend of the narrow channel).

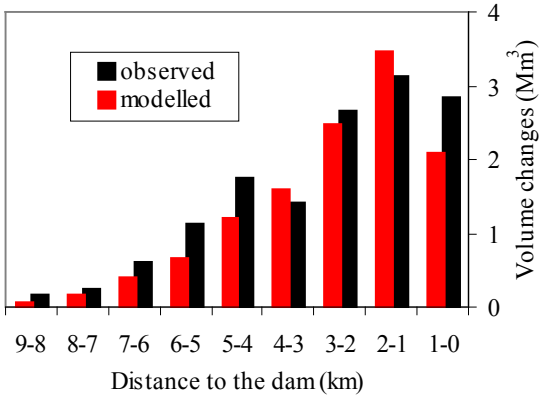


**Figure 5.7 Sediment volume changes along the longitudinal profile of the Barasona reservoir for the simulation period 1986-1993.**

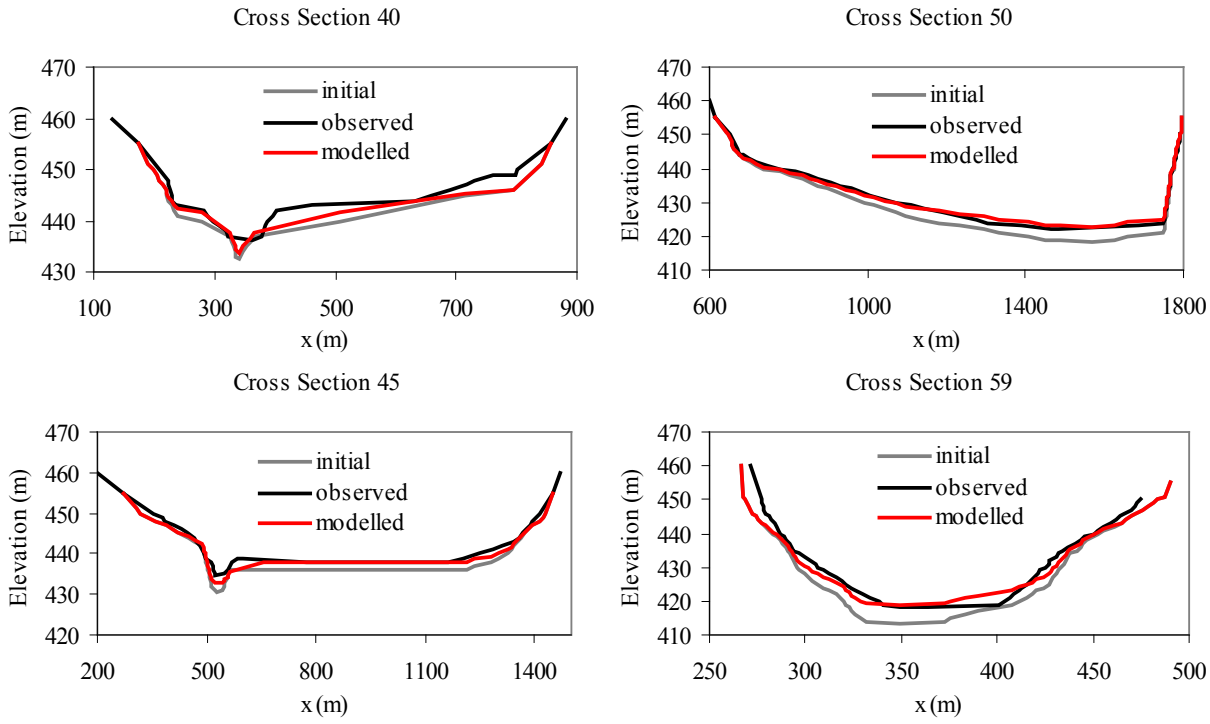


**Figure 5.8 Bed elevation changes at four different cross-sections of the Barasona reservoir for the simulation period 1986-1993.**

The parameterization derived from the model calibration for the period 1986-1993 was set and applied to the period 1995-1997 (case 1). Unfortunately, the model was not able to simulate the high sediment release caused by yearly flushing operations, as depicted in Figure

5.9. In case 1, deposition processes continue to be the driving force in explaining sediment distribution within the Barasona reservoir.

According to Morris and Fan (1997), reservoir drawdown by opening a low-level outlet to temporarily establish riverine flow along the reservoir results in a retrogressive channel erosion through the deposits and high sediment release through the outlet. Retrogressive erosion is characterized by a zone of high slope and rapid erosion, moving upstream along a channel having a lower slope and erosion rate. It is the main process explaining the formation of flushing channels through reservoir deposits. The point of slope change, also called nickpoint, will move either upstream during flushing operations or downstream through delta development.

To account for retrogressive erosion during flushing operations, two new steps were included into the reservoir sedimentation model: identification of the movable nickpoint within the reservoir at the simulation time step; and application of a variable $f_{act}$ within the downstream reach of the reservoir defined by the nickpoint. Slope changes along the longitudinal profile of the reservoir indicate the new position of the nickpoint. The parameter $f_{act}$ was assumed to vary linearly within the reach between the nickpoint and the dam, remaining constant at the upstream reach of the reservoir ($f_{act}$ = 3 cm.day$^{-1}$). The maximum value of $f_{act}$ ($f_{act,max}$) was calibrated for the simulation period 1995-1997. Four different scenarios concerning the longitudinal variability of the parameter $f_{act}$ were tested. The parameter $f_{act,max}$ was set to 3, 15, 25 and 35 cm.day$^{-1}$ depending on the scenario. Results of the model calibration for the different scenarios are presented in Figure 5.10. According to Figure 5.10, the model simulation using a $f_{act,max}$ of 25 cm.day$^{-1}$ presented the best results.

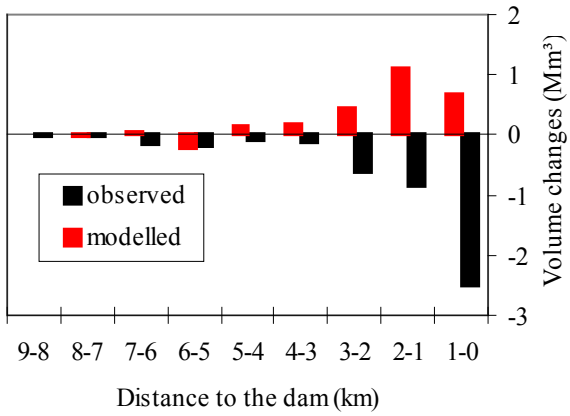


**Figure 5.9 Sediment volume changes along the longitudinal profile of the Barasona reservoir for the simulation period 1995-1997 (case 1).**

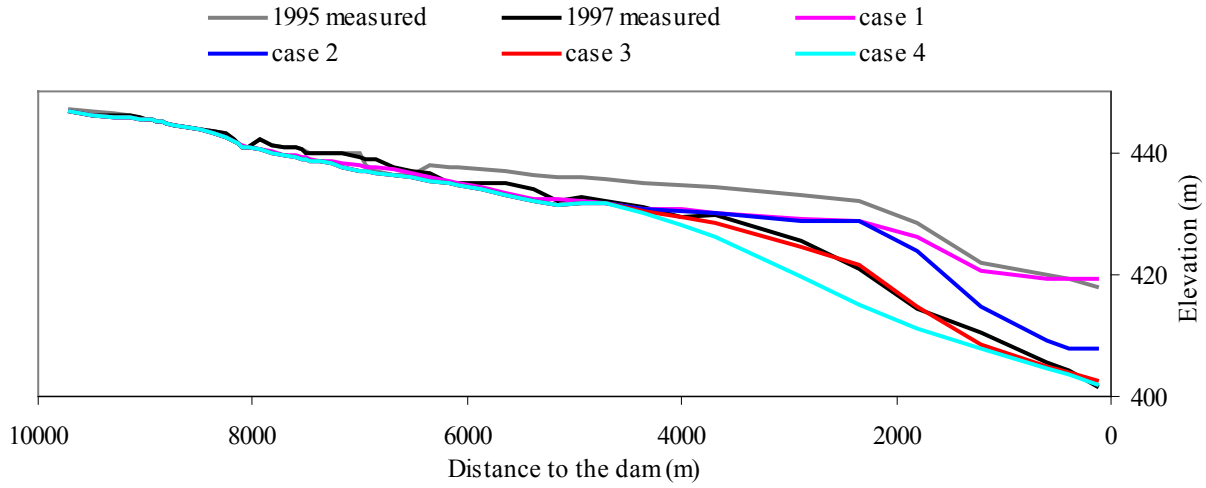


**Figure 5.10 Bed elevation changes along the longitudinal profile of the Barasona Reservoir (1995-1997) computed for different scenarios concerning the longitudinal variability of the parameter $f_{act}$: case 1 (3 cm.day$^{-1}$); case 2 (3 to 15 cm.day$^{-1}$); case 3 (3 to 25 cm.day$^{-1}$); and case 4 (3 to 35 cm.day$^{-1}$).**

To assess the ability of the model to simulate sediment volume changes along the longitudinal profile of the Barasona reservoir during the flushing operations (1995-1997), a $f_{act,max}$ of 25 cm.day$^{-1}$ was set (case 3). The results, summarized in Figure 5.11, showed that the model with those modifications concerning the identification of the nickpoint and the use of a variable $f_{act}$ was able to simulate the processes related to flushing operations. Further results concerning the bed elevation changes are presented in Figure 5.12 for four different cross-sections. For the cross-section 50, the model was not able to predict changes on the position of the deepest point, although the computed sediment volume changes are quite similar to the observed ones. At the cross-sections 40 and 59, a marginal overestimation of the volume of sediment remobilized during the flushing operations was observed. Overall, the results of sediment distribution along the longitudinal profile and the cross-sections of the Barasona reservoir are in good agreement with observed values derived from the high-resolution bathymetric survey of 1998.

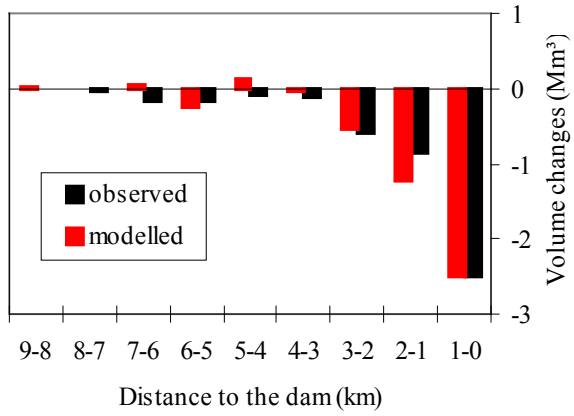


**Figure 5.11 Sediment volume changes along the longitudinal profile of the Barasona reservoir for the simulation period 1995-1997 (case 3).**

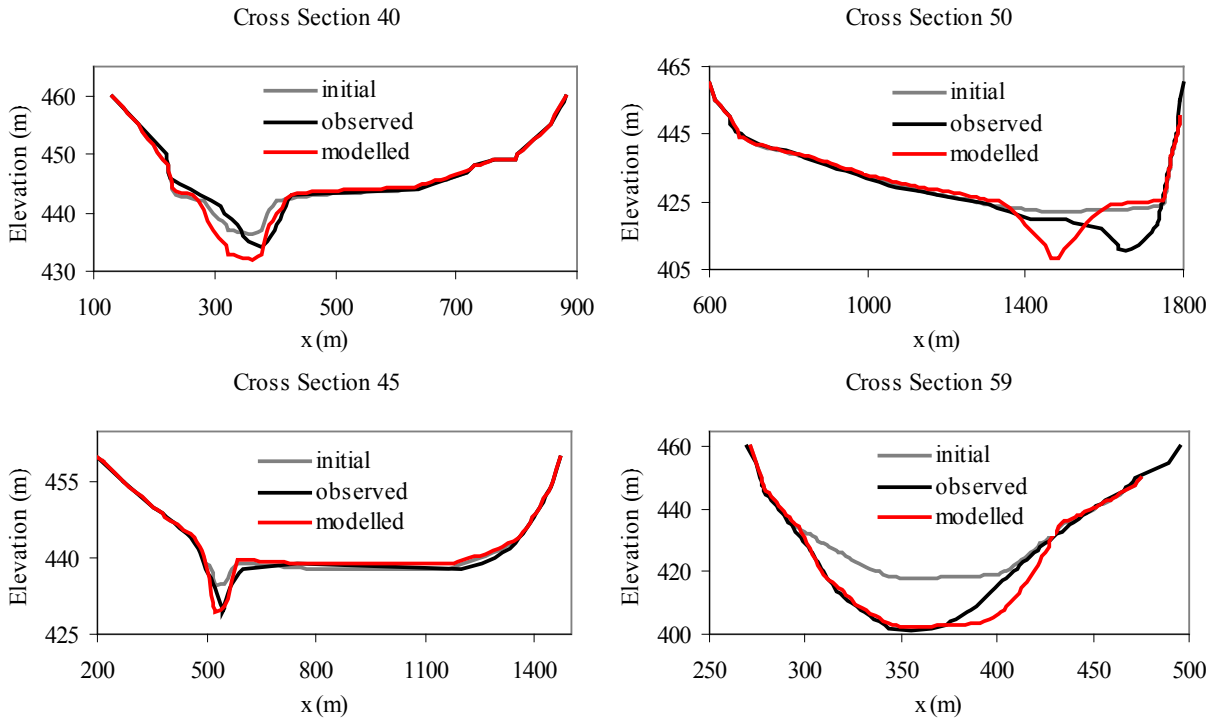


**Figure 5.12 Bed elevation changes at four different cross-sections of the Barasona reservoir for the simulation period 1995-1997.**

### 5.1.3. Validation

To evaluate the efficiency of the reservoir sedimentation model, it was applied to the simulation of a 10-year period of sediment deposition at the Barasona reservoir (1998-2006). The model parameters that produced the best model performance at the calibration stages were set. The high-resolution bathymetric survey of 2007 was used to check the model results.

Figure 5.13 shows the bed elevation changes along the longitudinal profile of the Barasona reservoir for the simulation period 1998-2006. As presented in Figure 5.13, the reservoir sedimentation model was able to simulate the vertical variation of the longitudinal profile caused by either deposition or remobilization of sediment. Nevertheless, at the downstream part of the reservoir, the model overestimated sediment remobilization, whereas at the reach between 2 and 4 km away from the dam, it overestimated deposition processes, which may explain the underestimation of sediment deposition close to the dam.

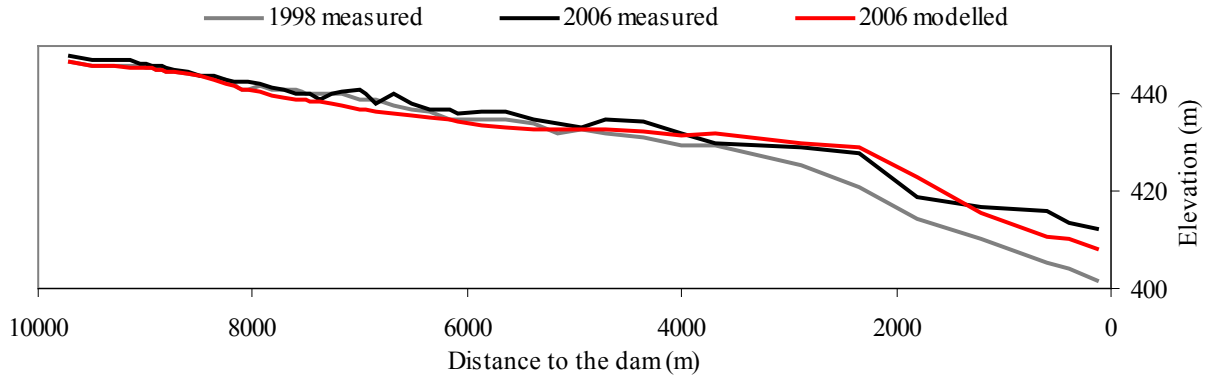


**Figure 5.13 Bed elevation changes along the longitudinal profile of the Barasona Reservoir for the simulation period 1998-2006.**

Changes in sediment volumes along the longitudinal profile of the Barasona reservoir for the simulation period 1998-2006 were also checked. The results, depicted in Figure 5.14, showed that the model overestimates to some extent the total volume of sediment deposited in the Barasona reservoir, particularly at an intermediate reach between 2 and 4 km away from the dam. The observed overestimation may be explained by the uncertainties of the QRF model in the prediction of sediment inflow discharges or further issues presented in Section 5.1.4.

Concerning the bed elevation changes for the cross-sections, model results are plotted for four different sections, as shown in Figure 5.15. Apart from section 40, where the model overestimated the sediment remobilization, the distribution of sediment at the other three cross-sections was well reproduced by the reservoir sedimentation model. At the most downstream cross-section (section 59), the model underestimated the total volume of incoming sediment, as a result of a high deposition rate for the upstream cross-sections.

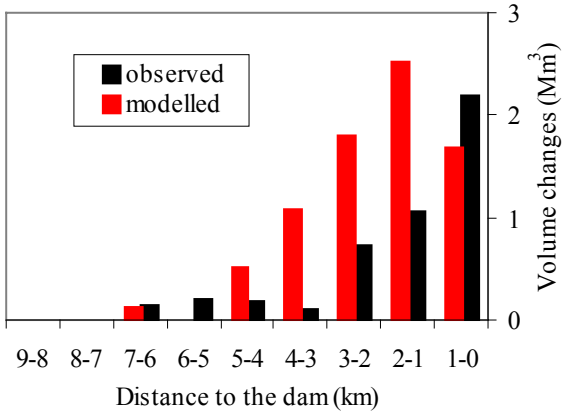


**Figure 5.14 Sediment volume changes along the longitudinal profile of the Barasona reservoir for the simulation period 1998-2006 (case 3).**

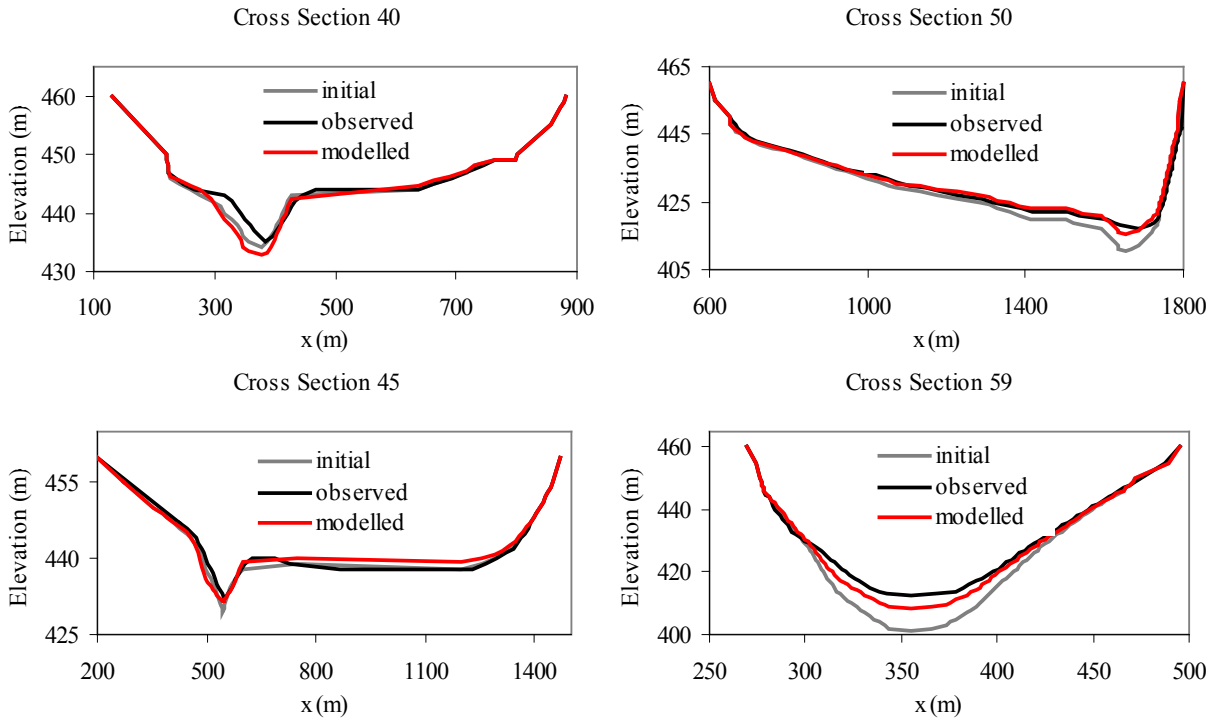


**Figure 5.15 Bed elevation changes at four different cross-sections of the Barasona reservoir for the simulation period 1998-2006.**

### 5.1.4. Sensitivity and Uncertainties

In the following, the reservoir sedimentation model is applied to evaluate its sensitivity to input data, parameters and model structure and to assess the related uncertainty. All model simulations were performed for the period 1986-1993 and the results were compared to those obtained from the best model performance on the calibration stages.

Firstly, the model performance was tested for different sediment transport equations: Wu et al. (2000a) and Tsinghua University (IRTCES, 1985). Figure 5.16 shows the sediment volume changes along the longitudinal profile of the Barasona Reservoir for both sediment transport equations, whereas Figure 5.17 illustrates the bed elevation changes along the longitudinal profile. The results summarized in Figures 5.16 and 5.17 showed that both sediment transport equations were able to reproduce the sediment deposition pattern for the period, as compared to measured data derived from high-resolution bathymetric surveys.

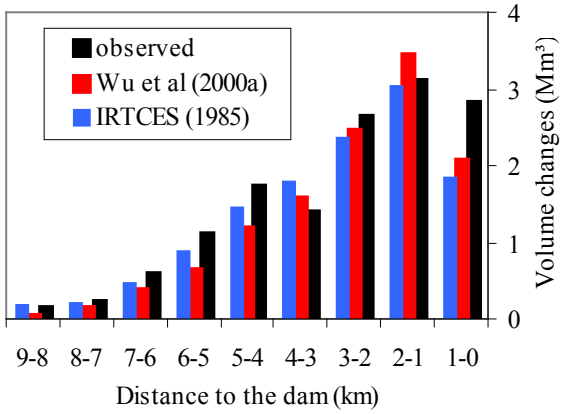


**Figure 5.16 Sediment volume changes along the longitudinal profile of the Barasona reservoir for the simulation period 1986-1993, computed using the equations proposed by Wu et al. (2000a) and Tsinghua University (IRTCES, 1985).**

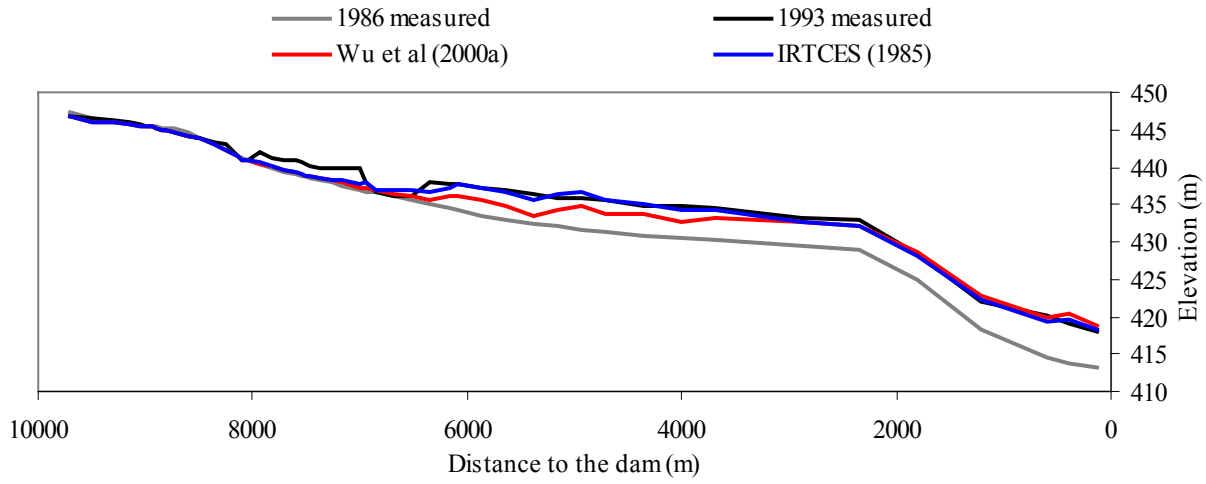


**Figure 5.17 Bed elevation changes along the longitudinal profile of the Barasona Reservoir for the simulation period 1986-1993, computed using the equations proposed by Wu et al. (2000a) and Tsinghua University (IRTCES, 1985).**

As the sediment transport equations proposed by Ackers and White (1973) and Ashida and Michiue (1973) are not applicable within the reservoir sedimentation model for the assessment of the transport of fine sediments ($d$ < 0.040 mm), a simulation using hypothetical data of grain size distribution of the incoming sediment was performed for the Barasona reservoir at the same period (1986-1993) to assess the model sensitivity to the four available equations. Results of sediment distribution along the longitudinal profile of the Barasona Reservoir are presented in Figure 5.18 for the four selected sediment transport equations. As shown in Figure 5.18, applications of the reservoir sedimentation model to simulate the transport of coarse sediment through a reservoir enable the assessment of delta development, characterized by rapid deposition of coarse sediment at the zone of inflow.

To assess the model sensitivity to different numbers of cross-sections, three model simulations were performed for the Barasona reservoir for 1986-1993 using 14, 27 and the minimum number of cross-sections obtained according to the selection rules presented in Section 5.1.1 (53 cross-sections). The model sensitivity to the number of cross-sections is evaluated through the simulation of sediment deposition along the longitudinal profile of the Barasona reservoir. The results, depicted in Figure 5.19, showed that the higher the discretization of the longitudinal profile (larger number of cross-sections), the better the model's ability to represent the bed elevation variation along the longitudinal profile.

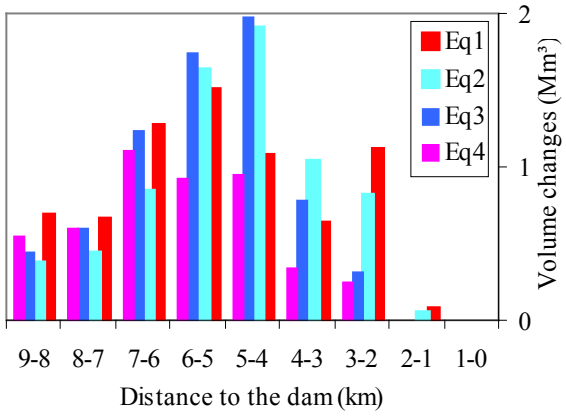


**Figure 5.18 Sediment distribution along the longitudinal profile of the Barasona reservoir for the simulation period 1986-1993, computed with four different equations: Eq1 (Wu et al., 2000a); Eq2 (Ashida and Michiue, 1973); Eq3 (IRTCES, 1985); and Eq4 (Ackers and White, 1973).**

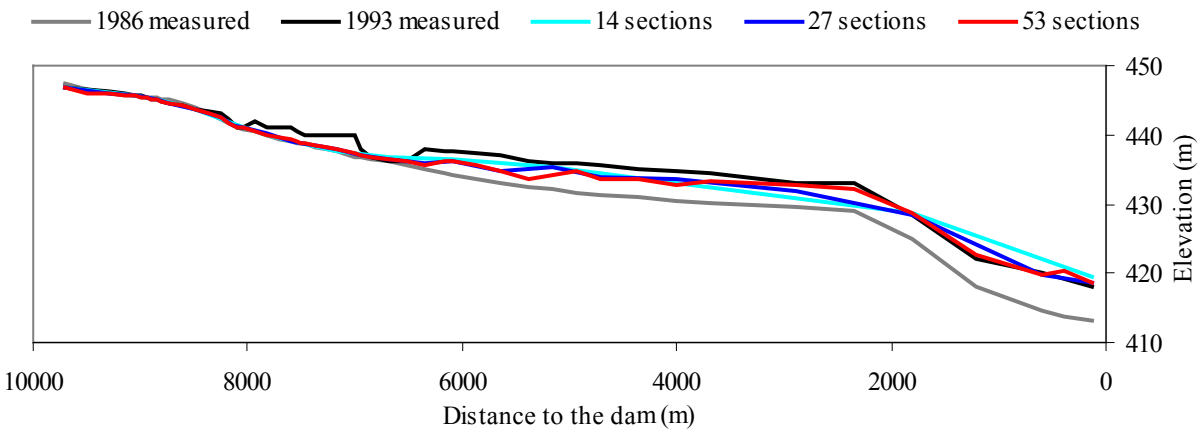


**Figure 5.19 Bed elevation changes along the longitudinal profile of the Barasona Reservoir (1986-1993), computed for a varied number of cross-sections (14, 27 and 53 sections).**

In order to evaluate the model sensitivity to the application of a varied number of grain size classes, simulations were performed for the Barasona reservoir for 1986-1993 using 3, 5 and 10 grain size classes. The limits of the particle size classes used in the model simulations are presented in Table 5.2. Sediment distribution along the longitudinal profile of the Barasona Reservoir was computed using the reservoir sedimentation model for 3, 5 and 10 particle size classes, as presented in Figure 5.20. The results of the model applications indicated that a decrease in the number of sediment classes causes an increase in sediment deposition at the upstream part of the reservoir. The discrepancy between the results from the three model simulations (3, 5 and 10 grain size classes) may be explained by the fact that the calculation of sediment transport through the reservoir is performed for the mean diameters of the particle size classes, which differ significantly from each other, depending on the discretization used. Therefore, the larger the number of the particle size classes, the higher the model accuracy in reproducing the non-uniform sediment transport represented by size classes.

Uncertainty in the simulation results was high, not only due to uncertainties of input data, such as sediment inflow discharges derived from QRF models, grain size distribution of incoming sediment and properties of the material previously deposited (bed composition, dry bulk density, deposition thickness), but also due to uncertainties in the model structure to represent adequately the transport of water and sediment through the reservoir. Furthermore, uncertainties in using the Rouse equation (Eq. 3.87) for the calculation of vertical distribution of suspended sediment concentration immediately upstream of the dam should be considered. Although the Rouse equation was developed for equilibrium conditions in rivers (Morris and Fan, 1997), it was included in the reservoir sedimentation model to account for the sediment release efficiency of outlet devices (see Section 3.4.6). According to the literature review, no other equation that accounts for vertical distribution of suspended sediment concentrations was found.

**Table 5.2 Limits of the particle size classes used in the model simulations for the Barasona reservoir (1986-1993).**

| Grain size classes | Limits (mm) | | |
|---|---|---|---|
| | 3 classes | 5 classes | 10 classes |
| 1 | 0.001 - 0.004 | 0.001 - 0.004 | 0.001 - 0.002 |
| 2 | 0.004 - 0.063 | 0.004 - 0.016 | 0.002 - 0.004 |
| 3 | 0.063 - 4.000 | 0.016 - 0.063 | 0.004 - 0.008 |
| 4 | | 0.063 - 1.000 | 0.008 - 0.016 |
| 5 | | 1.000 - 4.000 | 0.016 - 0.031 |
| 6 | | | 0.031 - 0.063 |
| 7 | | | 0.063 - 0.125 |
| 8 | | | 0.125 - 1.000 |
| 9 | | | 1.000 - 2.000 |
| 10 | | | 2.000 - 4.000 |

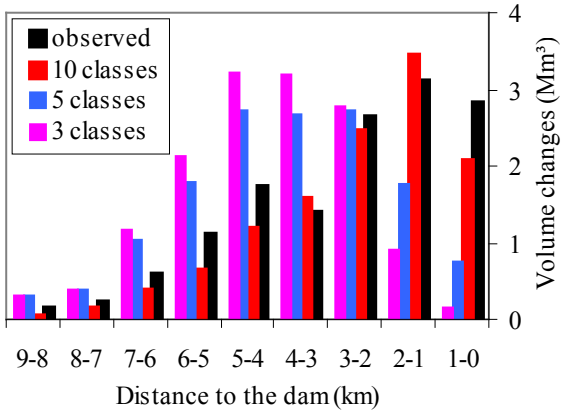


**Figure 5.20 Sediment distribution along the longitudinal profile of the Barasona reservoir (1986-1993), computed for four different number of grain size classes (3, 5 and 10 classes)**

## 5.2. Model Application to the Benguê Catchment in Brazil

### 5.2.1. Model Parameterization

**Catchment**

To simulate water fluxes within the Benguê catchment, the WASA-SED model was parameterized. Land cover characterization was performed by Creutzfeldt (2006). Climate data were derived from 16 climate stations located within and around the Benguê catchment by inverse-distance interpolation. High-resolution topographic maps generated from ASTER images were used to identify the spatial units of the corresponding catchment (sub-basins). For the characterization of soil units, data from RADAMBRASIL soil map (1981) were used. Spatial discretization resulted from the application of a semi-automated algorithm (Francke et al., in Press)

For the simulation of sediment fluxes, the USLE parameters were evaluated. The soil erodibility factor (*K*) was computed from the particle size distribution of the topmost horizon of each soil using an equation proposed by Williams (1995). The USLE cover and management factor (*C*) was either measured during fieldwork or obtained from tabulated values according to the land cover identified within the Benguê catchment. As no practice of erosion protection was observed in the study area, the support practice factor (*P*) was set to 1. The USLE topographic factor (*LS*) is calculated implicitly within the WASA-SED model, taking into account the topographic characteristics of the terrain components. Rough estimates of mean Manning's n for surface roughness were assigned according to land-use classes based on data obtained during fieldwork in the Benguê catchment or estimated for the remaining classes according to values given in the literature (Morgan, 2005).

**Reservoir Network**

The simplified modelling approach of reservoir sedimentation was tested for the Benguê catchment in Brazil. In total, 114 reservoirs with a wide range of surface areas (from 300 to 830,000 m²) were identified in the Benguê catchment, as presented in Appendix 1. Those reservoirs were classified into strategic reservoirs and small reservoirs, according to their size and location. Strategic reservoirs are medium and large-sized reservoirs located on main rivers at the sub-basin's outlet, whereas small reservoirs are located on tributary streams and represented in the model in an aggregate manner (see Section 3.5). Eleven reservoirs were selected as strategic, following its definition. They are characterised by means of their stage-area-volume curve, spillway geometry, water withdrawal, operating conditions of water intake devices, year of dam construction, etc. Amongst others, the 19.6-$Mm^3$ Benguê reservoir, located at the catchment outlet, is treated in the model simulation as a strategic reservoir.

The maximum surface area of the reservoirs was estimated using satellite imageries of very wet years in 2002 and 2004 with 15-m resolution. It was assumed that the maximum reservoir areas correspond to the maximum values obtained from the comparison of both years. Maximum storage capacities were computed using the Molle equation (Eq. 3.96). Average values of the empirical parameters of

the Molle equation (c = 2.7 and d = 1000) were tested for 21 reservoirs located in the Benguê catchment, as presented in Figure 5.21. The results are in good agreement with measured reservoir volumes.

For the application of the cascade routing scheme, the reservoirs of the Benguê catchment were grouped into five size classes according to their storage capacity. The range of the reservoir size classes was then defined for the Benguê catchment, as presented in Table 5.3.

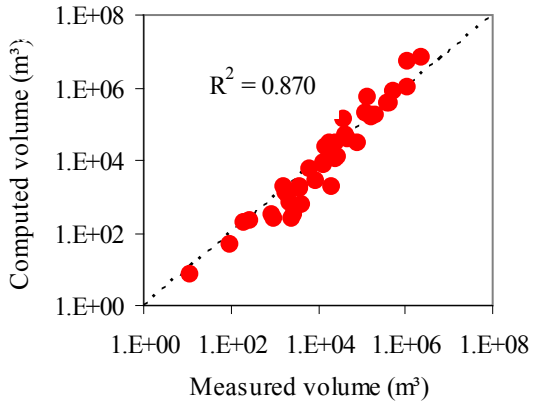


**Figure 5.21 Evaluation of applicability of the Molle parameters to 21 reservoirs located in the Benguê catchment.**

**Table 5.3 Reservoir size classes identified in the Benguê catchment according to their storage capacity.**

| Reservoir class | Range ($10^3 m^3$) | Number of reservoirs |
|---|---|---|
| 1 | < 5 | 43 |
| 2 | 5 - 25 | 36 |
| 3 | 25 - 50 | 9 |
| 4 | 50 - 100 | 6 |
| 5 | 100 - 250 | 9 |

Water and sediment transfer between reservoir classes and water and sediment retention in the small reservoirs were computed using the simplified modelling approach of reservoir sedimentation. For the strategic reservoirs, the water and sediment balance are calculated individually. Nevertheless, due to the lack of information about the geometric features of these reservoirs and physical properties of sediment deposits, a simplified sediment budget was carried out, as described in Section 3.5.3.

For the model simulations, the Benguê catchment was firstly divided into 11 sub-basins according to the location of the strategic reservoirs. The sub-basins that were still too large were further subdivided to maintain similar sizes, resulting in 30 sub-basins.

### 5.2.2. Calibration

WASA-SED model was calibrated for the 12-$km^2$ Aiuaba experimental catchment (see Fig. 4.1). The model performance was analysed using daily data of inflow discharges into the Boqueirao reservoir derived from reservoir level measurements. Sensitivity analyses were performed to test the effect of changes in parameters values on model results. The parameters used for the model calibration were: the soil depth; the scaling factor for bedrock hydraulic conductivity; the fraction of alluvial soils within the lowest terrain component; and the scaling factor $K_{fcorr}$, which was introduced in the model by Güntner (2002) to counteract the underestimation of rainfall intensities when the temporal resolution of the model is lower than that of rainfall events and their internal variability. The sensitivity analyses indicated that the model results are strongly affected by changes on the scaling factor $K_{fcorr}$. In the WASA-SED model, a constant value of the scaling factor $K_{fcorr}$ was primarily used. However, a significant variation of $K_{fcorr}$ observed in events with different intensities led to the establishment of a relationship between daily rainfall amount $R$ and $K_{fcorr}$, as presented in Figure 5.22.

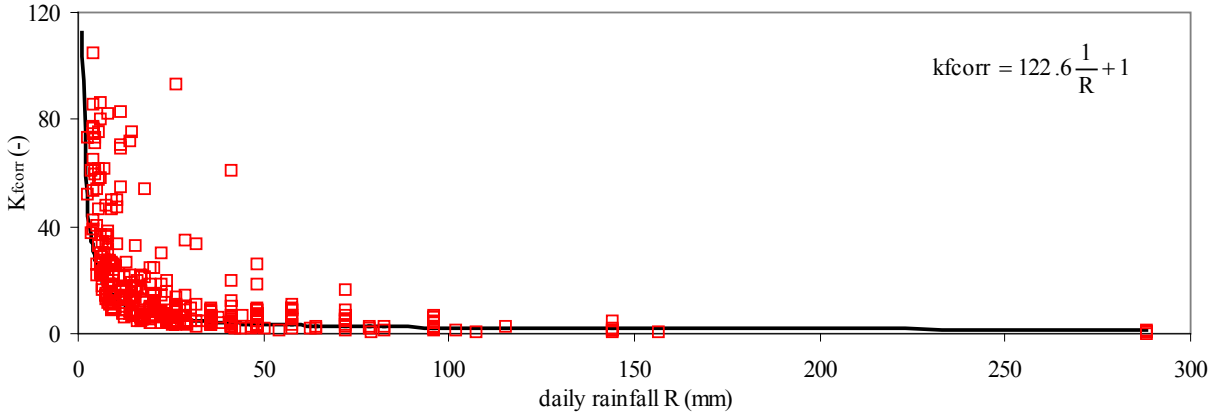


**Figure 5.22 Correlation between daily rainfall *R* and $K_{fcorr}$ observed in the Aiuaba experimental catchment for the period 2000-2006.**

## 5.2.3. Validation

**Reservoir Network**

The WASA-SED model was applied to the 933-km$^2$ Benguê catchment for the period 2000-2006 to test the cascade routing scheme for small reservoirs. The cascade routing scheme is a runoff distribution algorithm that accounts for water and sediment fluxes among reservoir classes (see Section 3.5). The first model simulation (case 1) was performed for 30 sub-basins using the original runoff distribution algorithm as proposed by Güntner (2002). According to Güntner (2002), the generated runoff within a sub-basin is distributed equally among the five reservoir classes and the same fraction is attributed to the water discharge at the sub-basin outlet without retention.

As there is no information about water and sediment fluxes between reservoirs of the study area, the validation of the modelling approach for small reservoirs was based on another model simulation using a detailed discretization of the Benguê catchment with 140 sub-basins. The model simulation using 140 sub-basins (case 2) attempts to give a detailed description of the study area in terms of contributing area for water and sediment yield, reservoir location, water and sediment retention and water and sediment fluxes among reservoir classes. Water and sediment balance are calculated individually for each reservoir and water and sediment transfer among reservoirs is computed using the natural sequence, according to the reservoir location. Due to the lack of test data, it was assumed that the model simulation using 140 sub-basins produces more realistic results through the use of a larger spatial discretization and by taking into account that all reservoirs are treated individually.

Comparing results of modelled inflow discharges into the reservoir classes (1-5) using the original runoff distribution algorithm (case 1) with those using 140 sub-basins (case 2), one notes a very poor model performance in the case 1, with Nash-Sutcliffe coefficients NS varying from minus 4.030 for the reservoir class 4 to 0.396 for the reservoir class 2, as depicted in Figure 5.23. Consequently, the estimation of sediment inflow into the reservoir classes was also not correctly represented by the original cascade routing scheme (see Fig. 5.24). Overall, the model simulation using the original runoff distribution algorithm overestimated the results of water and sediment inflow into the reservoir classes, which may be explained by the fact that the fraction of area controlled by each reservoir size class is smaller than that admitted in the original runoff distribution algorithm (one sixth of the catchment area).

In order to improve the model performance using the cascade routing scheme, another runoff distribution algorithm was applied, as proposed by Vries (2006). In the revised cascade routing scheme (case 3), the fraction of contributing area of each reservoir class is used to calculate the fraction of generated runoff that is attributed as water inflow into the reservoir classes (see Section 3.5.2). The WASA-SED model was applied again to 30 sub-basins of the Benguê catchment using the revised cascade routing scheme (case 3). Simulation results using the revised cascade routing scheme (case 3) were compared to those obtained from the simulation with 140 sub-basins (case 2). Figures 5.25 to 5.28 show the comparison between case 2 and case 3 in terms of water inflow, water outflow, water retention and water storage volume of the reservoir classes. The results showed a good model performance for simulations using the revised cascade routing scheme.

The revised cascade routing scheme was also applied to calculate sediment fluxes into the reservoir classes and sediment transfer among reservoir classes. The fraction of contributing area of each reservoir class is used to calculate the fraction of sediment yield that is attributed as sediment inflow into the reservoir classes (see Section 3.5.3). The components of sediment balance in the reservoirs classes were calculated using the revised cascade routing scheme (case 3) and compared to those obtained from the simulation with 140 sub-basins (case 2). The results, summarized in Figures 5.29 to 5.32, are in good agreement with those computed using 140 sub-basins (case 2). For water and sediment inflow, NS values were greater than 0.89. Accordingly, the results indicated that the revised cascade routing scheme (case 3), firstly developed for the calculation of water transfer among reservoir classes, can be also used to model sediment transfer among the reservoir classes.

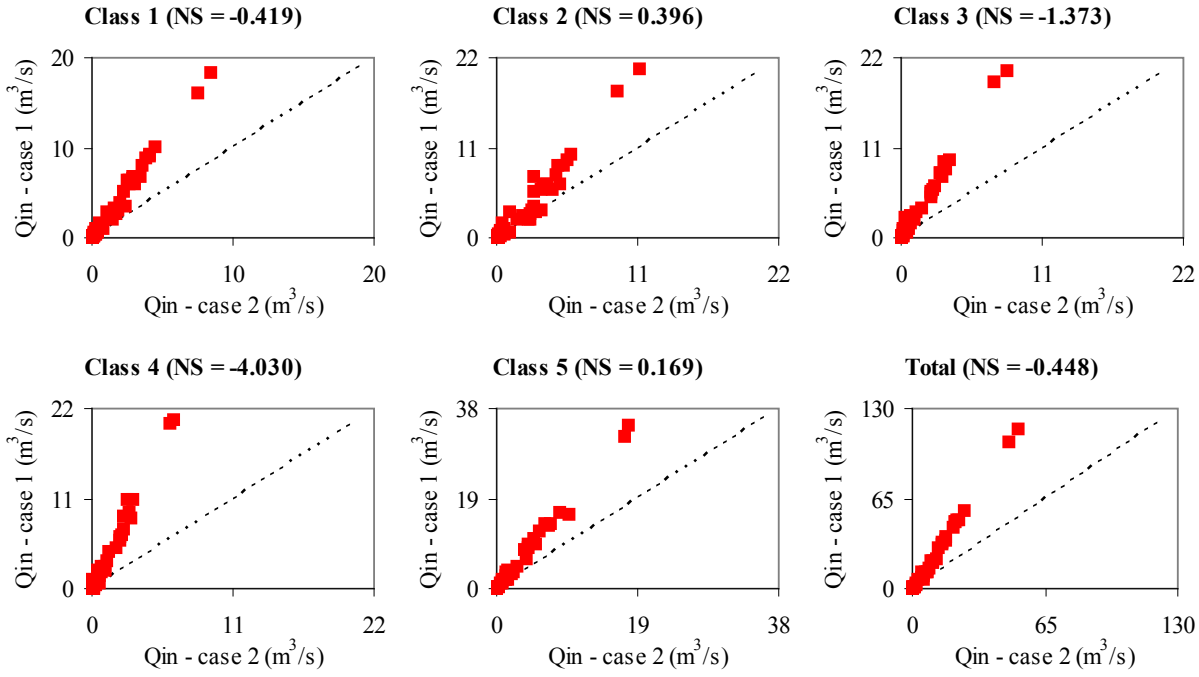


**Figure 5.23 Water inflow into the reservoir classes (1 to 5) and total value for all classes considering: simulation with 30 sub-basins using the original cascade routing scheme (case 1); and simulation with 140 sub-basins (case 2).**

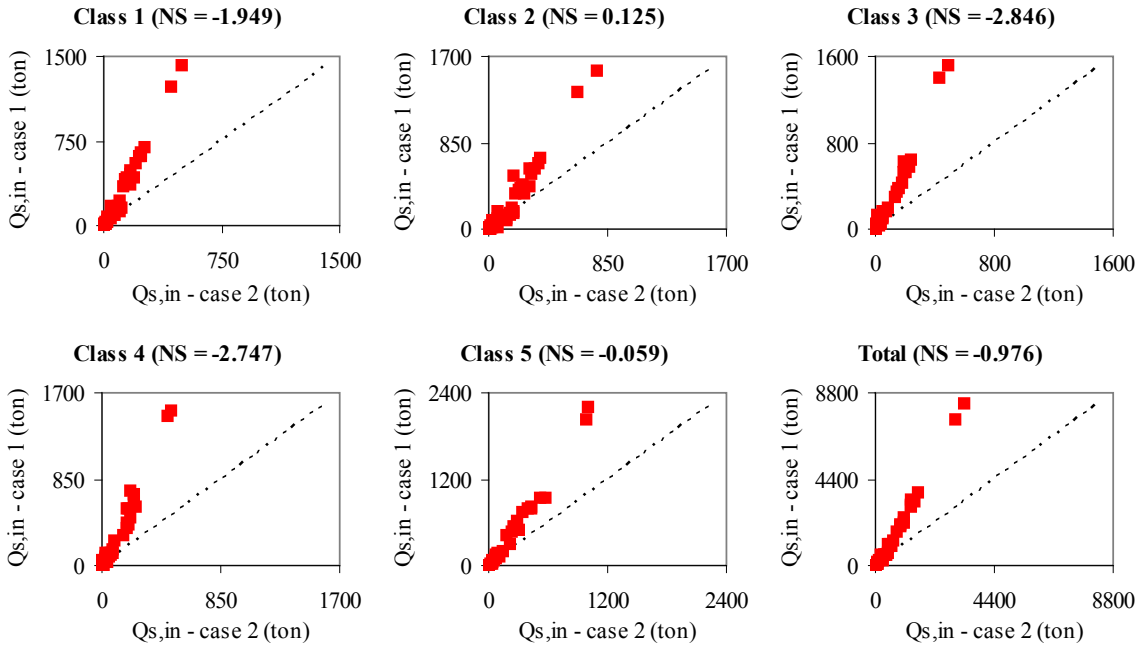


**Figure 5.24 Sediment inflow into the reservoir classes (1 to 5) and total value for all classes considering: simulation with 30 sub-basins using the original cascade routing scheme (case 1); and simulation with 140 sub-basins (case 2).**

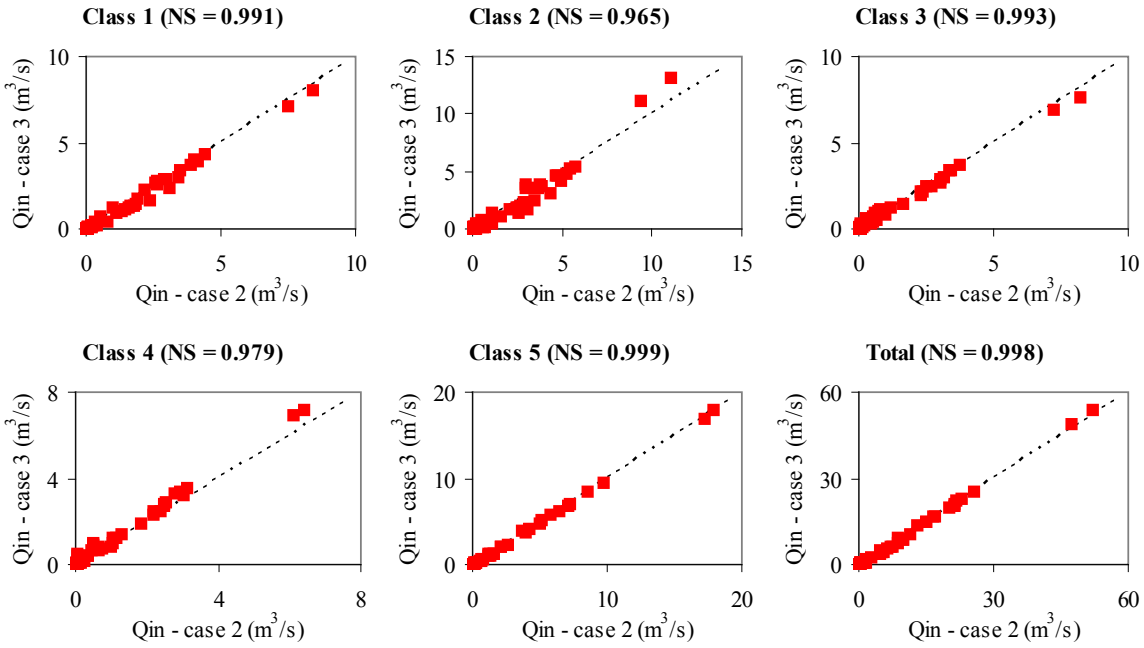


**Figure 5.25 Water inflow into the reservoir classes (1 to 5) and total value for all classes considering: simulation with 30 sub-basins using the revised cascade routing scheme (case 3); and simulation with 140 sub-basins (case 2).**

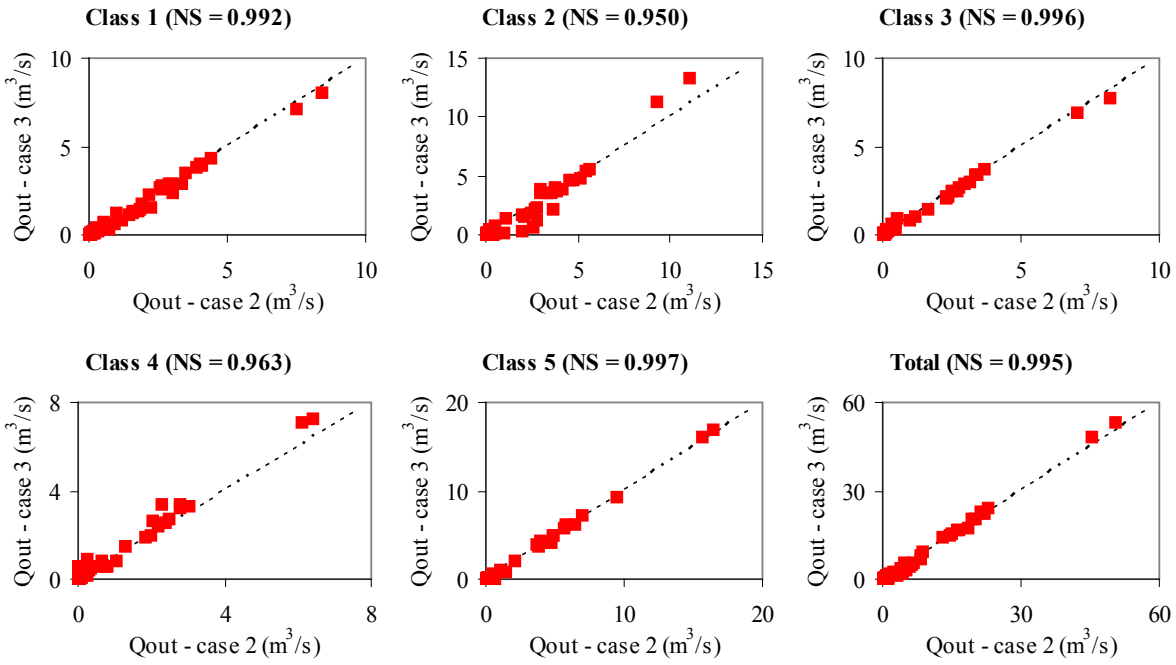


**Figure 5.26 Water outflow from the reservoir classes (1 to 5) and total value for all classes considering: simulation with 30 sub-basins using the revised cascade routing scheme (case 3); and simulation with 140 sub-basins (case 2).**

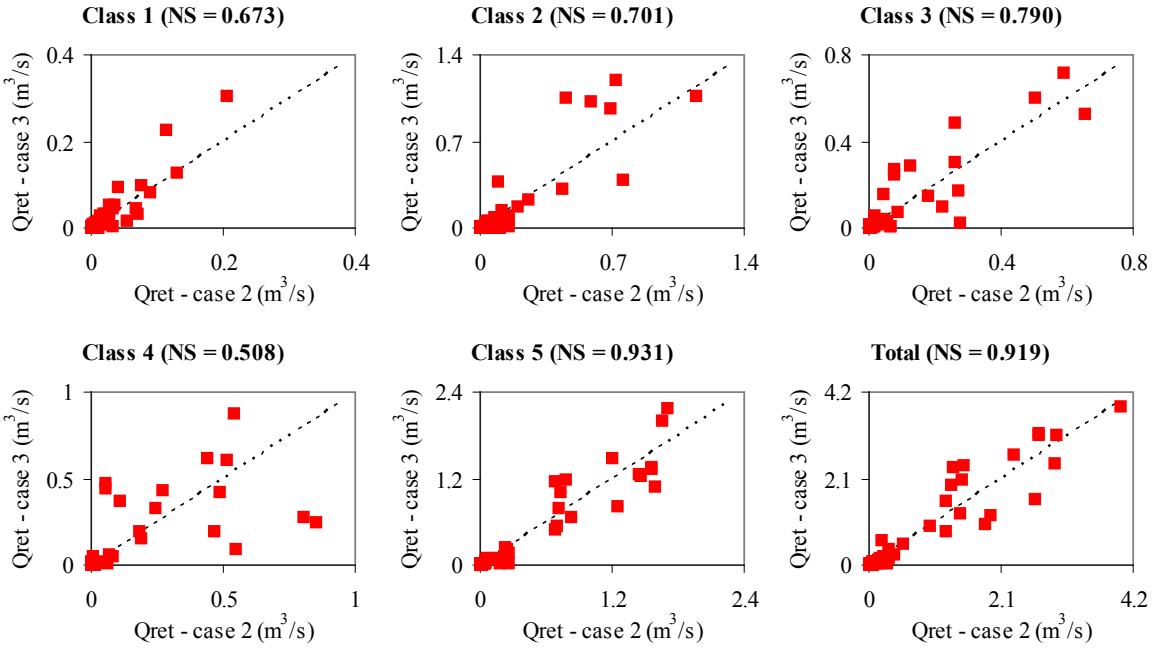


**Figure 5.27 Water retention in the reservoir classes (1 to 5) and total value for all classes considering: simulation with 30 sub-basins using the revised cascade routing scheme (case 3); and simulation with 140 sub-basins (case 2).**

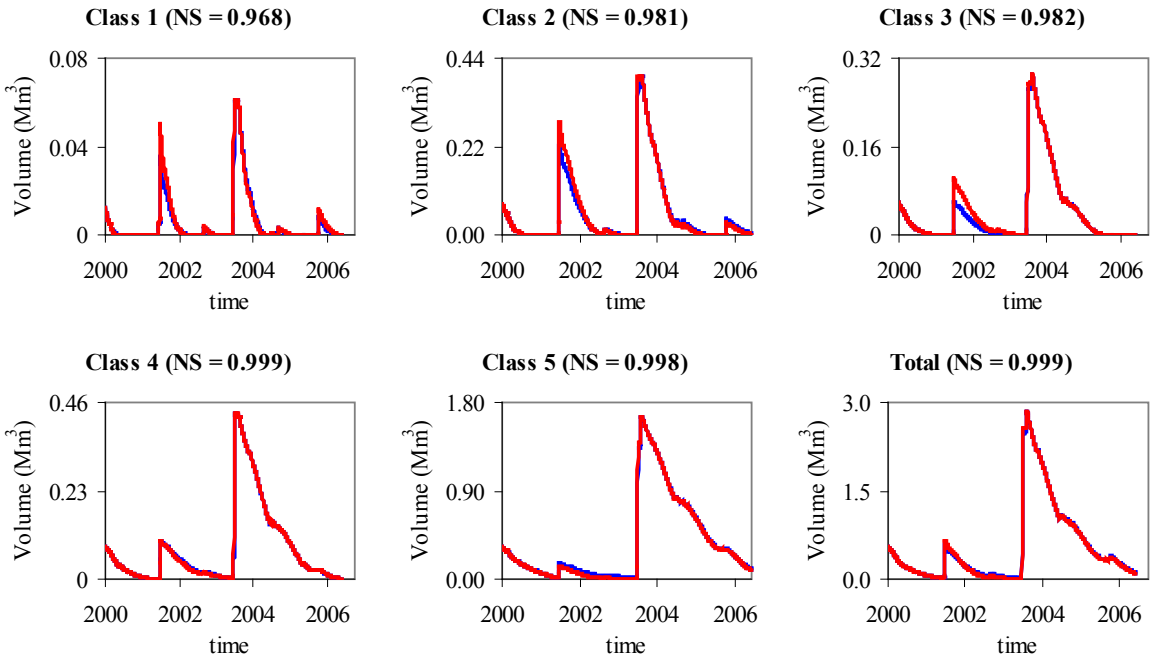


**Figure 5.28 Water volume in the reservoir classes (1 to 5) and total value for all classes considering: simulation with 30 sub-basins using the revised cascade routing scheme (case 3, red line); and simulation with 140 sub-basins (case 2, blue line).**

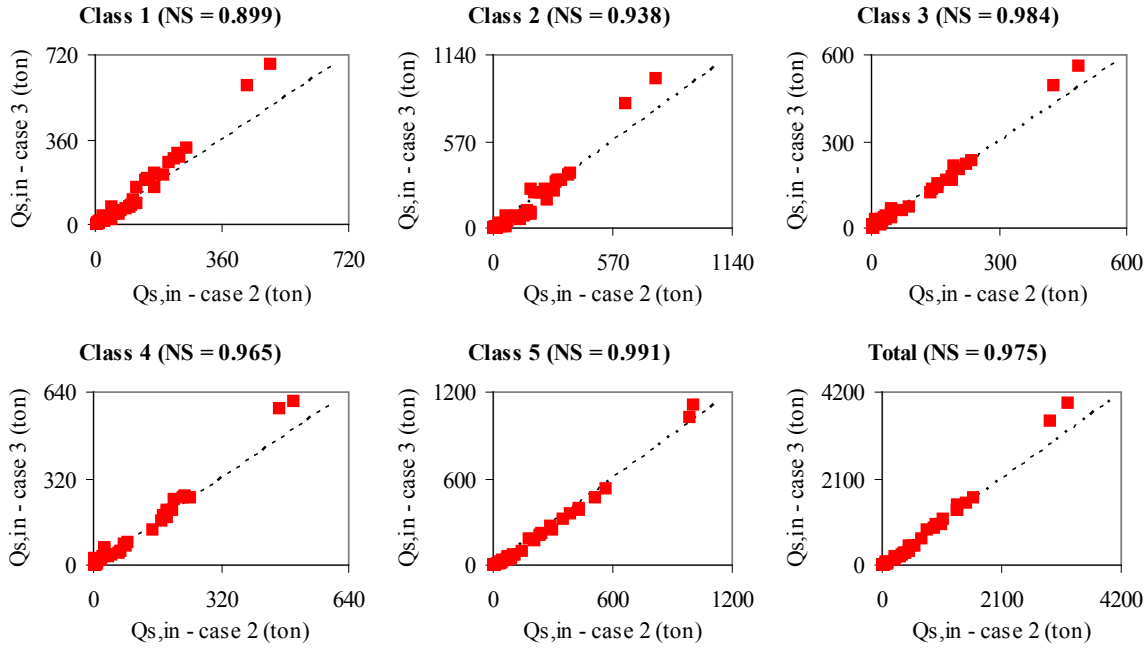


**Figure 5.29 Sediment inflow into the reservoir classes (1 to 5) and total value for all classes considering: simulation with 30 sub-basins using the revised cascade routing scheme (case 3); and simulation with 140 sub-basins (case 2).**

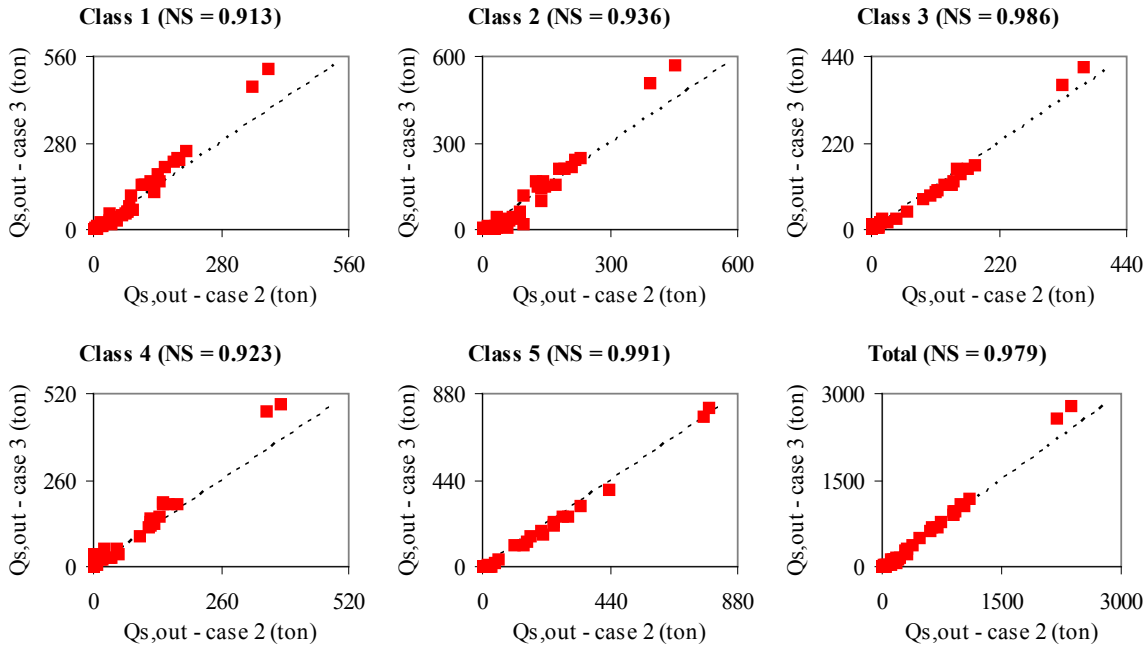


**Figure 5.30 Sediment outflow from the reservoir classes (1 to 5) and total value for all classes considering: simulation with 30 sub-basins using the revised cascade routing scheme (case 3); and simulation with 140 sub-basins (case 2).**

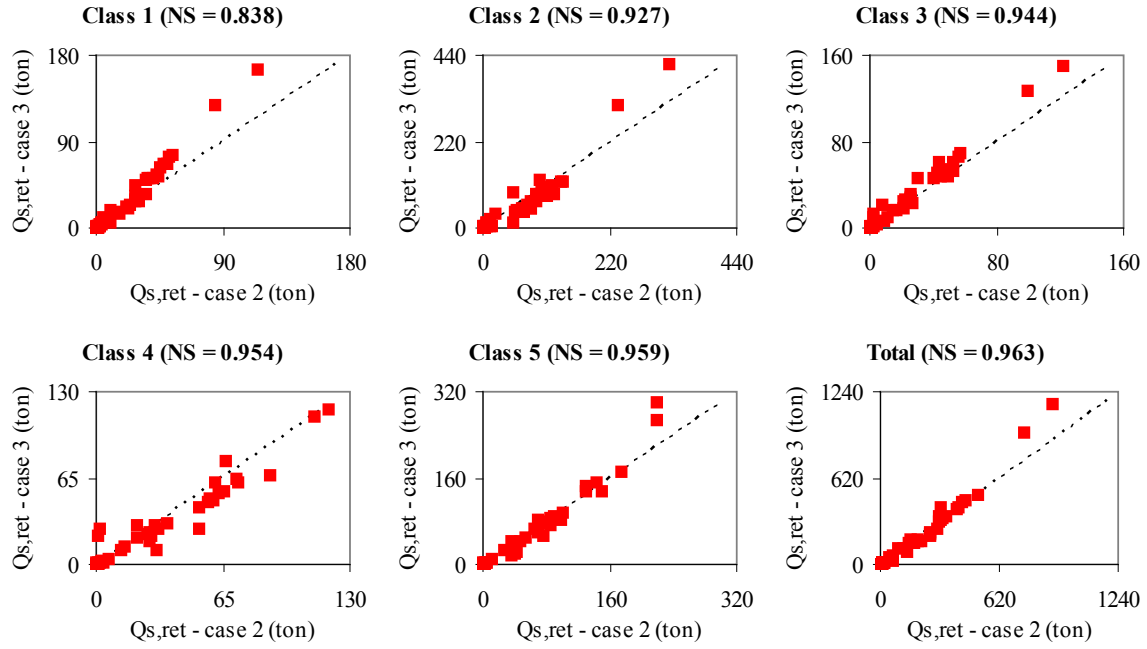


**Figure 5.31 Sediment deposition in the reservoir classes (1 to 5) and total value for all classes considering: simulation with 30 sub-basins using the revised cascade routing scheme (case 3); and simulation with 140 sub-basins (case 2).**

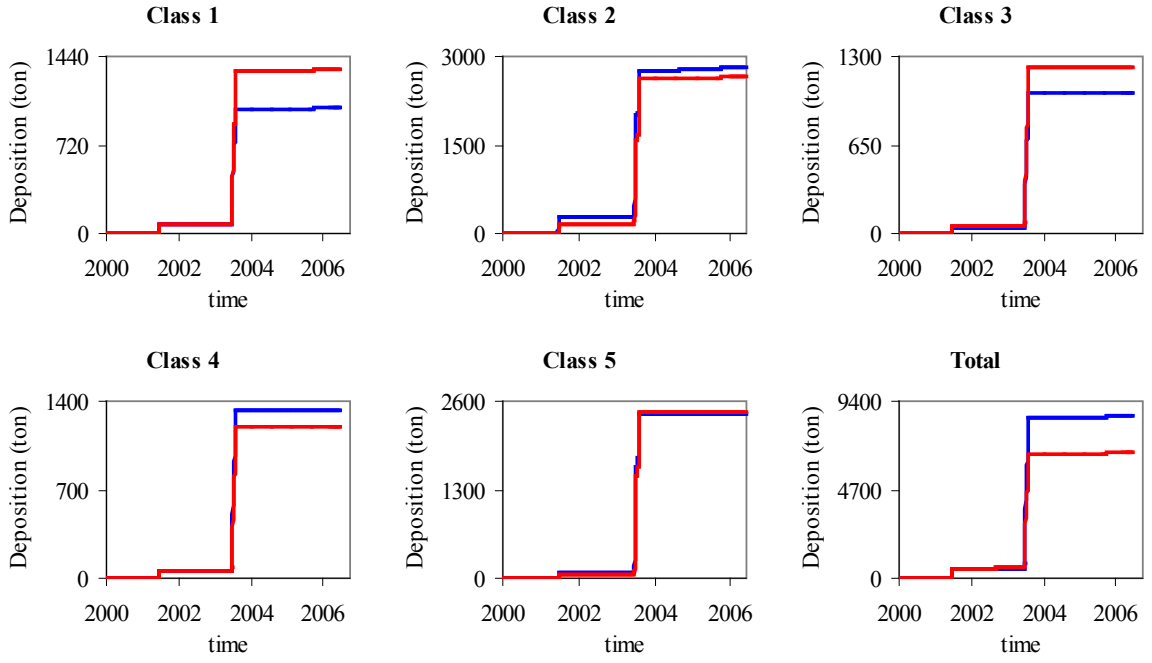


**Figure 5.32 Cumulative sediment deposition in the reservoir classes (1 to 5) and total value for all classes considering: simulation with 30 sub-basins using the revised cascade routing scheme (case 3, red line); and simulation with 140 sub-basins (case 2, blue line).**

**Benguê Reservoir**

The model application to the Benguê catchment enabled the analysis of water and sediment fluxes into the Benguê reservoir at the catchment outlet for the period 2000-2006. Two simulations were performed to check the ability of the WASA-SED model to reproduce rainfall-runoff processes within the catchment using 30 sub-basins: uncalibrated daily simulation (*sim1*) and calibrated daily simulation (*sim2*). In the uncalibrated daily simulation (*sim1*), the calibrating parameters were set to those obtained from the model calibration for the Aiuaba experimental catchment without readjustment. Unfortunately, the WASA-SED model overestimates the results of water inflow and water volume in the Benguê reservoir for the uncalibrated daily simulation (*sim1*), as presented respectively in Figures 5.33 and 5.34. As an attempt to improve the model performance, the scaling factor $K_{fcorr}$ was adjusted in the calibrated daily simulation (*sim2*). A correction factor of 0.15 was found by the calibration. The results, summarized in Figure 5.34, show that the adjustment of a single parameter, the scaling factor $K_{fcorr}$, improved the model results for the entire simulation period.

Sediment fluxes into the Benguê reservoir were computed using the WASA-SED model for the period 2000-2006. Unfortunately, measured data of sediment fluxes into the Benguê reservoir to test the WASA-SED model were not available for that time period. Furthermore, the assessment of sediment deposition for the period through bathymetric surveys was not possible because of the short time between surveys and low sedimentation rate. Nevertheless, to give an overview of temporal variation of sediment fluxes into the Benguê reservoir, modelled values are plotted in Figure 5.35 for the two model simulations (*sim1* and *sim2*). As depicted in Figure 5.35, the estimation of sediment yield flowing into the Benguê reservoir is strongly affected by changes to the scaling factor $K_{fcorr}$. Sedimentation rates of 0.57 and 0.18 cm.year$^{-1}$ were estimated with the uncalibrated daily simulation (*sim1*) and the calibrated daily simulation (*sim2*), respectively. The values of sedimentation rate for the two model simulations were considered low in

comparison to the average value of 1.17 cm.year$^{-1}$ observed for seven reservoirs located within the State of Ceará (Araújo, 2003). Values of suspended sediment concentration (SSC) computed for the model simulations (*sim1* and *sim2*) were within the range of 0.01 to 0.73 g.L$^{-1}$, whereas those measured during the rainy season of 2007 varied from 0.01 to 0.34 g.L$^{-1}$ for 29 small flood events (see Section 4.1.2).

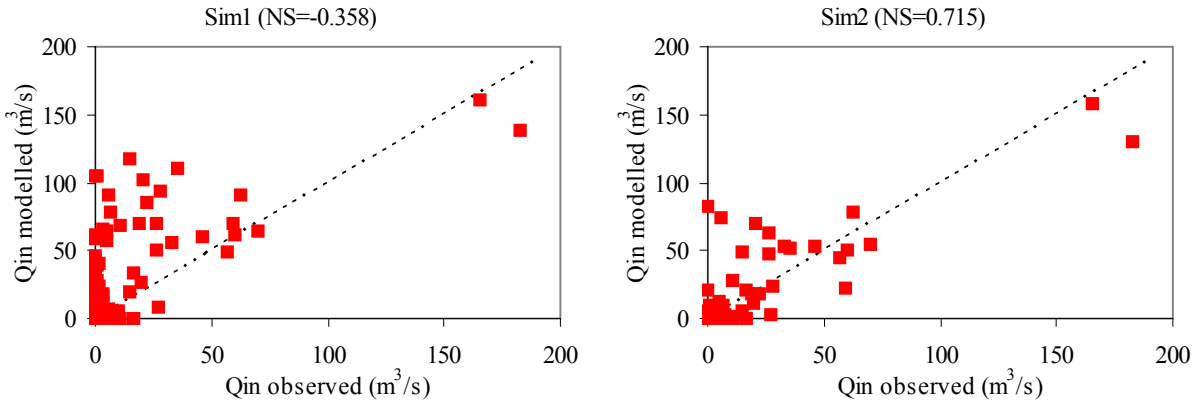


**Figure 5.33 Water inflow into the Benguê reservoir derived from the uncalibrated daily simulation (sim1) and the calibrated daily simulation (sim2).**

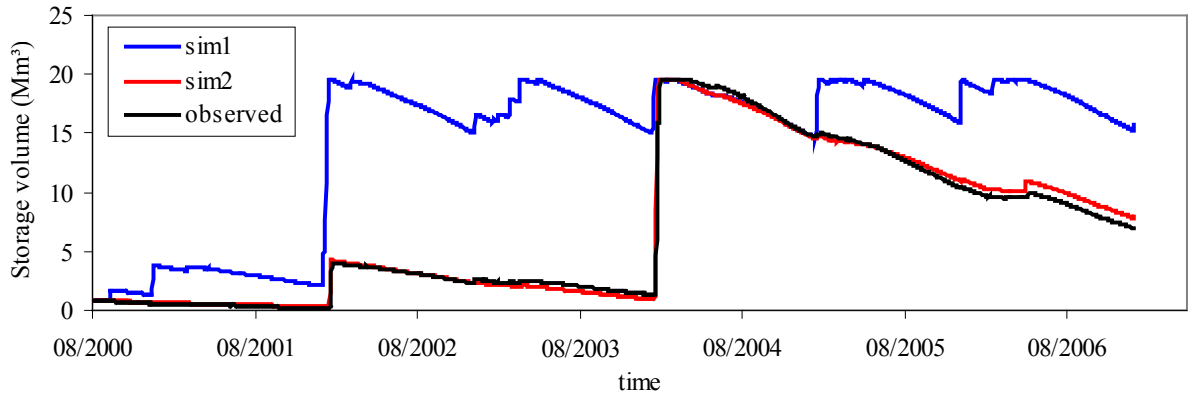


**Figure 5.34 Storage volumes of the Benguê reservoir derived from the uncalibrated daily simulation (sim1) and the calibrated daily simulation (sim2).**

Taking into account the lack of test data in the semi-arid region of north-east Brazil to validate the simplified modelling approach of reservoir sedimentation, the model was applied to the Barasona reservoir for the period 1986-1993, despite its characteristics of a large reservoir. The results of storage capacity decrease obtained from the model simulation using the simplified modelling approach for reservoir network (approach 2) were compared to those obtained from the simulation using the detailed modelling approach (approach 1), which was described in Section 3.4 and intensively tested previously (see Section 5.1). As depicted in Figure 5.36, the results of storage capacity decrease derived from modelling approaches for large reservoirs (approach 1) and for small reservoirs (approach 2) are in good agreement. Despite its good performance, approach 2 does not allow the simulation of either sediment management techniques, or the spatial distribution of sedimentation.

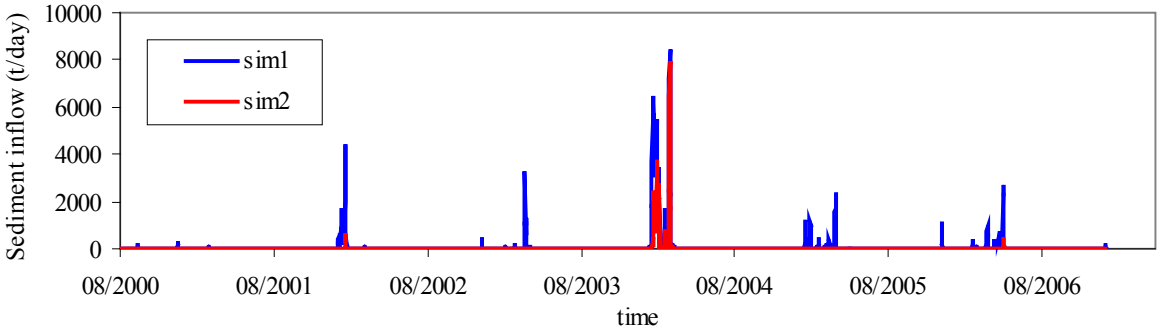


**Figure 5.35 Sediment inflow into the Benguê reservoir derived from the uncalibrated (sim1) and the calibrated (sim2) daily simulation.**

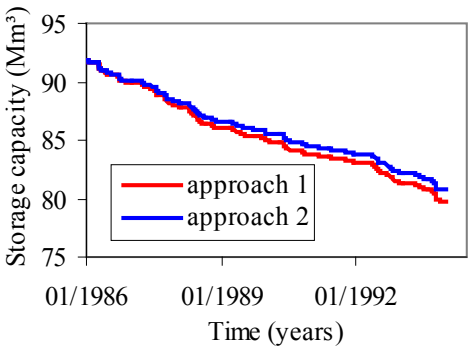


**Figure 5.36 Storage capacity decrease of the Barasona reservoir for the period 1986-1993, computed using the modelling approach for large reservoirs (approach 1) and that for small reservoirs (approach 2).**

## 5.2.4. Sensitivity and Uncertainties

Sensitivity of the modelling approach for small reservoirs to input data, parameters and model structure was evaluated using the WASA-SED model. Model simulations were performed for the Benguê catchment for the period 2000-2006. To account for the effects of upstream reservoirs on the water and sediment fluxes coming into the Benguê reservoirs, three different scenarios were considered: simulation without upstream reservoirs, i.e. neither small nor strategic ones (scenario 1); simulation with only strategic reservoirs (scenario 2); and simulation with all upstream reservoirs (scenario3). Results of water and sediment fluxes into the Benguê reservoir during flood events in the years of 2002, 2004 and 2006 are depicted in Figures 5.37 and 5.38 for the three scenarios considered, respectively. The results presented in Figure 5.37 indicated that the upstream reservoirs (scenarios 2 and 3) were able to retain a significant amount of water coming from the catchment, particularly for the years dominated by small flood events (2002 and 2006). For the year 2004, a similar behaviour of water retention in the upstream reservoirs was observed for the beginning of the rainy season. Once the water level of upstream reservoirs began to increase, the discrepancy between values of water discharges computed for scenarios 2 and 3 and those for scenario 1 decreased. As soon as the upstream reservoirs reached their maximum storage capacity, no difference in water inflow into the Benguê reservoir was observed for the scenarios.

According to the results presented in Figure 5.38, the behaviour of sediment retention in upstream reservoirs was quite different to that observed for water retention. The grain size distribution of the sediments seemed to be the main factor explaining the behaviour of sediment retention, because the coarser grains continued to be deposited in upstream reservoirs even during overflow. This tendency is clearly shown in Figure 5.38, in which sediment continued to be retained by the upstream reservoirs at the end of the wet period (March, 2004), whereas water retention was very low for the same period.

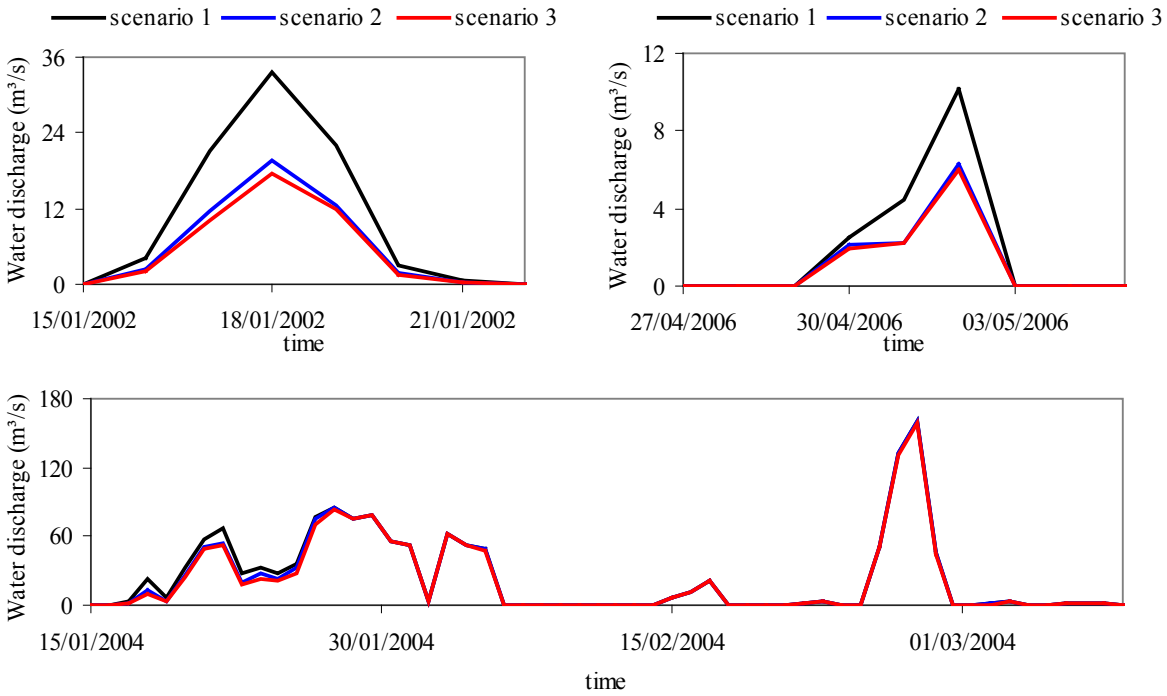


**Figure 5.37 Water inflow into the Benguê reservoir during flood events in the years of 2002, 2004 and 2006, obtained from the simulations: without upstream reservoirs (scenario 1); with only strategic reservoirs (scenario 2); and with all upstream reservoirs (scenario 3).**

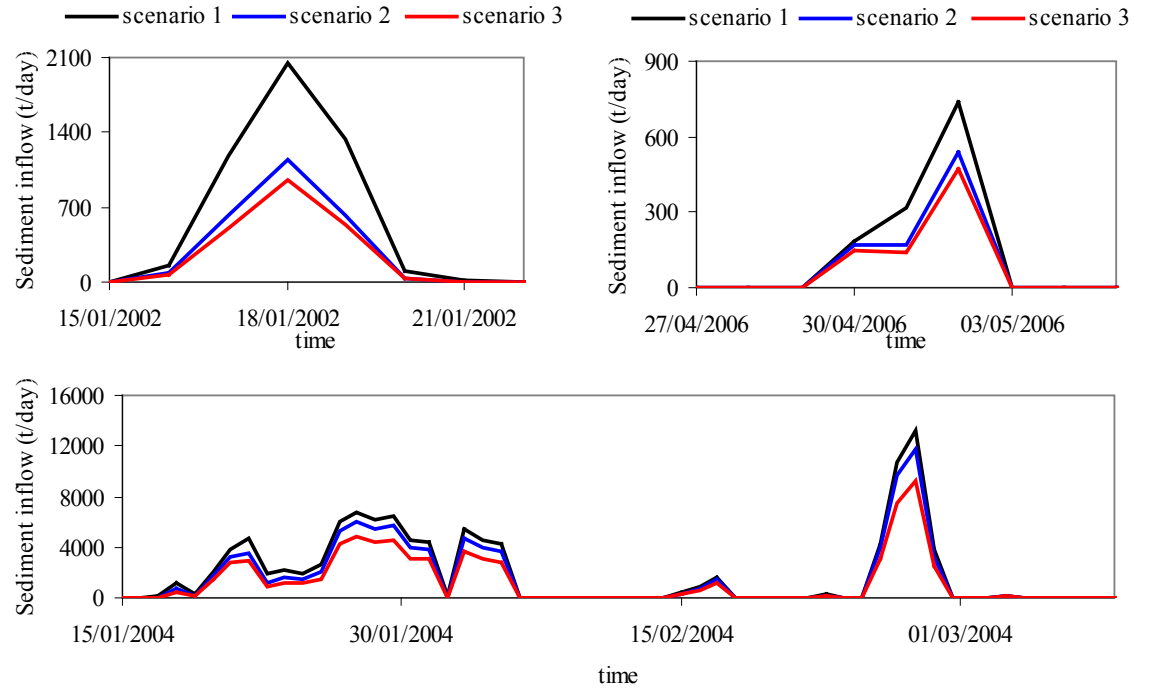


**Figure 5.38 Sediment inflow into the Benguê reservoir during flood events in the years of 2002, 2004 and 2006, obtained from the simulations: without upstream reservoirs (scenario 1); with only strategic reservoirs (scenario 2); and with all upstream reservoirs (scenario 3).**

To test the model sensitivity to the composition of the soils of the Benguê catchment, model simulations were carried out for the period 2000-2006, considering three different scenarios: loamy soils are predominant (60% of clay, 30% of silt and 10% of sand, *scenario a*); silty soils are predominant (30% of clay, 60% of silt and 10% of sand, *scenario b*); and sandy soils are predominant (10% of clay, 30% of silt and 60% of sand, *scenario c*). Mean grain size distributions were assigned to all soils of the Benguê catchment, according to the scenarios (*a* to *c*). The results of sediment retention within the small and strategic reservoirs are presented in Table 5.4 for the scenarios considered. As depicted in Table 5.4, the modelling approach applied for the assessment of sediment retention in upstream reservoirs was quite sensitive to changes in the composition of the soils of the catchment. Sediment retention varied from 36 to 87%, depending on the reservoir type (small reservoirs) and the scenario considered (*a* to *c*).

For the assessment of model sensitivity to the number of reservoir size classes of the Benguê catchment, simulations were performed considering 1, 3 and 5 classes. The limits of the reservoir size classes used in the simulations are presented in Table 5.5. Results of water and sediment balance of the small reservoirs considering 1, 3 and 5 reservoir size classes are summarized in Table 5.6. The results indicated that an increase in the number of reservoir size classes produced an increase in water and sediment fluxes into the reservoir classes, which may be explained by the fact that the water and sediment balance of small reservoirs were performed for each reservoir size class using one hypothetical representative reservoir with mean characteristics. A smaller number of reservoir size classes resulted in larger surface areas and storage capacities of the hypothetical reservoirs, reducing spillway overflow and, consequently, sediment release.

Uncertainties of model input data and parameters were of particular relevance in the study area with low data availability. There was little information available concerning the small reservoirs of the Benguê catchment. To estimate their maximum surface areas, satellite imageries of wet years with 15-m resolution were used. Furthermore, note the uncertainties inherent in using an area-volume relationship to estimate the storage capacities of the small reservoirs.

The upstream-downstream position of the reservoir size classes defined in the cascade routing scheme also involved uncertainties. On the one hand, reservoirs from the same size class may be located in an upstream-downstream sequence. On the other hand, smaller reservoirs may be located downstream of larger reservoirs.

**Table 5.4 Sediment retention within the small reservoirs (classes 1 to 5) and the strategic reservoirs of the Benguê catchment (2000-2006), computed for three scenarios according to the grain size distribution of soils within the catchment: loamy soils (scenario a); silty soils (scenario b); and sandy soils (scenario c).**

| Reservoir type | Sediment retention (%) | | |
|---|---|---|---|
| | loamy soils | silty soils | sandy soils |
| class 1 | 36.5% | 56.7% | 82.9% |
| class 2 | 46.1% | 66.8% | 87.4% |
| class 3 | 42.1% | 62.8% | 85.3% |
| class 4 | 40.6% | 61.8% | 84.5% |
| class 5 | 48.0% | 67.0% | 86.9% |
| strategic reservoir | 44.9% | 64.8% | 86.0% |

**Table 5.5 Limits of the reservoir size classes used to evaluate the model sensitivity.**

| Reservoir class | Range ($10^3 m^3$) | | |
|---|---|---|---|
| | Five classes | Three classes | One class |
| 1 | < 5 | < 25 | <250 |
| 2 | 5 - 25 | 25 - 50 | |
| 3 | 25 - 50 | 100 - 250 | |
| 4 | 50 - 100 | | |
| 5 | 100 - 250 | | |

**Table 5.6 Water and sediment retention within the small reservoirs (classes 1 to 5) of the Benguê catchment (2000-2006), computed for 1, 3 and 5 reservoir size classes.**

| Reservoir class | Water retention (%) | | | Sediment retention (%) | | |
|---|---|---|---|---|---|---|
| | Five classes | Three classes | One class | Five classes | Three classes | One class |
| 1 | 1.18% | 4.52% | 9.96% | 26.56% | 38.79% | 42.71% |
| 2 | 6.31% | 8.36% | | 43.04% | 33.89% | |
| 3 | 6.69% | 15.39% | | 35.47% | 38.14% | |
| 4 | 9.17% | | | 29.80% | | |
| 5 | 15.44% | | | 38.27% | | |
| all classes | 8.56% | 8.91% | 9.96% | 35.35% | 37.19% | 42.71% |

Uncertainty of model results in terms of runoff was high, particularly due to uncertainties in estimating the scaling factor $K_{fcorr}$, which counteracts the underestimation of rainfall intensities when the temporal resolution of the model is lower than that of rainfall events and their internal variability.

The estimation of spatial variability of climate data using an inverse-distance interpolation of measured data at climate stations included uncertainties. Rainfall data derived for sub-basins were usually attenuated by the interpolation, reducing peak runoff. Furthermore, for some days of the simulation period (2000-2006), rainfall data for the entire Benguê catchment had to be derived from only one climate station.

Uncertainties of simulation results obtained from the application of the modelling approach for small reservoirs, together with the WASA-SED model, should be mentioned. Water and sediment fluxes into the small reservoirs were derived from model results. No test data were available to calibrate and validate the modelling approach for small reservoirs. Nevertheless, as an attempt to evaluate the performance of the modelling approach for small reservoirs, it was tested for the Barasona reservoir, as described in Section 5.2.3.

Sediment yield from the Benguê catchment was calculated using the MUSLE equation, as described in Section 3.2.3. Uncertainties in data used to evaluate the parameters for the MUSLE equation were high, particularly the USLE cover and management factor (*C*), which is tabulated and may change by an order of magnitude, depending on the land cover and its seasonal dynamics. Furthermore, the estimation of grain size distribution of soils of the Benguê catchment involved uncertainties, mainly because of the low resolution of soil maps and scarce data availability concerning soil features.

## 5.3. Evaluation of Sediment Management Strategies for the Barasona Reservoir

### 5.3.1. Scenarios Considered

In order to achieve a sustainable water use of reservoirs subjected to high sediment deposition or those which provide the primary or sole reliable source of water for a region, sediment management strategies should be evaluated and implemented.

Considering the high water availability of the Barasona reservoir and the existence of bottom sluices, techniques of sediment pass-through such as partial drawdown, emptying and flushing can be considered for sediment management. The following sediment management scenarios were tested for the period 1995-1997 using the reservoir sedimentation model:

- *Scenario 1*: simulation of sediment deposition in the Barasona reservoir without sediment management, i.e. the bottom outlets remain closed during the simulation period.
- *Scenario 2*: simulation of flushing operation in the Barasona reservoir (*scenario 2* may be classified as seasonal emptying if most of the sediment is released by routing

rather than by degradation of sediment previously deposited). The bottom outlets are operated exactly as performed during the flushing in the years 1995, 1996 and 1997. They were opened after the irrigation season, when flood events usually occur, for a period of 64 days in 1995, 44 days in 1996 and 27 days in 1997. In the simulation, measurements of water inflow, water outflow and reservoir levels were used.

- *Scenario 3*: simulation of partial drawdown of the Barasona reservoir after the irrigation season. The reservoir water surface is maintained at a constant level of 430 m above sea level for 50 days, which corresponds to a storage volume of about 7.1 Mm³ at the beginning of the simulation period.
- *Scenario 4*: simulation of partial drawdown of the Barasona reservoir after the irrigation season. The reservoir water surface is maintained at a constant level of 425 m above sea level for 50 days, which corresponds to a storage volume of about 1.9 Mm³ at the beginning of the simulation period.

### 5.3.2. Application

To evaluate the sediment release efficiency of the sediment management scenarios described previously, the reservoir sedimentation model was applied to the Barasona reservoir for the period 1995-1997. The cumulative sediment release from the Barasona reservoir is shown in Figure 5.39 for all sediment management scenarios. The results indicated that *scenario 2* was the most efficient sediment management strategy, releasing almost 19 million tons of sediment coming from fluxes reaching the Barasona reservoir and erosion during the flushing operations. The other sediment management scenarios were able to release no more than 9 million tons of sediment. Nevertheless, even for the *scenarios 3* to *4*, a significant increase in sediment release was observed as compared to *scenario 1*, which represents the alternative without sediment management.

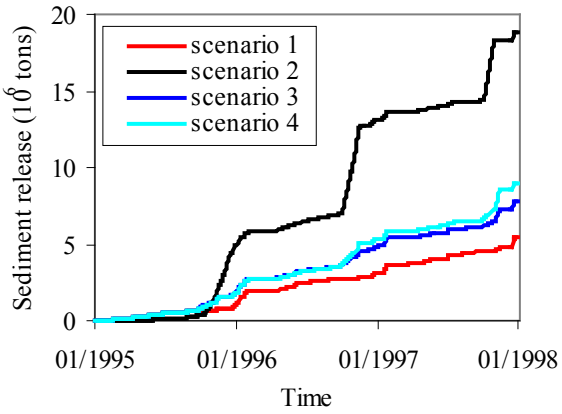


**Figure 5.39 Cumulative sediment release of the Barasona reservoir computed for four different sediment management scenarios (1995-1997).**

Figure 5.40 shows the storage capacity changes of the Barasona reservoir computed for the sediment management scenarios. For *scenario 2*, a considerable increase in storage capacity during the three flushing operations was observed, whereas for *scenarios 3* and *4* the storage capacity decreases, although at a lower rate compared to *scenario 1*. The strong increase in storage capacity observed in *scenario 2* may be explained by severe erosion along the main channel of the reservoir, created during the flushing operations. In *scenario 2*, almost a 5-$Mm^3$ gain in storage capacity was observed for the period. The bed elevation changes along the longitudinal profile of the Barasona reservoir are presented in Figure 5.41 for the sediment management scenarios. The results showed that *scenarios 3* and *4* were able to accelerate erosion processes at the upstream reach of the reservoir, but they were not suitable to remobilize the sediment deposited previously close to the dam because of the water volume stored there, thus reducing the flow velocity and, consequently, the sediment transport capacity.

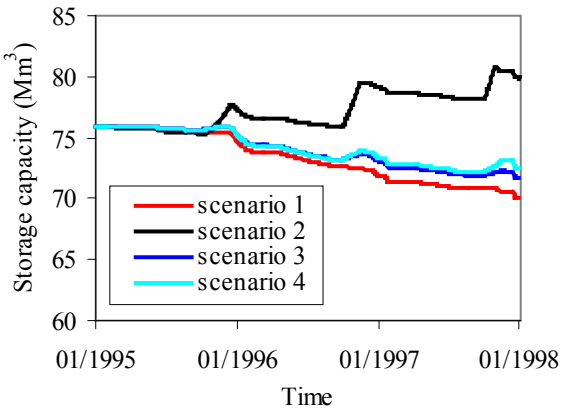


**Figure 5.40 Storage capacity changes of the Barasona reservoir computed for four different sediment management scenarios (1995-1997).**

In the prediction of the life time of the Barasona reservoir, sedimentation rates derived from the model simulations for the sediment management scenarios (1995-1997) are assumed to be representative of long-term sedimentation trend (see Table 5.7). For *scenario 1*, the reservoir would be completely full with sediments after 47 years. The application of sediment management *scenarios 3* and *4* will extend the reservoir life-time up to 64 and 80 years, respectively. For *scenario 2*, a negative value of sedimentation rate was observed for the period 1995-1997, which made it difficult to estimate the life-time of the Barasona reservoir as a function of sedimentation. The negative value for the sedimentation rate may be explained by the fact that the sediment release exceeded significantly the sediment inflow for the period due to high erosion of the material previously deposited. Nevertheless, at a larger time scale, a continuous storage decrease is expected for the Barasona reservoir. In wide reservoirs, such as the Barasona, flushing operations erode only a narrow channel through the deposits, creating a floodplain-type geometry (Morris and Fan, 1997). To maintain the channel, repeated flushing should be performed, usually at annual intervals. Nevertheless, during impounding periods, the incoming sediments will be continuously deposited on the floodplains. According to Morris and Fan (1997), the single flushing channel will produce only a temporary increase in storage capacity for wide reservoirs. The sediment deposition on the floodplains will cause a continuous storage capacity decrease to some stable volume, equal to the volume within the main flushing channel.

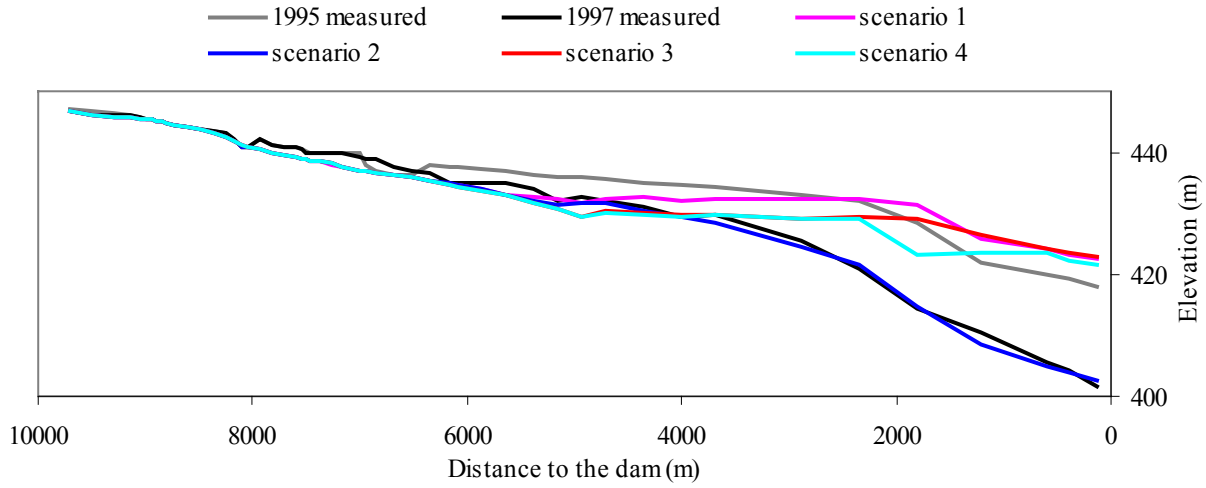


**Figure 5.41 Bed elevation changes along the longitudinal profile of the Barasona Reservoir computed for four different sediment management scenarios (1995-1997).**

**Table 5.7 Expected life time of the Barasona reservoir estimated considering that the sedimentation rates derived from the model simulations for the sediment management scenarios (1995-1997) are representative of long-term sedimentation trend.**

| Sediment management scenarios | Sedimentation rate ($Mm^3$/year) | Expected life time (years) |
|---|---|---|
| 1 | 1.95 | 47 |
| 2 | (-1.32)* | - |
| 3 | 1.43 | 64 |
| 4 | 1.15 | 80 |

* The storage capacity of the Barasona reservoir increases at the time period (1995-1997) due to flushing operations (scenario 2)

For the assessment of the impacts in applying the sediment management techniques on the water availability of the Barasona reservoir in the period 1995-1997, results of water release for irrigation purposes derived from the *scenarios 2* to *4* were compared to those from *scenario 1* (without attention to sediment management). Figure 5.42 shows the results of cumulative water release through the intake devices, which should fulfil the daily water demand for the period. As depicted in Figure 5.42, the reservoir water yield varied from about 1,806 $Mm^3$ (*scenario 2*) to 2,091 $Mm^3$ (*scenario 1*) at the period, which means that almost 284 $Mm^3$ were lost due to the implementation of the sediment management technique related to *scenario 2* (flushing operations). Accordingly, the results of water loss were calculated for each of the sediment management scenarios, as presented in Table 5.8. Taking into account the water loss for the implementation of the sediment management techniques (*scenarios 2* to *4*), it was possible to calculate the costs related to each scenario (see Table 5.8). A unit water cost of 0.09 €.$m^{-3}$ was used according to the Spanish System of Information about Water (HISPAGUA, in 2004). The costs varied from 13 to 26 million €, depending on the scenario considered.

The costs to dredge the same amount of sediment released using the sediment management scenarios are presented in Table 5.9. A mean unit cost of 50 €.$m^{-3}$ of sediment derived from an actual price research at some companies was used. The amount of sediment effectively released using the sediment management techniques (*scenarios 2* to *4*) is calculated as the sediment release excess obtained from the comparison with the *scenario 1* (without sediment management). The costs vary from about 77 to 490 million euros, depending on the scenario. Therefore, the sediment management techniques (*scenarios 2* to *4*) are economically attractive as compared to those related to sediment removal by hydraulic dredging. However, at some cases, excavation and hydraulic dredging are the only management options available. Furthermore, these techniques are more efficient in removing sediment from the floodplains.

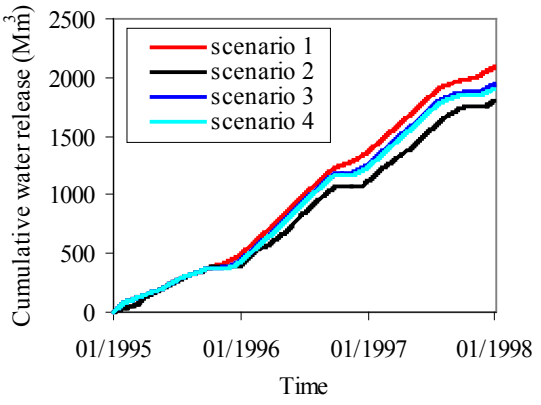


**Figure 5.42 Cumulative water release from the Barasona Reservoir for irrigation purposes, computed for four different sediment management scenarios (1995-1997).**

**Table 5.8 Estimated costs for the implementation of the sediment management scenarios at the Barasona reservoir for the period 1995-1997 using a unit water cost of 0.09 €.$m^{-3}$ (Hispagua, in 2004)**

| Sediment management scenarios | Water loss ($Mm^3$) | Estimated costs (million €) |
|---|---|---|
| 1 | 0 | 0.00 |
| 2 | 284 | 25.58 |
| 3 | 149 | 13.44 |
| 4 | 184 | 16.58 |

**Table 5.9 Estimated costs to dredge the same amount of sediment effectively released by the sediment management techniques (scenarios 2 to 4) using a unit cost of 50 €.m$^{-3}$ (price survey at some companies)**

| Sediment management scenarios | Effective sediment release (Mm$^3$) | Estimated costs (million €) |
|---|---|---|
| 1 | 0.00 | 0.00 |
| 2 | 9.80 | 489.86 |
| 3 | 1.54 | 76.99 |
| 4 | 2.38 | 118.82 |

## 5.4. Closure

The reservoir sedimentation model was firstly applied to the Barasona reservoir located in the Pre-Pyrenean Mediterranean zone of Spain. The model calibration consisted of two stages: an application for the simulation periods 1986-1993 characterized by high sedimentation rate as a consequence of no application of sediment management technique, i.e. the bottom outlets remained closed during the entire period; and an application for the simulation period 1995-1997, which included yearly flushing operations. The parameter $f_{act}$, which accounts for the maximum thickness of the active layer available for erosion, was calibrated for both conditions, enabling the application of the reservoir sedimentation model to a wide variety of situations. To validate the reservoir sedimentation model, it was applied to the Barasona reservoir for the simulation period 1998-2006, which was characterized by intensive operation of the bottom outlets, but however without using pool drawdown for sediment management. The model was able to simulate that situation, as discussed in Section 5.1.3. However, it overestimated to some extent the sediment deposition in the Barasona reservoir.

Another application was carried out on the 933-km² Benguê catchment, located in the semi-arid region of north-east Brazil. Taking into account the large number of reservoirs identified within this catchment and the lack of information about them, a simplified modelling approach was developed and coupled with the WASA-SED model to account for water retention and sedimentation processes of those reservoirs. The reservoirs were grouped into size classes according to their storage capacity and a cascade routing scheme was applied to describe the upstream-downstream position of the classes. The strategic reservoirs located on the main rivers of the catchment were analysed individually in terms of water and sediment balance, including the 19.6-Mm$^3$ Benguê reservoir. The WASA-SED model was applied to the Benguê catchment for the simulation period 2000-2006 using the original runoff distribution algorithm proposed by Güntner (2002). As no test data were available to assess the performance of the original representation, a detailed discretization of the Benguê catchment was used to describe the study area in terms of contributing area for water and sediment yield, reservoir location, water and sediment retention and water and sediment fluxes among reservoir classes. This detailed discretization enabled the calculation of water and sediment balance of each small reservoir and water and sediment transfer among reservoirs following the natural upstream-downstream sequence according to the reservoir location. The original representation overestimated the results of water and sediment fluxes into the reservoir classes, as compared to those obtained from the detailed discretization, which was assumed to be more realistic. As an attempt to improve the model performance using the cascade routing scheme, another runoff distribution algorithm was applied. In the revised representation, the fraction of water and sediment inflow attributed to each reservoir class was defined by the fraction of its contributing area. The model results of the simulation using the revised representation were in good agreement with those obtained from the simulation using the detailed discretization.

Finally, the reservoir sedimentation model was applied to the Barasona reservoir for the period 1995-1997 to evaluate the sediment release efficiency of sediment management strategies. Four sediment management scenarios were considered: no sediment management (*scenario 1*); yearly flushing operations exactly as occurred at that period (*sce-*

*nario 2*); partial drawdown to a constant level of 430 m above sea level (*scenario 3*); and partial drawdown to a constant level of 425 m above sea level (*scenario 4*). According to the results, *scenarios 3* and *4* were able to reduce sediment deposition by increasing the sediment release during pool drawdown, as compared to those obtained from *scenario 1*. However, they were not suitable to remobilize the sediment deposited previously close to the dam, as observed in *scenario 2*, for which a storage capacity increase of about 5 $Mm^3$ was computed. Cost analysis indicated that *scenario 2*, which is the most efficient in releasing sediment, would be up to 90% more expensive than the other sediment management techniques (*scenarios 3* and *4*), but a lot cheaper than dry excavation and hydraulic dredging.

# CHAPTER 6

# 6. Conclusions and Recommendations

## 6.1. General Conclusions

In this study, a reservoir sedimentation model was developed and coupled within the WASA-SED model, which simulates rainfall-runoff processes and sediment transport operating on the hillslope and within the river network. The reservoir sedimentation model comprises two modelling approaches depending on size of the reservoir and data availability: a detailed modelling approach; and a simplified modelling approach. The detailed modelling approach of reservoir sedimentation is deterministic, process-based and one-dimensional. It is able to simulate sediment transport through the reservoir and spatial distribution of sedimentation. Furthermore, it enables the assessment of changes on the sediment deposition caused by sediment management practices. On the other hand, the simplified modelling approach is suitable to assess water and sediment retention in dense reservoir networks, characterized by scarce data availability.

### 6.1.1. Detailed Modelling Approach of Reservoir Sedimentation

The reservoir sedimentation model was applied to the Barasona reservoir to test the detailed modelling approach. Measured data of water inflow discharges into the Barasona reservoir were used to minimize uncertainties of using the rainfall-runoff module of the WASA-SED model. The attempt to estimate sediment inflow discharges using a simple sediment rating curve derived from measured data of SSC and water discharges was unsuccessful, giving a weak correlation ($R^2 = 0.0053$). Instead, a Quantile Regression Forest model (QRF model) was used to explain the temporal variability of SSC values through the analysis of ancillary variables, which act as driving forces or proxies for processes (rainfall, cumulative discharge, rising/falling limb data). The comparison between measured and predicted SSC values for a 15-min time scale indicated that the QRF model was able to predict SSC values using ancillary data ($R^2 = 0.92$). At the daily time scale, a lower correlation ($R^2 = 0.38$) was observed between mean daily SSC derived from observed 15-min data and mean daily SSC derived from the QRF model. However, the proposed approach still worked adequately in the prediction of SSC and enabled the analysis of time periods for which only daily data were available.

A two-stage calibration of the reservoir sedimentation model was performed to account for changes in the sediment deposition pattern caused by sediment management practices. Firstly, the model was applied to the Barasona reservoir for the simulation period 1986-1993, which was characterized by high sedimentation rate as a consequence of no application of sediment management technique. The parameter $f_{act}$, which accounts for the maximum thickness of the active layer available for erosion, was calibrated for that situation. The best model performance was obtained for a $f_{act}$ of 3 $cm.day^{-1}$. Bed elevation changes along the longitudinal profile and cross-sections were well represented by the model. The reservoir sedimentation model was also able to distribute sediment deposits within the Barasona reservoir. Secondly, two new steps were implemented into the reservoir sedimentation model to account for retrogressive erosion caused by flushing operation, which includes the identification of the point of slope changes along the longitudinal profile of the reservoir (nickpoint) and a variable $f_{act}$ within the downstream reach defined by the nickpoint. The improved reservoir sedimentation model was applied to the Barasona reservoir for the simulation period 1995-1997, which was characterized by yearly flushing operations. The parameter $f_{act}$ was

assumed to increase linearly from the nickpoint to the dam, remained constant at the upstream reach of the reservoir ($f_{act}$ = 3 cm.day$^{-1}$, derived from the first stage of the model calibration). The maximum value of the $f_{act}$ (close to the dam) was obtained by calibration ($f_{act,max}$ = 25 cm.day$^{-1}$). The new model configuration enabled the reproduction of channel formation by flushing operations.

For the validation of the reservoir sedimentation model, an application on the Barasona reservoir was carried out for the period 1998-2006, which was characterized by intensive use of the bottom outlets to manage sediments. According to the model results, the modelling approach was able to assess changes in the sediment deposition caused by sediment management without using of pool drawdown. Nevertheless, the model overestimated the total volume of sediment deposition. The sediment trapping efficiency estimated using volume changes between bathymetric surveys and sediment inflow discharges derived from the QRF models was 33%, whereas that computed using the reservoir sedimentation model was 53%. The overestimation observed may be related to the uncertainties of the QRF model in the prediction of sediment inflow discharges.

Despite the model uncertainties, one may conclude that the proposed reservoir sedimentation model is a helpful tool to assess the complex behaviour of sediment deposition and bed erosion with accuracy.

### 6.1.2. Simplified Modelling Approach of Reservoir Sedimentation

A simplified modelling approach was developed to assess water balance and sediment budget of reservoirs with limited data availability in terms of their geometric characteristics, such as those identified in the Benguê catchment. For the aggregate description of the water balance of reservoirs that cannot be represented explicitly in the WASA-SED model, a storage approach respecting different reservoir size classes and their interaction via river network was applied. For each class, the water balance was calculated for one hypothetical representative reservoir of mean characteristics. The simplified approach of the reservoir sedimentation model was used to simulate the effects of upstream reservoirs on the water and sediment yield from the Benguê catchment (2000-2006). Three spatial model configurations were tested as follows:

- Original runoff distribution algorithm (Güntner, 2002), which assumes that the generated runoff within a sub-basin is distributed equally among the reservoir classes and the same fraction is attributed to the water discharges at the sub-basin outlet without retention.
- Detailed discretization, which enables the calculation of water and sediment balance of each reservoir, to which a contributing area is associated, derived from digital elevation models. Due to the lack of test data, the large spatial discretization of this representation and its ability to simulate the natural upstream-downstream sequence of sediment transfer between reservoirs, it was used as a reference scenario.
- Revised runoff distribution algorithm, which assumes that the fraction of contributing area of each reservoir class defines the fraction of water and sediment inflow that is attributed to each class, respectively.

Water and sediment fluxes into the reservoir size classes were not correctly represented by the original runoff distribution algorithm according to the results obtained from the detailed discretization, with Nash-Sutcliffe coefficients *NS* within the ranges -4.030 to 0.396 and -2.846 to 0.125, respectively, depending on the class. Overall, the original discretization overestimated the results, which may be explained by the fact that the fraction of area controlled by each reservoir size class is smaller than that admitted in the original runoff distribution (one sixth of the catchment area).

The revised runoff distribution algorithm was then developed and tested for the Benguê catchment. Results for the components of water and sediment balances in the reservoir classes, such as water and sediment inflow, water and sediment retention, and water and sediment out-

flow, were compared with those derived from the detailed discretization. Overall, the revised representation showed good results, with NS values for water and sediment inflow discharges being increased to over 0.89. The results indicated that the water and sediment balance of small reservoirs and sediment transfer between reservoir classes were well represented by the cascade routing scheme admitted in the revised runoff distribution algorithm. The revised representation was able to capture intra-annual and inter-annual variability of water storage volume and sediment retention in the reservoirs. For instance, over 90% of the sediment deposition of the reservoir classes during the simulation period is associated with the extremely high flood events that occurred in 2004.

The application of the simplified modelling approach of reservoir sedimentation to the Benguê catchment (2000-2006) enabled the assessment of the role of upstream reservoirs in retaining water and sediment generated within the catchment. According to model results, about 11% of runoff was retained in upstream reservoirs. Nevertheless, the simulation period included an atypical year (2004) with very high runoff generation, which may explain the low runoff retention, since most of the small reservoirs overflowed. For regular years with lower runoff generation, it is estimated that the water retention would be larger, since overflow of small reservoirs is not usual for these conditions and the area controlled by upstream reservoirs is around 45% in the Benguê catchment. Concerning sediments, the model results indicated that the upstream reservoirs retained almost 20% of the sediment generated within the catchment. According to the sensitivity analysis presented in Section 5.2.4, the amount of sediment retention in the upstream reservoir is impacted not only by overflow frequency but also by the grain size distribution of the transported material.

### 6.1.3. Sediment Management Strategies

The proposed reservoir sedimentation model was developed not only to assess the sediment deposition pattern and quantify sedimentation rates, but also to serve as a tool to evaluate the effects of implementing sediment management techniques and their abilities in extending the life-time of existing reservoirs subjected to severe sedimentation. To evaluate the sediment release efficiency of different sediment management strategies, the model was applied to the Barasona reservoir for the period 1995-1997, considering four scenarios, as follows:

- No sediment management (*scenario 1*).
- Yearly flushing operations exactly as occurred at that period (*scenario 2*).
- Partial drawdown to a constant level of 430 m above sea level (*scenario 3*).
- Partial drawdown to a constant level of 425 m above sea level (*scenario 4*).

According to the model results, all sediment management techniques described in scenarios 2 to 4 were able to reduce sediment deposition in the Barasona reservoir for that period, as compared with that observed for scenario 1. Sedimentation rates of 1.43 and 1.15 $Mm^3.year^{-1}$ were computed for scenarios 3 and 4, respectively, whereas scenario 1 presented a significantly higher sedimentation rate of 1.95 $Mm^3.year^{-1}$. For scenario 2, a negative value of sedimentation rate was observed as a consequence of an increase of 5 $Mm^3$ in water storage volume due to erosion during flushing operations. The increase in water storage volume observed in scenario 2 may be explained by high erosion rates along the main channel of the Barasona reservoir during the simulation period, which had been accumulating sediment since the last flushing operation in 1978. Nevertheless, after repeated flushing operations, a decrease in sediment release is expected as a consequence of limited sediment availability at the flushing channel and continuous sediment deposition on the floodplains. Admitting that the sedimentation rates computed for the scenarios (except for scenario 2) are representative of long-term trend, they were used to predict the life time of the Barasona reservoir, which may vary from 47 years (scenario 1) to 80 years (scenario 4), depending on the scenario. In the case of scenario 2, it was not possible to predict the life-time of the Barasona reservoir using the sedimentation rate (negative value). However, a longer reservoir life-time as a function of sedimentation is expected.

Costs for the implementation of the sediment management techniques (scenarios 2 to 4) were estimated, considering the total water loss related to each scenario. A water unit cost of 0.09 €.m$^{-3}$ was used according to the Spanish System of Information about Water (HISPAGUA, in 2004). The costs varied from 13 to 26 million €, depending on the scenario considered. To dredge the same amount of sediment released using the sediment management strategies (scenarios 2 to 4), the costs may increase up to 490 million €.

Considering the high water availability of the Barasona reservoir and the existence of bottom outlets, techniques for sediment pass-through such as those described in scenarios 2 to 4 were technically and economically attractive. Nevertheless, regular flushing operations (yearly) seems to be the most promising sediment management strategy, despite the higher costs associated with its implementation, as compared to scenarios 3 and 4. Two disadvantages of this technique should be mentioned: it is not suitable for removing sediment deposition on the floodplains; and the extremely high concentration of sediments released during the operations can cause unacceptable environmental and geomorphological impacts downstream of the reservoir.

As an alternative strategy to release sediments, one may propose the combination of two methods, such as the application of partial drawdown (every year) and flushing operations (every five or ten years), reducing water loss and downstream impacts and increasing reservoir water yield.

## 6.2. Discussion

In semi-arid environments, such as the Brazilian Northeast, water scarcity due to droughts is commonly the most important aspect affecting water availability. In this region, water supply depends strongly on storage in surface reservoirs and sediment deposition in these reservoirs represents a great risk for both qualitative and quantitative conservation of water resources. For an assessment of the importance of the reservoir network in disconnecting water and sediment transfer within basins, the results from the model application to the Benguê catchment (Section 5.2.3) are discussed here.

On the one hand, the reservoir network is able to retain a significant amount of water, reducing the water availability of the 19.6-Mm$^3$ Benguê reservoir located at the catchment outlet, particularly in regular years characterized by small flood events (see Fig. 5.37, Section 5.2.3). On the other hand, the water stored in upstream reservoirs may be used for irrigation purposes in small farms and for drinking, enabling a better spatial distribution of water resources. Nevertheless, smaller reservoirs are usually unable to supply water for the entire dry season, drying up a short time after the rainy season, as depicted in Figure 5.28 (Section 5.2.3), due to the poor ratio between storage volume and losses through evaporation and infiltration. In this sense, smaller reservoirs are hydrologically inefficient, and alternative water sources are required in these situations, such as water transfer from larger reservoirs and cisterns.

Concerning sediments, upstream reservoirs serve as sediment detention basins, retaining a considerable amount of sediment generated within the catchment and extending the life-time of larger reservoirs located downstream. Nevertheless, the sediment retention in those reservoirs may impact their water availability quantitatively by decreasing their storage capacity and qualitatively by pollutants adsorbed onto the transported sediment. Consequently, reservoir siltation will enhance the risks of water stress in those areas due to relatively high evaporation and overflow water losses. The impact of upstream reservoirs on water and sediment fluxes within the catchment is mainly related to their storage capacity. Smaller reservoirs retain low water amounts and are inefficient in trapping sediments, since overflow occurs frequently.

In semi-arid regions, such as those where the Benguê catchment is located, the implementation of sediment management techniques, particularly sediment pass-through (see Section 2.4.2), is constrained by water availability. As an attempt to minimize sediment deposition and water loss, one may propose that the reservoir outlets are opened completely during spillway overflow. Nevertheless, smaller reservoirs are usually provided neither with bottom

outlets nor with intake devices, thus not allowing the application of this technique. Therefore, in those cases, techniques for erosion control are usually the most appropriate method to reduce sediment delivery to reservoirs.

Another situation is observed in dryland environments in Spain, where reservoir siltation is aggravated by the Mediterranean regime of the rivers with frequent floods and a considerably smaller number of reservoirs in uplands. In such regions, the life-time of reservoirs may be reduced to a few decades due to siltation. Therefore, it is indispensable to manage sediment as well as water to achieve their sustainable long-term use. Within this study, the Barasona reservoir located in the Pre-Pyrenean Mediterranean zone of Spain was analysed in detail to give an overview of the sediment deposition pattern of Spanish reservoirs and to evaluate the applicability of sediment management scenarios. As discussed in Section 5.3, all the sediment management techniques considered are able to minimize sediment deposition in the Barasona, but differing according to efficiency and costs. Currently, only limited effort is put into the implementation of such measures (bottom gates are open only once a month regardless of sediment conditions), leaving a considerable margin for optimizing sediment management.

Nevertheless, a sustainable sediment management encompasses the entire fluvial system, including river and reservoir network. The sediment released from a reservoir during sediment management operations will certainly produce impacts on rivers and reservoirs downstream. Therefore, some aspects should be considered before applying sediment management techniques:

- Analysis of the simultaneous application of sediment management techniques to all reservoirs within a basin. However, it may be constrained by water availability.
- Assessment of water demand as well as the severity of the sedimentation problem of reservoirs. In this case, the sediment retention in upstream reservoirs may ensure a sustainable long-term use of the main reservoirs located downstream.
- Assessment of the viability of building new reservoirs to serve as sediment detention basins. However, it may include large operational and capital costs.
- Evaluation of the viability of implementing erosion control practices to reduce sediment yield.

## 6.3. Perspectives

The reservoir sedimentation model was able to achieve the objectives described at the beginning of this research. Nevertheless, some further improvements could be done to the model, either including new features or modifying those already available. Some of these features are:

- In reservoirs with multiple major tributaries, the sediment deposition pattern can be strongly affected by lateral inflows and lateral sediment discharges, depending on their characteristics such as water temperature, grain size distribution and sediment concentration. Therefore, water and sediment contributions from tributaries could be considered in the reservoir sedimentation modelling, serving as internal boundary conditions.
- Fluvial processes observed in stream channels crossing deltas, such as meandering, levee formation, channel incision and armouring, could be modelled.
- As the sediments enter the reservoir and begin to settle, they tend to accommodate themselves in bottom layers that can suffer a compaction process over the years. Consolidation changes the thickness and density of the bed through decreases in porosity. Therefore, those processes could be included in the reservoir sedimentation model.
- Stratified flows occurs frequently in reservoirs because of density differences between the inflowing and the impounded water caused either by differences in temperature or by the presence of turbidity. Turbidity currents are often important processes in reservoir sedimentation by transporting fine material over long distances through the impoundment to the vicinity of the dam. Therefore, such phenomena could be considered in the reservoir sedimentation model.

Beyond the model implementation, some other aspects should be considered. An intensive monitoring campaign should be carried out to assess hydrological and sedimentological processes in reservoirs and to obtain enough test data to validate the reservoir sedimentation model that accounts for those processes. Not only sediment management techniques, but also techniques of erosion control and upstream sediment trapping within the catchment should be analysed in an integrated manner using a sediment-transport model system. Finally, the reservoir sedimentation model could be applied to evaluate the impacts of storage capacity loss of reservoirs on water availability in semi-arid areas such as the north-east Brazil, where the water supply for drinking and irrigation purposes is mostly provided by surface reservoirs. In such regions, reservoir sedimentation represents a great risk for both qualitative and quantitative conservation of the water resources.

# CHAPTER 7

## 7. References


Ackers, P. and White, W.R. (1973). Sediment transport: new approach and analysis. Journal of the Hydraulics Division, ASCE, 99, no. HY I I, pp. 2041-2060.

Alonso, C.V. (1980). Selecting a formula to estimate sediment transport capacity in nonvegetated channels. CREAMS A field scale model for chemicals, runoff; and erosion from agricultural management system, edited by W.G. Knisel, U.S.D.A. Conservation Research Report no. 26, Chapter 5, pp. 426-439.

American Society of Civil Engineers (ASCE), Task Committee on Relations Between Morphology of Small Stream and Sediment Yield (1982). Relationships between morphology of small streams and sediment yield. Journal of the Hydraulics Division, ASCE, 108, no. HY I I, pp. 1328-2365.

Annandale, G.W. (1984). Predicting the distribution of deposited sediment in southern African reservoirs. Challenges in African Hydrology and Water Resources, Proc. of Harare Symposium, IAHS Publication n. 144.

Araújo, J.C. (2003). Reservoir sedimentation in the Brazilian Semi-arid: modelling and validation. Brazilian Journal of Water Resources, Porto Alegre, 8(2), pp. 39-56.

Araújo, J.C., Fernandes, L., Machado Júnior, J.C, Oliveira, M.L.R. and Sousa, T.C. (2003). Sedimentation of reservoirs in semiarid Brazil. In: Gaiser, T., Krol, M.S., Frischkorn, H. and Araújo, J.C.: Global change and regional impacts: Water availability and vulnerability of ecosystems and society in the semi-arid Northeast of Brazil. Springer-Verlag, Berlin Heidelberg, Germany, 205-216.

Araújo, J.C., Güntner, A. and Bronstert, A. (2006). Loss of reservoir volume by sediment deposition and its impact on water availability in semiarid Brazil. Hydrological Sciences, 51(1), pp. 157-170.

Arnold, J.G., Williams, J.R., Griggs, A.D. and Sammons, N.B. (1990). SWRRB: A basin scale simulation model for soil and water resources management. Texas A&M Univ. Press, College Station, U.S.A.

Ashida, K. and Michiue, M. (1973). Studies on bed load transport rate in alluvial streams. Trans. Japan Society of Civil Engineers, 4.

Ashida, K., and Michiue, M. (1970). Study on suspended sediment (1). Annals DPRI, No. 13B : 233-242. (in Japanese)

Avendaño, C., Cobo, R., Sanz, M.E. and Gómez, J.L. (1997). Capacity situation in Spanish reservoirs. I.C.O.L.D. 19th Congress on Large Dams, 74, R.52, 849-862.

Bagnold, R.A. (1956). The flow of cohesionless grains in fluids. Phil. Trans. Royal Soc. Lond. A246 (964), pp. 235-297.

Barnes, H.H. (1967). Roughness characteristics of natural channels. Water Supply Paper No. 1849, U.S. Geological Survey, USA.

Borland, W.M. (1971). Reservoir sedimentation. In: River Mechanics, chap. 29, H.W. Shen (editor), Water Resources Publication, Forth Collins.

Borland, W.M. and Miller, C.R. (1958). Distribution of sediments in large reservoirs. Journal of Hydraulics Division, ASCE, 84(2).

Brownlie, W.R. (1981). Prediction of flow depth and sediment discharge in open channels. W.M. Keck Laboratory of Hydraulics and Water Resources, Report no. KH-R-43A, California Institute of Technology, Pasadena, California.

Brune, G. (1953). Trap efficiency of reservoirs. Trans. of Am. Geophysical Union, 34(3), pp. 407-418.

Brunner, G.W. (2002). HEC-RAS, River analysis system hydraulic reference manual. US Army Corps of Engineers, Hydrologic Engineering Center (HEC).

Campos, R. (2001). Three-dimensional reservoir sedimentation model. PhD thesis, University of Newcastle, Newcastle, pp. 25-45.

Chang, H. (1998). Fluvial processes in river engineering. Krieger, Malabar, FL.

Chen, B.F. and Hung, T.K. (1993) Dynamic pressure of water and sediment on rigid dam. ASCE. J. Mechanical Engineering, 19(7), pp. 1411-1433.

Chen, Y., Wai, O.W.H., Li, Y.S. and Lu, Q.M. (1999). Three-dimensional numerical modeling of cohesive sediment transport by tidal current in Pearl River Estuary. International Journal of Sediment Research, 14(2), pp. 107-123.

Choi, S. and Garcia, M. (2002). k-ε turbulent modeling of density currents developing two dimensionally on a slope. J. Hydraulic Eng., 128(1), pp. 55-63.

Chow, V.T. (1959). Open channel hydraulics. McGraw-Hill, New York, USA.

Chow, V.T., Maidment, D.R. and Mays, L.W. (1988). Applied hydrology. McGraw-Hill International Editions, Civil Engineering Series, Singapore.

Churchill, M.A. (1948). Discussion of "Analysis and use of reservoir sedimentation data" by C. Gottschalk, Proc. of Federal Interagency Sedimentation Conference, Denver.

Costa, A.C. (2007). Hydrology of an experimental catchment in preserved Caatinga vegetation in semi-arid environment. MSc thesis, Federal University of Ceará, Brazil. (in Portuguese)

Creutzfeldt, B.N.A. (2006). Remote sensing based characterisation of land cover and terrain properties for hydrological modelling in the semi-arid Northeast of Brazil. M.Sc. thesis, University of Potsdam, Germany.

Dallimore, C.J., Imberger, J. and Hodges, B.R. (2004). Modeling a plunging underflow. Journal of Hydraulic Engineering, 130(11), pp. 1068-1076.

De Cesare, G., Schleiss, A., Hermann, F. (2001). Impact of turbidity currents on reservoir sedimentation. Journal of Hydraulic Engineering, 127(1), pp. 6-16.

Einstein, H.A. (1950). The bedload function for sediment transport in open channel flow. U.S. Department of Agriculture Soil Conservation, Technical Bulletin No. 1026.

Engelund, F. and Hansen, E. (1972). A monograph on sediment transport in alluvial streams. Teknisk Forlag, Copenhagen.

Evans, G.P., Mollowney, B.M. and Spoel, N.C. (1990). Two-dimensional modelling of the Bristol channel, UK. Estuarine and Coastal Modeling Conference, ASCE, New York.

Fang, H. and Wang, G. (2000). Three-dimensional mathematical model of suspended-sediment transport. Journal of Hydraulic Engineering, 126(8), pp. 578-592.

Fargas, D., Martınez, J.A. and Poch, R.M. (1996). Identification of critical sediment source areas at regional level. Annales Geo-physical 14 Supplement II, 314, European Geophysical Society C.

Foster, G.R. and Lane, L.J. (1983). Erosion by concentrated flow in farm fields. Proceedings, D.B. Simons Symposium on Erosion and Sedimentation, Colorado State University, Ft. Collins, CO, pp. 9.65-9.82.

Francke, T., López-Tarazón, J.A., Vericat, D., Bronstert, A. and Batalla, R.J. (submitted). Flood-based analysis of high-magnitude sediment transport using a non-parametric method. Earth Surface Processes and Landforms.

Francke, T., Güntner, A., Bronstert, A., Mamede, G.L. and Müller, E.N. (in Press). Automated catena-based discretisation of landscapes for the derivation of hydrological modelling units. International Journal of Geographical Information Science, DOI: 10.1080/13658810701300873.

Gladkow, G.L. and Söhngen, B. (2000). Modellierung des geschiebetransports mit unterschiedlicher korngröße in flüssen. Mitteilungsblatt der Bundesanstalt für Wasserbau, 82, pp. 123-129.

González, J., Tamburrino, A. and Niño, Y. (2006). Reservoir sedimentation: 1D model of turbidity currents and delta deposits. Proc. of the International Conference on Fluvial Hydraulics (River Flow 2006), (2), pp. 1607-1616, Taylor & Francis Group.

Govers, G. (1990). Empirical relationships on the transport capacity of overland flow. In: Proceedings of the Jerusalem Workshop, Erosion, Transport and Deposition Processes, March-April 1987, 5(189), pp. 45-63.

Graf, W.H. (1984). Hydraulics of sediment transport. McGraw-Hill, New York, Water Res. Publ., Littleton, CO, USA.

Graf, W.H. and Altinakar, M.S. (1998). Fluvial hydraulics – flow and transport processes in channels of simple geometry. John Wiley & Sons LTDA. ISBN 0-471-97714-4.

Greco, M. and Molino, B. (1997). Two dimensional model for sediment transport and diffusion simulation. Proceeding of Second International Conference on Environmental Management, Wollongong.

Güntner, A. (2002). Large-scale hydrological modelling in the semi-arid North-East of Brazil. PhD thesis, Potsdam Institute for Climate Research, Germany. PIK-Report No. 77.

Güntner, A. and Bronstert, A. (2004a). Representation of landscape variability and lateral redistribution processes for large-scale hydrological modelling in semi-arid areas. Journal of Hydrology, 297(1-4), pp. 136-161.

Güntner, A., Krol, M., Araújo, J.C. and Bronstert, A. (2004b). Simple water balance modelling of surface reservoir systems in a large data-scarce semiarid region. Hydrological Sciences Journal, 49, pp. 901-918.

Guy, H.P. (1969). Laboratory theory and methods for sediment analysis. Techniques of Water-Resources Investigations of the United States Geological Survey. Book 5 Chapter C1.

Haan, C.T., Barfield, B.J., and Hayes, J.C. (1994). Design hydrology and sedimentology for small catchments. New York: Academic Press.

Han, Q. and He, M. (1990). A mathematical model for reservoir sedimentation and fluvial processes. International Journal of Sediment Research, 5, pp. 43-84.

Han, Q.W. (1980). A study on the non-equilibrium transportation of suspended load. Proc. Int. Symps. on River Sedimentation, Vol.2 (Beijing China), pp. 793-802.

Hayter, E.J., Hamrick, J.M., Bicknell, B.R. and Gray, M.H. (2001). One-dimensional hydrodynamic/sediment transport model for stream networks. Technical Report, U.S. Environmental Protection Agency, National Exposure Research Laboratory, Athens, GA.

Hoggan, D.H. and Twiss, D.E. (1993). Two-dimensional hydrodynamic modeling with a computer graphics system. Hydraulic Engineering Conference, ASCE, New York.

Huang, H., Imran, J. and Pirmez, C. (2005). Numerical model of turbidity currents with a deforming bottom boundary. Journal of Hydraulic Engineering, 131, pp. 283-293.

Huang, J. (2001). A mathematical model of reservoir sedimentation. International Journal of Sediment Research, 16(2), pp. 244-250.

Huang, J., Hilldale, R.C. and Greimann, B.P. (2006). Cohesive sediment transport. In: Yang, C.T. (ed.), Erosion and sedimentation manual. U.S. Bureau of Reclamation, Technical Service Center, Denver, CO., chapter 4.

IRTCES (1985). Lecture notes of the training course on reservoir sedimentation. International Research of Training Center on Erosion and Sedimentation, Sediment Research Laboratory of Tsinghua University, Beijing, China.

Julien, P.Y. (1995). Erosion and sedimentation. Cambridge University Press. ISBN: 0521442370.

Kalinske, A.A. (1947). Movement of sediment as bedload in rivers. American Geophysical Union Transactions, 28, pp. 615-620.

Karaushev, A. (1966). The silting of small reservoirs and ponds: theory and calculation methods. Soviet Hydrology, n. 1.

Lane, E.W. and Koelzer, V.A. (1943). Density of sediments deposited in reservoirs. Report no. 9, in: A Study of Methods Used in Measurement and Analysis of Sediment Load in Streams, University of Iowa.

Langendoen, E.J. (2000). CONCEPTS - conservational channel evolution and pollutant transport system software manual. USDA-ARS National Sedimentation Laboratory, Research Report 16, Oxford, Mississippi.

Lara, J.M. (1962). Revision of procedures to compute sediment distribution in large reservoirs. US Bureau of Reclamation, Denver.

Lara, J.M. and Pemberton, E.L. (1963). Initial unit weight of deposited sediments. Proc. of Federal Interagency Sedimentation Conference, Denver.

Laursen, E.M. (1958). The total sediment load of streams. Journal of the Hydraulics Division, ASCE, 84, no. HY 1, 1530-1 through 1530-36.

Letter, J.V., Donnell, B.P., McAnally, W.H. and Thomas, W.A. (2000). Users guide to SED2D WES version 4.5. U.S. Army, Engineer Research and Development Center, Waterways Experiment Station, Coastal and Hydraulics Laboratory.

Lopes, J.L. (1978). Mathematical modelling of sediment deposition in reservoirs. PhD Thesis, Colorado State University, Fort Collins, USA.

Mamede, G.L., Bronstert, A., Araújo, J.C., Batalla, R.J., Güntner, A., Francke, T. and Müller, E.N. (2006). 1D process-based modelling of reservoir sedimentation: a case study for the Barasona reservoir in Spain. Proc. of the International Conference on Fluvial Hydraulics (River Flow 2006), (2), pp. 1585-1594, Taylor & Francis Group.

McAnally, W.H. (1989). STUDH: a two-dimensional numerical model for sediment transport. Sediment Transport Modelling Conference, ASCE, New York.

Mehta, A.J., Hayter, E.J., Parker, W.R., Krone, R.B. and Teeter, A.M. (1989). Cohesive sediment transport. I: Process description. Journal of Hydraulic Engineering, 115(8), pp. 1076-1093.

Merril, W.M. (1974). Reservoir sedimentation: a computer simulation. The Kansas Water Resources Institute, University of Kansas.

Meyer-Peter, E. and Müller, R. (1948). Formulas for bed-load transport. Proc. 2nd Congress IAHR, Stockholm, Sweden.

Miller, C.R. (1953) Determination of the unit weight of sediments for use in sediment volume computations. US Bureau of Reclamation, Denver.

Molle, F. (1989). Evaporation and infiltration losses in small reservoirs.. Serie Hydrologia, 25, SUDENE / ORSTOM, Recife, Brazil. (in Portuguese)

Monteith, J.L. (1965). Evaporation and environment. Symo. Soc. Exp. Biology, 19, 205-234.
Morgan, R.P.C. (2005). Soil erosion and conservation. Blackwell, Oxford.
Morris, G. L. and Fan, J. (1997). Reservoir Sedimentation Handbook, McGraw-Hill, New York.
Olsen, N.R.B. (1991). A three-dimensional numerical model for simulation of sediment movements in water intakes. DrIng. Thesis, Norwegian Institute of Technology, University of Trondhein, Norway.
Olsen, N.R.B., Jimenez, O., Lovoll, A. and Abrahamsen, L. (1994). Calculation of water and sediment flow in hydropower reservoirs. IAHR Int. Conf. on Modelling, Testing and Monitoring of Hydropower Plants, Budapest.
Palmieri, A., Shah, F. and Dinar, A. (2001). Economics of reservoir sedimentation and sustainable management of dams. Journal of Environmental Management, 61, pp. 148-163.
Parker, G. (1990). Surface-based bedload transport relation for gravel rivers. Journal of Hydraulics Research, 28(4), pp. 501-518.
Parker, G. and Sutherland, A.J. (1990). Fluvial Armor. J. Hydraul. Res., 28, 529-544.
Penman, H.L. (1948). Natural evaporation from open water, bare soil and grass. Proceedings Royal Society London, A 193, pp. 120-145.
Pereira, L. (2006). Isotopic and hydro-chemical analysis of surface and groundwater in the Aiuaba ecological station. PhD thesis. Federal University of Ceará, Brazil.
Peschke, G. (1977). Ein zweistufiges Modell der Infiltration von Regen in geschichtete Böden. Acta hydrophysica, 22(1), pp. 39-48.
Peschke, G. (1987). Soil moisture and runoff components from a physically founded approach. Acta hydrophysica, 31(3/4), pp. 39-48.
RADAMBRASIL Project (1981). Soil exploitation map. Levantamento dos Recursos Naturais, vol. 23, Rio de Janeiro (in Portuguese).
Ribberink, J.S. (1998). Bed-load transport for steady flows and unsteady oscillatory flows. Coastal Eng., 34, pp. 59-82.
Rickenmann, D. (1991). Bedload transport and hyperconcentrated flow at steep slopes. Fluvial Hydraulics of Mountain Regions, Springer-Verlag, New York, edited by A. Armanini and G.D. Silvio, pp. 429-441.
Rickenmann, D. (2001). Comparison of bed load transport in torrents and gravel bed streams. Water Resour. Res., 37(12), 3295-3306.
Rijn, L.C. van, (1984a), Sediment transport, Part I: Bedload transport. J. of Hydr. Eng., ASCE, 110(10), pp. 1431-1456.
Rijn, L.C. van, (1984b), Sediment transport, Part II: suspended load transport. J. of Hydr. Eng., ASCE, 110(11), pp. 1613-1641.
Rottner, J. (1959). A formula for bedload transportation. LaHouille Blanche, 14(3), pp. 285-307.
Rubey, W.R. (1933). Settling velocities of gravel, sand and silt particles. American Journal of Science, 21, pp. 325-338.
Scheer, P. van der, Ribberink, J.S. and Blom, A. (2002). Transport formulas for graded sediment. Research Report 2002R-002, Civil Engineering, University of Twente, The Netherlands, 123 p.
Scheer, P. van der. (2000). Transport formulae for graded sediment – verification with flume data. M.Sc. thesis, University of Twente, Enschede.
Schoklitsch, A. (1934). Der geschiebetrieb und die geschiebefracht, Wasserkraft und Wasserwirtschujl, 29(4), pp. 37-43.
Schoklitsch, A. (1950). Handbuch des wasserbaues. Springer: Vienna.
Schulits, S. and Hill Jr., R.D. (1968). Bedload formulas. Pennsylvania State University, College of Engineering, State College, Pennsylvania.
Schulla, J. (1997). Hydrologische modellierung von flussgebieten zur abschätzung der folgen von klimaänderungen. Zürcher Geographische Schriften, Band 69, Geographisches Institut, Eidgenössische Technische Hochschule, Zürich, Switzerland, pp. 161.
Shen, H.W. and Julien, P.Y. (1992). Erosion and sediment transport. In: Maidment, R.D., Handbook of Hydrology, McGraw Hill, New York, pp. 12.1-12.61.
Shojaeefard, M.H., Goudarzi, K. and Ghasvari Jahromi, H. (2007). Numerical simulation of 2_D turbidity currents and wall jet. American Journal of Applied Sciences 4(11), 882-888.
Shuttleworth, W.J. and Wallace, J.S. (1985). Evaporation from sparse crops - an energy combination theory. Quart. J. Roy. Meteorol. Soc., 111, pp. 839-855.
Siddique, M. (1991). A nonequilibrium model for reservoir sedimentation. Ph.D. Thesis, Colorado State University, Forth Collins, USA.
Simoes, F.J.M. and Yang, C.T. (2006). Sedimentation modeling for rivers and reservoirs. In: Yang, C.T., ed., Erosion and Sedimentation Manual, U.S. Bureau of Reclamation, Technical Service Center, Denver, CO., chapter 5.
Sloff, C.J. (1997). Sedimentation in reservoirs. PhD Thesis, Delft University of Technology, Holland.
Smart, G.M. and Jaeggi, M. (1983). Sediment transport on steep slopes. Mitt. Der Versuch-

sanst. fur Wasserbau, Hydrol. und Glaziol., 64, Zurich Inst. of Technol., Zurich, Switzerland.

Tang, L. and Chen, J. (1998). One-dimensional model of a reservoir sedimentation and its application in calculating water intake of a power plant. Journal of Hohai University, 26(5), (in Chinese).

Tarela, P. and Menendez, A. (1999). A model to predict reservoir sedimentation. Lakes & Reservoirs: research and management, 4, pp. 121-133.

Timothy, J.R. and Blair, G. (2006). Dam decomissing and sediment management. In: Yang, C.T., ed., Erosion and Sedimentation Manual, U.S. Bureau of Reclamation, Technical Service Center, Denver, CO., chapter 8.

Toffaleti, F.B. (1969). Definitive computations of sand discharge in rivers. Journal of the Hydraulics Division, ASCE, 95, no. HY I, pp. 225-246.

Toniolo, H. and Parker, G. (2003). 1D numerical modeling of reservoir sedimentation. Proceedings, IAHR Symposium on River, Coastal and Estuarine Morphodynamics, Barcelona, Spain, pp. 457-468.

U.S. Army Corp of Engineers. (1991). HEC-6 scour and deposition in rivers and reservoirs. User's Manual, Hydrologic Engineering Center, Davis, Calif.

Valero-Garces, B.L., Navas, A., Machin, J. and Walling, D.E. (1999). Sediment sources and siltation in mountain reservoirs: a case study from the Central Spanish Pyrenees. Geomorphology, 28, pp. 23-41.

Vetter, M. (1989). Total sediment transport in open channels. Report no. 26, Institute of Hydrology, University of the German Federal Army, Munich, Germany (translated from Gesamttrarzsport van Sedimenterz in OfSenen Gerirznen into English by the U.S. Bureau of Reclamation, Denver, Colorado).

Vries, M.J. de (2006). Assessment of WASA's reservoir storage model by using data from the Benguê Watershed, Ceará, Brazil. MSc Thesis, University of Twente, The Netherlands.

Wang, S.S.Y., Combs, P. and Hu, K.K. (1989). New developments in modelling 3-D sedimentation phenomena. Sediment Transport Modelling Conference, ASCE, New York.

White, W.R. and Bettes, R. (1984) The feasibility of flushing sediments through reservoirs. Proc. Symposium on Challenges in African Hydrology and Water Resources, Harare, Zimbabwe.

White, W.R., Milli, H. and Crabe, A.D. (1975). Sediment transport theories: a review. Proceedings of the Institute of Civil Engineers, London, Part 2, 59, pp. 265-292.

Wilcock, P.R. and Crowe, J.C. (2003). Surface-based transport model for mixed-size sediment. Journal of Hydraulic Engineering, 129(2), pp. 120-128.

Williams, D.T. and Julien, P.Y. (1989). Applicability index for sand transport equations. J. Hyd. Div. ASCE, 115(11), pp. 1578-1581.

Williams, J.R. (1975). Sediment-yield prediction with universal soil equation using runoff energy factor. In: Present and prospective technology for predicting sediment yield and sources: Proceedings of the sediment-yield workshop, USDA Sedimentation Lab., Oxford, MS, November 28 – 30, 1972, ARS-S-40, pp. 244-252.

Wilson, B.R, Barfield, B.J. & Moore, I.D. (1982) A hydrology and sedimentology watershed model. I. Modeling technique. Dept. of Agric. Engineering, University of Kentucky, Lexington, New York, USA.

Wu, W. and Vieira, D.A. (2002). One-dimensional channel network model CCHE1D Version 3.0 – Technical Manual. Technical Report No. NCCHE-TR-2002-1, National Center for Computational Hydroscience and Engineering, The University of Mississippi.

Wu, W., Rodi, W and Wenka, T. (2000a). 3D numerical modeling of flow and sediment transport in open channels. J. Hydr. Engrg., 126(1), pp. 4-15.

Wu, W., Wang, S.S.Y. and Jia, Y. (2000b). Nonuniform sediment transport in alluvial rivers. J. of Hydr. Res., 38(6), pp 427-434.

Yang, C.T. (1973). Incipient motion and sediment transport. Journal of the Hydraulic Division, ASCE, 99, no. HY 10, pp. 1679-1704.

Yang, C.T. (1976). Discussion of sediment transport theories - a review by W.R. White, H. Milli, and A.D. Grabble. Institute of Civil Engineering, Part 2, 61, pp. 803-810.

Yang, C.T. (1979). The movement of sediment in rivers. Geophysical Survey 3, D. Reidel, Dordrecht, pp. 39-68.

Yang, C.T. (1984). Unit stream power equation for gravel. Journal of Hydraulic Engineering, ASCE, 110 (12), pp. 1783-1797.

Yang, C.T. (1996). Sediment transport: theory and practice. McGraw-Hill, New York.

Yang, C.T. and Huang, C. (2001). Applicability of sediment transport formulas. International Journal of Sediment Research, 16(3), Beijing, China, pp. 335-343.

Yang, C.T. and Molinas, A. (1982). Sediment transport and unit stream power function. Jour-

nal of the Hydraulics Division, ASCE, 108, no. HY6, pp. 776-793.

Yang, C.T. and Simoes, F.J.M. (2000). User's manual for GSTARS 2.1 (Generalized Stream-Tube model for Alluvial River Simulation version 2.1). U.S. Bureau of Reclamation Technical Service Center, Denver CO, 80225.

Yang, C.T. and Simoes, F.J.M. (2002). User's manual for GSTARS3 (Generalized Sediment Transport model for Alluvial River Simulation version 3.0). U.S. Bureau of Reclamation Technical Service Center, Denver, CO, 80225.

Yang, C.T. and Wan, S. (1991). Comparison of selected bed-material load formulas. Journal of Hydraulics Engineering, ASCE, 117(8), pp. 973-989.

Yang, C.T., Huang, J.V. and Greimann, B.P. (2004). User's manual for GSTAR-1D 1.0 (Generalized Sediment Transport for Alluvial Rivers – One Dimensional, Version 1.0). U.S. Bureau of Reclamation Technical Service Center, Denver, CO, 80225.

Yang, C.T., Molinas, A. and Song, C.C.S. (1989). GSTARS – Generalized Stream Tube model for Alluvial River Simulation. Twelve Selected Computer Stream Sedimentation Models Developed in the United States, U.S. Interagency Subcommittee Report on Sedimentation, edited by S. S. Fan, Federal Energy Regulatory Commission, Washington D.C., pp. 148-178.

Yang, C.T., Treviño, M.A. and Simoes, F.J.M. (1998). User's manual for GSTARS 2.0 (Generalized Stream Tube model for Alluvial River Simulation version 2.0), U.S. Bureau of Reclamation Technical Service Center, Denver, CO, 80225.

Zhang R.J. and Xie, J.H. (1993). Sedimentation research in China. Systematic Selections, China Water and Power Press, Beijing.

# APPENDIX

## Appendix

**Appendix 1 Location of Small and Strategic Reservoirs within the Benguê Catchment**